THE CONTROL AND STABILITY ANALYSIS OF TWO–WHEELED ROAD VEHICLES

SIMOS EVANGELOU

Submitted to the University of London
for the degree of
Doctor of Philosophy

Electrical and Electronic Engineering
Imperial College London

September 2003

Abstract

The multibody dynamics analysis software, AUTOSIM, is used to develop automated linear and nonlinear models for the hand derived motorcycle models presented in (Sharp, 1971, 1994*b*). A more comprehensive model, based on previous work (Sharp and Limebeer, 2001), is also derived and extended. One version of the code uses AUTOSIM to produce a FORTRAN or C program which solves the nonlinear equations of motion and generates time histories, and a second version generates linearised equations of motion as a MATLAB file that contains the state-space model in symbolic form. Local stability is investigated via the eigenvalues of the linearised models that are associated with equilibrium points of the nonlinear systems. The time histories produced by nonlinear simulation runs are also used with an animator to visualise the result. A comprehensive study of the effects of acceleration and braking on motorcycle stability with the use of the advanced motorcycle model is presented. The results show that the wobble mode of a motorcycle is significantly destabilised when the machine is descending an incline, or braking on a level surface. Conversely, the damping of the wobble mode is substantially increased when the machine is ascending an incline at constant speed, or accelerating on a level surface. Except at very low speeds, inclines, acceleration and deceleration appear to have little effect on the damping or frequency of the weave mode. A theoretical study of the effects of regular road undulations on the dynamics of a cornering motorcycle with the use of the same model is also presented. Frequency response plots are used to study the propagation of road forcing signals to the motorcycle steering system. It is shown that at various critical cornering conditions, regular road undulations of a particular wavelength can cause severe steering oscillations. The results and theory presented here are believed to explain many of the stability related road accidents that have been reported in the popular literature. The advanced motorcycle model is improved further to include a more realistic tyre-road contact geometry, a more comprehensive tyre model based on Magic Formula methods utilising modern tyre data, better tyre relaxation properties and other features of contemporary motorcycle designs. Parameters describing a modern high performance machine and rider are also included.

Acknowledgements

I wish to thank Professor David Limebeer and Professor Robin Sharp for their support and guidance throughout this project and for taking care of the necessary funding. It has been a unique experience to work with such outstanding researchers and to know that I could constantly trust their scientific judgements, which, I must say, they always explained with great enthusiasm. I really enjoyed their pleasant, humorous and open-hearted character and I doubt I will ever forget the exhilarating trip to Snetterton race track on the back seat of Prof. Limebeer's Kawasaki ZX-9R.

Finally, my deepest gratitude goes towards my family for their endless love and support. Their confidence in me has been tremendously encouraging and provided me with strength to accomplish my task. I feel very lucky to have such a caring family and to know that I can always rely upon them.

Contents

List of Figures

List of Tables

Part I

Introduction and Literature Review

Chapter 1

Introduction

In recent years there has been an increased motorcycle sales momentum in various parts of the world. In China alone, "Guang Cai Motorcycle Association of Imports and Exports"[1] estimates the two-wheeler sales for a typical month in year 2000 to be around 5.8 million, giving an increase of 13.72% from the same month in the previous year. During this period the trend has been for people to shift towards machines with higher engine capacities. The Ministry of Road Transport & Highways, Government of India, gives the total number of registered two-wheelers as on 31 March 2000 to be just less than 34 million compared with 4.57 million for cars[2], while according to the Japan Automobile Manufacturers Association[3] the total number produced in Japan was in excess of 2 million for year 2002.

Motorcycles are typically used for commuting or for pleasure. Lighter vehicles with smaller engines are usually cheaper than their heavier counterparts and provide the primary means of transport in a lot of Asian countries. "Harley-Davidson" type tourers are very popular in the United States while a wide variety of Japanese exports come to Europe. Pleasure is mostly acquired from riding powerful sports road bikes that nowadays have designs and engine performances that can easily be compared with full racing machines only a decade old. It is also common for police to use big powerful machines and often they have to ride them under difficult circumstances at high speeds. Needless to say, a lot of investment nowadays goes into motor racing and development of state-of the-art high technology machines.

On the negative side, even though motorcycles have been developed and manufactured for a long time, they are still known to possess behavioural problems. Typically, they can exhibit lightly damped oscillatory behaviour under certain circumstances, which can seriously compromise rider safety with possible loss of control and serious injury as a result. Several lightly damped modes exist, the most important being wobble and weave. Weave is a low frequency mode associated with high speed operation, while high frequency wobble is associated with lower speeds. There is anecdotal evidence to suggest that wobble frequency steering oscillations can occur at much higher speeds also.

[1] http://www.cn-motorcycle.com/content3/tongji.htm#

[2] http://morth.nic.in/motorstat/mt5.pdf

[3] http://www.jama.org/statistics/motorcycle/production/mc_prod_year.htm

Several cases of serious accidents that involve no other road user have been reported in the popular motorcycle press over the past decade and these are believed to have been based on one or more of the above phenomena. Even though this type of accident has been known for a long time, it has proven remarkably difficult to obtain a complete understanding of the mechanisms involved. The main reasons for this seem to be the following: Firstly, unlike aircraft, motorcycles do not possess "black boxes" and therefore the accidents are poorly documented, and usually not witnessed by independent observers. Secondly, the investigating authorities and manufacturers tend to prematurely blame the rider for the accident. Thirdly, an unusual combination of circumstances has to occur for such accidents to happen. These involve the motorcycle type and setup, the speed, the lean angle, the rider's stature and the road profile. Finally, the underlying mechanics of these phenomena are complex as will be presented later on.

Apart from the social costs and loss of life, motorcycle accidents can also cause large financial costs. The Metropolitan police estimate that the total cost arising from the death of one of their officers involved in one such accident is approximately £1.2 M (Metropolitan Police, 2000).

There is therefore an increasing need to gain a complete understanding of the behavioural properties of single track vehicles and to seek solutions to any problems. The knowledge acquired can be used in the design, testing and development process to cut down costs associated with trial-and-error methods that are employed by manufacturers, and could aim at increasing rider safety and other quality features such as manoeuvrability and handling. Further to that, skills can be developed that could be used for rider training purposes.

The dynamic stability under small perturbations from straight running and steady cornering conditions for motorcycles has been studied extensively prior to this work. Most of the work carried out involved studies using theoretical models that have been derived by manual methods or by making use of computer assisted multibody dynamics software. The latter methods have given a significant boost to the complexity that can be included in a model compared with old fashioned hand derivations. There has been limited experimental work carried out as well and in general results are in agreement with the theory.

The purpose of this thesis is to make use of multibody dynamics analysis software to improve existing mathematical models by adding complicated features that are important to the accuracy of predicted behaviour. The focus is on high performance motorcycles. Work is then carried out in explaining the behaviour of motorcycles under acceleration and deceleration and also to quantify the machine response to regular road undulations through theoretical analysis. Attempts have been made in the past to study acceleration and deceleration in particular, but the hand derived models used proved to be unsuccessful in predicting behaviour that is aligned with common experience. This failure, as we will see later on, was primarily attributed to the relative simplicity of the model employed. As far as the present author is aware, no attempt has been made in the past to study the effects of road forcing from regular road undulations. These topics are covered in Parts II and III of this thesis following Part I with the introductory material. The rest of the work before conclusions and appendices (Parts V and VI) is contained in Part IV and

is involved with bringing the automated computer model up to date. This is ongoing research and is not complete at this stage. Central issues in modelling that will be tackled are representation of frame flexibilities, tyre–road contact geometry and tyre shear forces and moments. Many previous findings relate to motorcycle and tyre descriptions which are now somewhat dated and to tyre models that have a limited domain of applicability. Therefore, it is of interest to obtain a parametric description of a modern machine, and to utilise a more comprehensive tyre force model with parameter values to correspond to a modern set of tyres. In this way steady turning, stability, response and parameter sensitivity data for comparison with older information can be obtained, in order to determine to what extent it remains valid, and to better understand the design of modern machines.

To elaborate further, in the next Chapter (Chapter 2) a literature review is provided. Chapter 3 describes how a "simple" linear motorcycle model (Sharp, 1971) is derived using the multibody building software Autosim and how it compares with the prior art. In a similar respect Chapter 4 describes and compares with the prior art, the computer modelling of a more complicated design (Sharp, 1994*b*). These two chapters together build up the knowledge towards Chapter 5 that describes the state-of-the-art model. This was mostly developed elsewhere (Sharp and Limebeer, 2001) and only a revision is given here together with the necessary add-ons required for the results in subsequent chapters. Chapter 6 explains how it is possible to use a simple animator program to visualise the computer generated time responses. Chapter 7 makes use of the model of Chapter 5 to explain the behaviour of the wobble and weave modes under acceleration and deceleration, while Chapter 8 is concerned with quantifying the machine response to regular road undulations through theoretical analysis with the same model. Further modelling upgrades are described in Chapter 9 together with new parametric descriptions for the motorcycle design and tyres. Chapter 10 provides the conclusions and Chapter 11 gives an account of future research directions.

Chapter 2

Literature Review

The purpose of this Chapter is to give an overview of the state of knowledge on the steering behaviour of single-track vehicles up to date. The issues covered are presented roughly in chronological order and relate to theoretical studies through mathematical modelling and also to experimental results and observations that have occurred in the last 30 years.

Even though the scientific study of the motions of two-wheelers has been in progress for more than 100 years, early work was progressing slowly and many conflicting conclusions were drawn initially. Readers who are interested in the historical development of this topic are referred to the comprehensive survey article (Sharp, 1985). It can be seen from this paper that the early literature modelled the vehicle using simple rigid body representations for the front and rear frames, while the road-tyre rolling contact was treated as a non-holonomic constraint. Over time, this sequence of models treated the tyres as more and more sophisticated moment and force producers, and they also evolved to include the effects of various frame flexibilities and rider dynamics.

An important step in the theoretical analysis of motorcycles was achieved by (Sharp, 1971). Sharp carried out a Lagrangian analysis of the motions of a motorcycle with a rider, treating the vehicle as two rigid frames joined at an inclined steering axis, the rider being rigidly attached onto the rear frame. Four degrees of freedom were allowed, lateral motion, yaw, roll and steer, and only small perturbations from straight running were considered in the motion, essentially making the model linear. The tyres were assumed as producing steady state forces and moments that were linearly dependent on side-slip and camber angle, with the instantaneous forces and moments obtained from the steady state ones via a first order differential equation that modelled the tyre relaxation property. Aerodynamic effects were not included.

Sharp used this model to carry out a stability analysis by calculating the eigenvalues of the linear model as functions of forward vehicle speed under constant speed conditions. Two separate cases were considered, one with the steering degree of freedom present, giving rise to the "free control" analysis, and the other with the steering degree of freedom removed, giving rise to the "fixed control" analysis. The free control analysis exposed some important results. It predicted the presence of important modes throughout the speed range, some of which were os-

cillatory. These were given the names “capsize”, “weave” and “wobble”. Capsize is a slow speed divergent instability of the whole vehicle falling onto its side and is usually easily controlled by the rider’s use of his weight and steering torque to balance the motorcycle. Weave is a low frequency (2-3 Hz) oscillation of the whole vehicle involving roll, yaw and steer motions, and is well damped at moderate speeds but becomes increasingly less damped and possibly unstable at higher speeds. Wobble is a higher frequency (typically 7-9 Hz) motion that involves primarily the front steering system rotating relative to the rear frame, and at the time theory predicted that this mode is highly stable at low speeds becoming lightly damped at high speeds. At this point it became apparent that the full model employed represented minimum requirements for at least qualitatively correct predictions, and also that the tyre relaxation was an important addition to the model since the absence of it was dramatically stabilising the wobble mode. The fixed control stability characteristics appeared unattractive due to the predicted divergent instability throughout the speed range, an instability that is most severe at low speeds. Contrary to double track vehicle cases, the fixed control characteristics of the motorcycle were therefore found to be unimportant since the rider, given the choice, would almost certainly opt to exercise torque control.

Sharp also used his model to obtain stability characteristics for many parameter variations, and found the results to agree qualitatively well with known behaviour. In particular, he demonstrated the stabilising effect of steering damping on the wobble mode and destabilising effect on the weave mode, the positive effect of moving the rear frame mass centre forward, the criticality on stability of steering head angle, mechanical trail and front frame mass centre offset from the steering axis, and the improvement in wobble and weave behaviour by reduced lag in the tyre forces. Often changes in parameters had conflicting effects on various aspects of the behaviour or at various forward speed ranges.

The work by (Cooper, 1974) showed the importance of aerodynamic effects in the performance and stability of high speed motorcycles. Wind tunnel measurements were obtained for steady aerodynamic forces acting on a wide range of motorcycle-rider configurations separated into two groups: road machines and racing–record machines. The experiments were done for a range of wind speeds and yaw angles each time measuring three components of aerodynamic force and three aerodynamic moments. The steady aerodynamic side force coefficients for road machines were found to be low compared to those for highly streamlined motorcycles, resulting in low coefficients for the yawing and rolling moments. The lift coefficients for road bikes were found to be close to zero and the drag and pitching moment coefficients were high. Aiming to explain the very high speed weave problem, Cooper included these aerodynamic effects into Sharp’s model using parameters for a streamlined machine and carried out stability analyses that showed no considerable change in wobble mode, but revealed low weave damping at high speeds only when unsteady aerodynamic forces were included. These were measured in the wind tunnel via the replacement of the motorcycle shape by an equivalent shape (airfoil). For production motorcycles, Cooper’s results appear to suggest that the effect of aerodynamic side forces and moments on vehicle lateral stability are not large, and the only influence comes from drag, lift

and pitching moment affecting the tyre side forces via change of tyre loading with speed.

(Sharp, 1974) extended his original model to allow torsional flexibility of the rear wheel relative to the rear frame, restrained by a linear spring and damper. It was found that reduced stiffness in this freedom would deteriorate weave mode damping at medium and high speeds, while capsize and wobble would stay relatively unaffected. Compared with conventional frames found on motorcycles of that time, a degree of torsional flexibility was tolerable, but further increase in the stiffness would result in diminishing returns.

(Jennings, 1974) pointed out the existence of a modified weave mode that occurred under cornering conditions, in which the suspension system plays an important role in its initiation and maintenance. In order to investigate the effect of suspension damping on cornering weave, Jennings benchmarked several front and rear suspension dampers in laboratory experiments and riding tests and concluded that motorcycle stability is sensitive to suspension damping characteristics and cornering weave instability is to some extend controllable with rear suspension damping. He also found that as the speed is increased, cornering weave is produced at smaller roll angles. In a separate study (Sharp, 1976*a*) demonstrated by a simple analysis the possibility of interaction between pitch and weave modes at high forward vehicle speeds, where the lightly damped weave mode natural frequency approaches that of the pitch mode. It was clear that for straight running the coupling of in-plane and out-of plane motions would be weak but for steady cornering the coupling between the two modes would increase with increased lean angle, indicating that the inclusion of pitch and bounce freedoms in motorcycle models was desirable for further handling studies involving cornering.

(Singh *et al.*, 1974) obtained measurements for steady state tyre side force, aligning moment and overturning moment for free rolling scooter tyres, and by measuring responses to lateral slip input they also determined the relaxation length associated with side force and moment transient response. (Singh and Goel, 1975) used these data together with other obtained scooter parameters to build a five degree of freedom model, and the dynamic characteristics deduced from the model were in good agreement with (Sharp, 1971). They also used their model to investigate the effects of various design changes.

According to (Segel and Wilson, 1975) the tyre side force and overturning moment due to camber had to be described more accurately, both statically and dynamically, than what was available at the time, in order to predict the dynamics of single-track vehicles with more accuracy. They carried out experiments whereby they measured the transient behaviour of camber thrust and overturning moment, and found that the overturning moment was mostly generated in phase with the inclination, but the camber thrust had only a small proportion generated in phase with the rest lagging the input with a relaxation length about twice as much as that associated with side-slip generated forces.

Moving away from the constant forward speed case, (Sharp, 1976*b*) represents the first attempt to study the effects of acceleration and deceleration on the stability of motorcycles. However, the rather simplistic approach used, which regarded the longitudinal equations of motion as uncoupled from the lateral equations, and treated the longitudinal acceleration as a parameter

of the lateral motion contributing to longitudinal "inertia force", lead to some unsubstantiated conclusions. Even so, the stabilising effect of acceleration on the capsize mode was evident from the results suggesting that the capsize mode is mainly influenced by a roll angle to yawing moment feedback term arising from the rear frame "inertia force". It is generally recognised by motorcycle riders that at low speeds steering feels much better when accelerating, and usually they develop a low speed cornering technique to take advantage of this.

(Roe and Thorpe, 1976) set out to find cures for the wobble instability by measuring steer angle fluctuations on machines ridden 'hands off' at the onset of instability. The observed self excitation was strongest at midrange speeds (15 to 20 m/s) indicating that theoretical calculations of the time, predicting wobble problems at much higher speeds, were inconsistent with practice in this respect. The experiments of Roe and Thorpe showed that telescopic forks had insufficient lateral stiffness to prevent the onset of flutter and stiffening them as well as stiffening torsionally the rear frame made a considerable improvement to stability. Rear loading was found to make the behaviour worse and on the basis of their results it was suggested that there is a limit to the lateral stiffness attainable with a telescopic fork.

Following the postulate (Segel and Wilson, 1975) that a more elaborate treatment of the tyre was needed, (Sharp and Jones, 1977) developed a comprehensive tyre model and evaluated the influences of various parameters of the model, in order to determine which aspects of real tyre behaviour are important to describing the straight running behaviour of the motorcycle. In the absence of comprehensive experimental data on motorcycle tyres, Sharp and Jones based their model on constructed data from a taut string tyre model whose parameter set was obtained from existing tyre data. In 'taut string' theory, the tyre tread band is represented as a number of stretched strings elastically connected to the wheel rim. The tyre model together with aerodynamic load transfer effects were incorporated in the motorcycle model, and the stability results proved to be completely insensitive to whether camber forces were lagged or not, suggesting that the representation of the camber responses as instantaneous is adequate in the context of straight running stability. At this point it became clear that merely describing the tyre with greater accuracy was not enough to explain the discrepancy between theory and observation.

The main focus of (Weir and Zellner, 1978) was to investigate the rider control effects in connection with the established vehicle dynamic behaviour, acknowledging that the dynamics of the vehicle have a profound effect on the control activity employed by the rider. Theoretical analysis was used via a mathematical motorcycle model and a simple rider control model under straight running conditions, to demonstrate that the most influential rider control for lateral-directional operation is rider use of steer torque to control the vehicle roll angle–the same result was observed by (Eaton, 1973) some years before, by experiments he conducted which were based on theoretical work previously developed by (Weir, 1972). Weir and Zellner also verified that the lag of tyre camber force was unimportant and as far as lateral dynamics of the motorcycle were concerned, it was enough to assume that only side-slip generated forces were lagged. At the same time in a separate paper (Zellner and Weir, 1978), concentrating on steady cornering manoeuvres, measured steady state response data for five different motorcycles. Steer torque to roll

angle, steer torque to steer angle and yaw rate to steer angle ratios were presented against velocity and compared with the results from linear analyses with the mathematical model of (Weir and Zellner, 1978) under straight running conditions. The steer angle data were not predicted very well from the theory, but there was good agreement in the roll angle data and the speed where the steer torque to roll angle gain changed sign, which Zellner and Weir correctly referred to as the speed at which the capsize mode was crossing the stability boundary.

Further investigation was undertaken by (Weir and Zellner, 1979), this time under free control (open loop) conditions, to quantitatively determine the effects of various motorcycle design parameters and operating conditions on wobble and weave. Tests with a range of motorcycles and riders were carried out for straight running and steady cornering. Wobble was excited by a steering torque pulse input from the rider and was seen to be self sustained during straight running at moderate speeds (35–40 mph depending on rear loading of the vehicle), with frequency smaller than what theory predicted. More importantly, during steady cornering at limiting conditions and sometimes with worn or degraded shock absorbers, suspension bushings or other components, Weir and Zellner measured cornering weave responses that involved systematic participation from the suspension system. They found the weave oscillations to damp out once the rider reduced the roll angle, and they demonstrated that degraded damping of the rear suspension, rear loading and increased speed, amplified cornering weave tendencies. The frequency of wobble stayed relatively constant with speed, while that of weave increased with speed, as predicted by theory.

(Sakai *et al.*, 1979) carried out experiments on laboratory testing machines and provided comprehensive steady state force and moment response data for several types of free rolling motorcycle tyre. (Otto, 1980) investigated theoretically via computer simulation, validating by experiments, the effects of adding a travel trunk, saddlebags, and frame and handlebar mounted fairings to two large touring motorcycles. He concluded that certain combinations of accessories (including rigidity of mounting brackets) can actually improve the stability of a baseline motorcycle, but they are more likely to result in some destabilisation in one or more modes usually at high speeds. It was emphasised that tyre characteristics and inflation pressures are important variables in the behaviour of the motorcycle at high speeds, and it was considered that the self limiting behaviour observed in some forms of oscillations might be due to the tyre side force saturation from limiting adhesion with the road. Otto also considered that rider actions can profoundly influence the results from otherwise inconsequential events.

The discrepancy between theory and observation (mainly with respect to the damping of the wobble mode), was substantially explained and overcome by (Sharp and Alstead, 1980) and (Spierings, 1981) by including structural frame flexibilities in the theoretical models of motorcycles which up to that time assumed the frame to be rigid. Sharp and Alstead used a tyre model more realistic than before in their analyses based on taut string theory. It included consideration of tread width, longitudinal tread rubber distortion, tread mass gyroscopic effects, adjustment of the parameters according to the load, and "parabolic" approximation to the exact response. The camber responses were modelled empirically as instantaneous and were superposed. The new

freedoms in the model were a torsional flexibility of the front frame about an axis parallel to the steering axis, lateral flexibility of the wheel relative to the forks along the spindle axis, and a torsional flexibility at the steering head about an axis normal to the steering axis, in all cases restraining movement in these freedoms by linear springs and dampers. Full parameter sets (frame stiffnesses, mass and geometric properties) representative of four large production motorcycles of the time were used to carry out the standard eigenvalue type analyses of the linearised straight running model. Changes in the torsional stiffness associated with the flexibility parallel to the steering axis resulted in very small changes in the stability properties, but common levels of lateral stiffness at the wheel spindle deteriorated the wobble mode damping substantially with significant changes in the wobble frequency as well, and slight reduction in the weave mode damping at high speeds. The predicted change in wobble mode damping was for all speeds and therefore these results alone could still not explain the observations, but the inclusion of the rear frame torsional flexibility had the required result, whereby the damping of the wobble mode was reduced for midrange speeds and increased for higher speeds, without affecting the frequency strongly and slightly reducing weave mode damping at high speeds. It was suggested that from a stability point of view it is desirable to make the lateral stiffness as large as possible, with the possibility of an optimum value for the torsional stiffness of the rear frame.

(Spierings, 1981) through an independent study confirmed the main result above. Apart from varying the torsional stiffness he also investigated the effect of changing the height of the lateral fork bending joint. He used further analysis to evaluate the separate contributions from lateral distortion and from gyroscopic torques on the total influence of the lateral flexibility on stability and found that while the gyroscopic term had a stabilising effect, the lateral distortion was acting in the opposite manner with their relative importance changing with speed, and he concluded that lateral distortion should be opposed as much as possible by locating the front fork torsional axis as low as possible.

(Giles and Sharp, 1983) tried to estimate rear and front frame stiffness properties by static and dynamic loading at the wheel rim of a large conventional road motorcycle that was anchored to a baseplate. Dynamic loading of the frame was provided by means of a sinusoidally driven shaker, deflections were obtained by means of an accelerometer and frequency response information was produced via electronic data processing. The measured responses for the front frame showed a single resonance at about 12 Hz and it was concluded that the lumped mass assumption used to model frame flexibilities in theoretical studies was adequate. However, the value of the torsional stiffness and location of the twist axis at the steering head of the front frame predicted by the dynamic loading method, were remarkably different from the results of the static loading tests, and the differences were shown to be very significant in relation to the theoretical wobble mode prediction.

A significant step in the motorcycle theoretical analysis was made by (Koenen, 1983) building on his previous work (Koenen and Pacejka, 1980) and (Koenen and Pacejka, 1981). The model developed considered small perturbations about straight running conditions but also about unprecedented steady cornering conditions. The nominal situation was the starting point for the

calculations, the stationary situation had been described by a set of non-linear algebraic equations and linear differential equations were superposed to determine the non-stationary response. The coupling of the in-plane and out-of-plane motions increases with increased roll angle, and thereby it was recognised that bounce, pitch and suspension freedoms should be included in the model. The tyres were treated as thin discs that were radially flexible, and their width was taken into account by adding overturning moments arising from geometric considerations of the lateral migration of the contact point around the tyre profile. Side forces and aligning moments were assumed to be applied at the contact points in response to side-slip angle, camber angle and turn-slip, and the relation between them was based on a combination of specific measurements, the qualitative character of published measurements (Sakai *et al.*, 1979) and theoretical considerations. The variation of the side force with side-slip was assumed linear with a cornering stiffness that was linearly dependent on the camber angle, and the camber thrust was found from the experiments to vary approximately parabolically with camber angle, both of these forces varying linearly with normal load. Dependencies of the aligning moments on the wheel loads were constructed from considerations of how the tyre parameters depend on the contact length and possibly the width, and that the length and width vary in proportion to the square root of the wheel load. Relaxation properties were introduced via first order differential equations consistent with taut string theory, and relaxation lengths were assumed to vary proportionally to the square root of the normal load and to be the same for all camber and speed conditions. Aligning moments due to camber and turn-slip, and overturning moments were taken to arise instantaneously, and tread band mass gyroscopic effects were also included. Koenen inserted the rider upper body in the model with the freedom to roll relative to the lower body that was rigidly attached onto the main frame, with stiffness and damping parameters derived from simple laboratory experiments, acknowledging that these parameters were expected to vary widely depending on rider choice and stature. Aerodynamic lift and drag forces and pitching moment were included together with torsional frame flexibility at the steering head, consistent with (Sharp and Alstead, 1980) and (Spierings, 1981) findings. The parameter values for the flexibility were obtained from experimental static measurements.

Koenen used his model to calculate the eigenvalues of the small perturbation linearised motorcycle, with the results for straight running being consistent with the conventional wisdom, predicting weave and wobble modes varying with speed and front and rear suspension pitch and wheel hop modes depending only very slightly on speed. Under cornering conditions the interaction of these otherwise uncoupled modes produces more complicated modal motions. The cornering weave and combined wheel hop/wobble modes were illustrated and many root loci were plotted to observe the sensitivity of the results to parameter variations. Surprisingly, it was predicted that removing the suspension dampers hardly affects the stability of the cornering weave mode, contrary to the experiences of (Weir and Zellner, 1979) and (Jennings, 1974).

(Takahashi *et al.*, 1984) investigated experimentally the influence of tyre parameters on the straight running weave response of a motorcycle that was fitted with various sets of tyres, exciting weave behaviour by a rear mounted nitrogen gas-jet disturbance system. The measured

responses were compared with theoretical calculations obtained from a model based on (Sharp, 1971). This model had a slightly expanded linear tyre model which included lagged side-slip, camber angle and turn-slip generated forces and aligning moments, and strangely enough overturning moments not only due to camber but also side-slip. Parameters for the vehicle and tyres were measured and used in the model, and the calculated results and experimental measurements with respect to weave mode damping and frequency at various speeds agreed at least qualitatively. The tyre parameters were varied in the model and it was found that the largest contribution to the weave damping came from the cornering and camber stiffnesses and relaxation length of the rear tyre and not so much from the same parameters of the front tyre.

(Nishimi *et al.*, 1985) focused on the straight running stability by building a twelve degree of freedom motorcycle model which also included an elaborate rider structural model, with leaning freedom of the upper body relative to the lower body and lateral movement freedom of the lower body relative to the main frame. The parameters were measured experimentally and the rider data, in particular, were measured by means of excitation bench experiments, whereby the frequency responses from vehicle roll to rider body variables were obtained. The frequency and damping ratios of wobble and weave modes were calculated at various speeds and compared with results obtained by full scale running experiments for various motorcycles. A model without rider freedom was also compared but in general there was better agreement of the full model with the experiments, even though it predicted the weave mode with a discontinuity in a vehicle speed range between 40–60 km/h which was not observed in practice. The discontinuity was attributed to interference between the weave mode and rider lean mode which had similar frequencies at those speeds. The effect of individual rider parameters on stability were also investigated analytically and it was found that mass, moment of inertia and longitudinal location of rider's mass centre have a large influence on wobble and weave, while the rigidity, damping and height of the mass centre of the upper body influence weave mode and rigidity and damping of lower body influence wobble mode.

(Hasegawa, 1985) used partially reconstructed motorcycles that were able to develop weave instabilities at practical speed ranges and measured weave responses at high speeds. He compared the measurements with calculated results via an extensive motorcycle model and found good agreement. Meanwhile, (Bridges and Russell, 1987) used a scale model with rider and topbox in wind tunnel tests and demonstrated a regularity of vortex shedding in the wake of a topbox. Interpreted at full scale, and using theoretical model calculations, the aerodynamic forcing frequency was shown to coincide with the wobble mode frequency at a moderate road speed, clearly suggesting a possibility of coupling between the two mechanisms. Sensitivity of the straight running weave mode damping to variations in motorcycle design parameters were determined experimentally by (Bayer, 1988). Amongst others, stiff frames, a long wheelbase, a long trail and a flat steering head angle were found to increase weave mode damping.

(Katayama *et al.*, 1988) employed a motorcycle model with a rider model similar to that in (Nishimi *et al.*, 1985), in order to investigate which aspects of rider actions are important in the description of real behaviour. The rider model in this case included a lower body free

to lean relative to the frame instead of moving laterally, also considering rider control actions by steering torque and upper and lower body lean torques linearly related to roll angle and to a heading error from a desired path. Simulations were obtained for single lane change manoeuvres and were compared with the responses from real experiments with various riders. The results suggested that the major source of control is steering torque, while it is possible to control the motorcycle with lower body lean movement but much larger torques are required in that case. Normally, lower body control is utilised to assist steering torque control, and the upper body is controlled only to keep the rider in the comfortable upright position.

Consolidating on previous work, (Sharp, 1994*b*) developed a motorcycle model for straight running studies with design parameters and tyre properties obtained from laboratory experiments. The main constituents of this model were as in (Sharp, 1971) with the addition of lateral and twist frame flexibilities at the steering head, flexibility of the rear wheel assembly about an inclined hinge, roll freedom of the rider upper body, in-plane aerodynamic effects, and more elaborate tyre model. The tyre model was described by lagged side-slip generated side forces and aligning moments, and instantaneous side forces, aligning moments and overturning moments in response to camber angle. The outputs of the tyre model were related to the inputs in a linear fashion, consistent with small perturbations from straight running, and the constants of proportionality were dependent on tyre load. The overturning moment was obtained by virtue of replacement of the normal load applied at the real contact point of the rolling tyre, with a force and a moment that are applied on the theoretical contact point of an infinitely thin tyre. More detailed aspects of the tyre behaviour, such as turn-slip effects, tyre tread width effects and tread band mass effects, were known from previous work (Sharp and Alstead, 1980) to be small and were therefore neglected here. Sharp used his model to convey the sensitivity in stability from various design parameters displaying results of changes in the eigenvalue real parts corresponding to 10% increases in parameter values, at those speeds that the calculated root-loci exposed critical behaviour. “Hands-on” and ”hands-off” cases were presented, the difference between them being merely the amount of steering stiffness and damping, and moment of inertia of the front frame. His results were in agreement with empirical observations and with the main experimental findings of (Bayer, 1988), showing the advantage to the weave mode damping from a long wheelbase and a large steering head angle.

(Imaizumi *et al.*, 1996) introduced a very complex rider model that consisted of twelve rigid bodies, representing the arms, the trunk, the legs, etc. of the rider with appropriate mass and inertia properties. Linear springs and dampers with appropriate coefficient values were assumed to exist in the joints between the various parts, and rider motions such as steering, leaning of the body, pitching of the body, weight shift and knee grip were possible. Rider actions associated with these freedoms were also possible and were applied via proportional control elements.

(Ishii and Tezuka, 1997) investigated the handling performance of motorcycles with respect to the tyre properties. Steady state tyre side forces and aligning moments for a range of camber angles and side-slip angles were obtained for a front and a rear tyre via a flat plank tyre tester, and used with a motorcycle model to calculate steady cornering responses. The same manoeuvres

were executed experimentally and compared. Good agreement was obtained but only in steady state values. It was emphasised that care should be taken in estimating the side-slip angle from the experiments as this was small, and a method for doing so was demonstrated. The measured side-slip angle as a function of lateral acceleration was compared with the same angle from simulations and at least qualitative agreement was obtained. Other variables such as steer torque were also shown to follow to some extent the experimental measurements. As a final remark Ishii and Tezuka pointed out that both the aligning moment and side force, and therefore the tyre properties, are likely to be connected to the handling properties of the vehicle (steer torque, steer angle), which is not surprising at all.

Special attention was given to the front fork suspension in (Kamioka *et al.*, 1997) with respect to riding qualities of the motorcycle. A typical suspension unit was modelled on the basis of the inner structure and internal operation giving rise to spring forces, viscous damping forces, friction forces and oil lock forces. Sine wave excitation, and constant velocity in compression excitation experiments found the model to represent the unit relatively accurately. Further experiments were conducted, this time to check the validity of the combined fork unit model together with a simplified motorcycle model that involved only vertical and longitudinal dynamics, and the results over bumps and under braking agreed with measurements. Subsequently, the influence of the suspension characteristics on riding qualities of the vehicle was found by simulation and experiments verified the findings. Meanwhile, (Imaizumi and Fujioka, 1998) looked at the influence on system stability of rear load (top-box) mounts of different stiffnesses. The rear load assemblies considered were composed of the rigidly attached base, the load and the suspension mechanism. Two types of mechanism were used, the first being guide roller bearings with spring and damper allowing movement only laterally, and the second being vibration isolation rubbers at various points in the plane between the base and the load. Simulation and experiments were conducted at various speeds at hands off conditions with the rider applying a steering torque impulse to initiate oscillations, and in both cases it was shown that rear load assemblies with appropriate stiffness and damping were successful in damping out weave and wobble oscillations.

Diverting the attention to tyres, it can be seen that a considerable number of tyre models that describe steady state tyre forces and moments had been available up to that time. These are roughly divided into three categories: 1) physically founded models which require computation for their solution, such as the multi-radial-spoke model developed by (Sharp and El-Nashar, 1986; Sharp, 1991) 2) physically based models which are simplified sufficiently to allow analytical solution, such as the brush model described in (Fujioka and Goda, 1995*a*,*b*) and 3) formula based empirical models as described in (Bakker *et al.*, 1989; Pacejka and Bakker, 1991; Pacejka and Besselink, 1997). The principle on which the physical models are based is that of viewing the tyre as consisting of independent structural elements that can flex and compress when loaded, reminiscent of the bristles in a brush. It is also possible for the empirical models to contain physically based judgements. The first two models will not be described any further and the interested reader is referred to (Pacejka and Sharp, 1991) for a review on these issues. The third category consists of the so called “Magic Formula” model that became known for its ability

to match real tyre behaviour closely. It describes the steady state longitudinal force, side force, aligning moment and possibly overturning moment as functions of longitudinal slip, side-slip, camber angle and normal load, with constraints on the parameters to prevent the behaviour from becoming unrealistic in any operating condition. The context in which it was developed represented the car tyre behaviour where side-slip is the dominant input. Realising that there was a deficiency for motorcycles, where large camber angles are common, (de Vries and Pacejka, 1997) improved the original set of equations to make them suitable for the motorcycle case.

De Vries and Pacejka performed a series of measurements on public roads using a tyre test trailer, and acquired steady state forces and moments for front and rear tyres under a range of side-slip angles, camber angles and normal loads. The data were used for parameter identification, with a parallel aim of physically correct representations outside the measured data range. Plots that show accurate fits were presented although no magic formula parameter values were disclosed. At the same time effort was put in the investigation of the dynamic behaviour of the tyres via laboratory tests with pendulum and yaw oscillation test rigs. Two different dynamic models were considered in order to process the results, a first order relaxation model consistent with 'taut string' theory, and a rigid ring model. Cornering stiffnesses and relaxation lengths for small oscillations were identified via the first order relaxation model from frequency response data at various operating conditions of camber angle, normal load and forward speed, showing the relaxation length to be roughly the ratio of cornering stiffness and effective lateral stiffness of the tyre. A further indication from the identification procedure was that the relaxation length grows as the speed increases, to a significant degree at high speeds, and this was attributed to the inability of the first order model to deal with the gyroscopic effects of the tyre belt. In the more complex rigid ring model, the tyre belt with mass and inertia properties is considered to be elastically suspended from the rim thus representing a flexible carcass. This model (the rigid ring) was found to describe very accurately the tyre response through a greater range of frequencies than for the relaxation model, using only velocity independent tyre parameters. In (de Vries and Pacejka, 1998) a conventional fixed relaxation length tyre, applied with a simple motorcycle model, was claimed to be more physically consistent than the velocity dependent relaxation length model due to its similar predictions with the rigid ring model with respect to the damping of the high speed weave. The use of the variable relaxation length tyre model was leading to unstable weave predictions at high speeds unlike the other two. The magic formula equations were further improved in (Tezuka *et al.*, 2001) and (Pacejka, 2002) for motorcycle tyres.

(Cossalter *et al.*, 1999*a*) used a simple mathematical model of a motorcycle under steady cornering to evaluate those factors that influence the steering torque, relating to vehicle manoeuvrability. The tyre was modelled as having thickness and therefore correct representation of the lateral movement of the contact point was achieved. Lateral and longitudinal forces, and rolling resistance, aligning and twisting moments were assumed to appear in response to side-slip, longitudinal slip, and roll angle. Solutions were obtained for the steady cornering algebraic equation, and it was shown that the steering torque comprises at least seven components. Significant terms arise from mass, inertia, tyre force, tyre moment and gyroscopic properties at the

front of the vehicle, which vary in their relative influence with speed. Meanwhile, (Cossalter *et al.*, 1999*b*) introduced a new approach for the evaluation of vehicle handling and manoeuvrability, which uses optimal control methods to obtain the maximum distance manoeuvre a vehicle can execute given certain time, initial condition and path criteria.

By this time, stimulated by advances in computer power and technology, and the immense effort required to derive equations of motion by hand analysis for multibody systems other than very simple ones, several computer packages for assisted mechanical modelling had made their appearance over the preceding few years. These can in principle be separated in two categories, numerical or symbolic. Numerical codes prepare and solve equations in number form only, and post-process the results to give outputs in graph form or as animations. Symbolic codes derive equations of motion using symbols instead of numbers, similar to the approach of a human analyst, and naturally they require number substitution and further processing before any meaningful output can be obtained (linear analysis, time histories via numerical integration, etc.). Although symbolic equations are more difficult to obtain than numerical ones, once obtained for a particular system, they never need generating again, and naturally they are better suited for real time simulations that require fast code execution. Some of the commercially available numerical software are ADAMS and DADS, and symbolic AUTOLEV, AUTOSIM, MESA-VERDE, NEWEUL and SD/FAST. A review on the application of multi-body computer codes to road vehicle dynamics modelling problems is given in (Sharp, 1994*a*).

AUTOSIM is the modelling package used in this thesis and therefore it deserves further attention. It is a symbolic code generation language that was built on top of the standardised artificial intelligence language COMMON LISP (Steele and Guy, 1984), utilising many of the nice features of that language such as its extensibility and symbol manipulation capabilities (Sayers, 1991*a*). A tree topology multibody formalism was originally employed (Sayers, 1991*b*), based on the approach of (Kane and Levinson, 1983, 1985), which is an alternative statement of the Newton-Euler-Jourdain (virtual power) principle. It has been proven that with this method less operations are needed to derive equations of motion (Kane and Levinson, 1983), compared with the well known Lagrange's energy-based method, that can only accommodate holonomic constraints and introduces many cancelling terms in the computations. The rule based procedure for formulating the equations includes the sort of judgements a human analyst makes in formulating equations of motion, with rules to determine definitions for generalised coordinates and speeds (speeds not always arising from time derivatives of generalised coordinates) and a minimal equation set in generalised coordinates is constructed. Further techniques that lead to economy without inaccuracy are pursued and consequently lead to highly efficient computer code. The input from the dynamicist is in the form of a high-level language (Anon., 1998). The output is in the form of a low-level computer language code, such as FORTRAN, C, Simulink C (CMEX), ready to compile and solve the equations to obtain motion time histories, or a MATLAB M-file that contains symbolic state-space A, B, C, D matrices for linear analysis.

Acknowledging the necessity for automated methods in multibody building exercises, (Sharp and Limebeer, 2001) set out to confirm and extend the most elaborate hand derived motorcycle

model of the time using such methodologies. The modelling tool used was AUTOSIM and the target model was the one described by (Koenen, 1983). Koenen's model was reproduced as accurately as possible, using where possible the same parameter values, and straight running and steady cornering root-loci in the same fashion Koenen had presented were calculated and presented, with generally similar but not the same predictions. The high level of complexity of the model was apparent from this study, and the need for computer assisted methods for the analysis of such models was demonstrated. One of the original aims of Sharp and Limebeer was to investigate the apparent conflict with experimental evidence (Jennings, 1974; Weir and Zellner, 1979) and anecdotal evidence, in Koenen's prediction of the negligible influence of suspension damping on the stability of cornering weave. The cornering root-loci with rear suspension damping varied were reproduced and the damping was found to have a significant influence, indicating a possible error in Koenen's calculations. (Sharp, 2000) extended further the previous model to include a practically feasible variable geometry active rear suspension, and demonstrated the possibility of cornering weave stabilisation by this system, through employment of a speed adaptive control law.

Conclusions

The main mode of operation of a motorcycle is in free control, associated with the free steering system. Alternatively the rider can exercise fixed control, but under such circumstances the vehicle is unstable in roll at all speeds and therefore this method is not preferred. There are many influences on the self steering action, all of which can be observed and quantified when considering a vehicle under non-zero roll angle. Contributions are connected strongly to the design detail of the steering system and mainly arise from mass, inertia, tyre force, tyre moment and gyroscopic properties at the front of the vehicle, their relative importance being dependent on speed. It is also true that some have a stabilising and others destabilising nature, but in general the vehicle is able to self stabilise without too much effort from the rider. Nevertheless, the self-steering capability of the motorcycle inevitably leads to oscillatory behaviour, and it is a requirement that any motorcycle can self-stabilise effectively, without becoming too oscillatory under any circumstances.

In straight running, the most obvious instability is the capsizing of the whole vehicle at low speeds, where it essentially behaves as an inverted pendulum about to fall over. Strictly speaking the instability is slightly more complicated than this, and it involves contributions both from the capsizing of the whole vehicle and the divergence of the steering system to the side. In mathematical terms these start as two real modes with positive eigenvalues at very low speeds that coalesce, when the speed is increased, to form a complex conjugate pair with a positive real part. At this point weave starts to form and at around 8 m/s is stabilised and has a frequency of about 0.7 Hz as shown in the left root-locus plot in Figure 2.1. This mode involves movement of the whole vehicle-rider system with almost equal contributions from yaw and roll freedoms, and less from steer, with specific phase angle differences between them. With further speed increase

the damping of the weave mode is increased until about 20 m/s and subsequently it begins to decrease, becoming lightly damped at high speeds. The frequency increases monotonically with speed reaching a value of about 3.5 Hz at high speeds. There are several parameters that could change the stability properties of this mode and these have been studied in the literature.

Under straight running conditions there is a possibility for another higher frequency lightly damped mode to appear, usually called wobble mode. It is mainly seen as relative motion between the fork assembly and the main frame of the motorcycle. The resonant frequency of this mode (6–9 Hz) is relatively unaffected by speed variations and is mainly set by the inertia of the steering assembly about the steer axis, the mechanical trail and the front tyre cornering stiffness. The damping depends strongly on the torsional flexibility in the steering head region, with less stiff frames resulting in lightly damped conditions at moderate speeds, as shown in Figure 2.1. The damping can also be altered by steering dampers and the nature of the rider's grip on the handle bars, and together with the limited road speed, this phenomenon becomes an annoyance rather than a hazard. There is also a possibility of resonant forcing of the lightly damped motion via imperfections in the tyre or wheel assembly. Anecdotal evidence suggests that wobble oscillations can appear at much higher speeds, possibly associated with stiffer frames, and an unusually large disturbance may be necessary to initiate the problem. This behaviour could lead to large oscillations, eventually causing the handlebars to hit the steering lock stops. The severity of this problem is clear, and it is believed that the presence of steering friction might have something to do with it, but obviously a better understanding of this behaviour is required.

In-plane modes present in straight running conditions are shown in Figure 2.1. These are associated with the suspension, and tyre flexibility freedoms, referred as front suspension pitch, rear suspension pitch, front wheel hop etc. They are insensitive to speed variations and are decoupled from the out-of plane modes described above.

The cornering situation is considerably more complicated. Steady state configurations require fixed values for forward speed, lateral acceleration, roll angle, yaw rate and tyre side forces. These can be found by solving the non-linear algebraic equations of the equilibrium condition. The linear stability analysis involves small perturbations about the cornering trim condition, and the corresponding state variable values are required in the calculation of the linear analysis coefficients.

The in-plane and out-of-plane modes become coupled under cornering and this cross-coupling increases with roll angle. As a consequence several modes join together to form combined modes with particular characteristics as shown in the right root-locus plot in Figure 2.1. Cornering weave is similar in frequency to straight running weave at high speeds, with decreasing damping as the lean angle increases, but now there is systematic involvement from the suspension system in the oscillations. This has been observed experimentally and the influence of suspension damping on this mode has been demonstrated both analytically and experimentally. Wobble possibly involves some suspension motions as well, and the previously speed independent suspension pitch and wheel hop modes now vary considerably with speed. A combination of front wheel hop with wobble could occur when the two modes are close enough to join, and

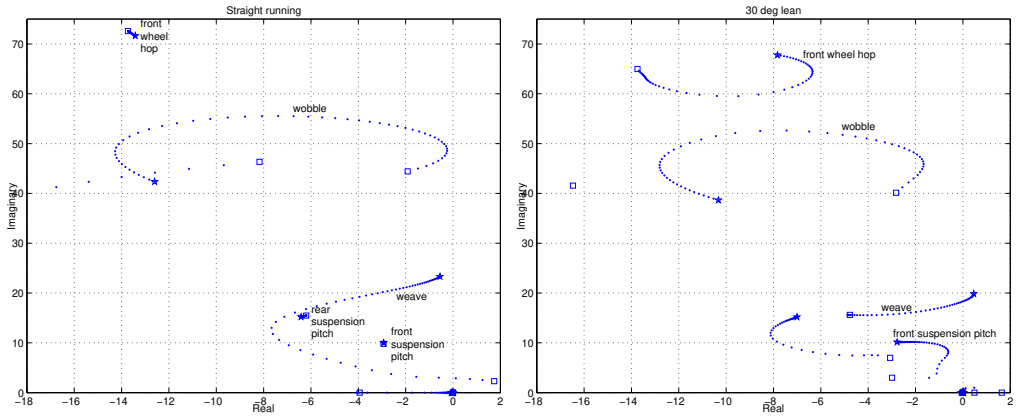

Figure 2.1: Straight running root-locus (left) and 30 deg roll angle root-locus (right) with speed the varied parameter. The speed is increased from 5 m/s (□) (left), 6 m/s (□) (right) to 60 m/s (⋆).

this mode is possibly linked to patter, mainly known from anecdotal evidence at this point. The coupling of the in-plane and out-of-plane motions also suggests that there is a possibility for road excitation signals to be transmitted into the lateral motions of the vehicle, causing steering oscillations by road profiling under cornering.

The rider has effect on the motorcycle in two ways, firstly, as a structural part, adding to the mass and inertia of the vehicle-rider system, and secondly as a controller. The control position the rider takes depends strongly on the open loop dynamics of the vehicle discussed above. It seems likely that the rider stabilises the roll response to permit good path following and performance to occur, and that the weave mode can be influenced by rider control under some conditions, with the possibility of destabilising effects from some stabilisation and path following control actions. The frequency of the wobble mode is well beyond the rider's capability to supply control, but yet it can be influenced by the damping provided from the rider holding the handlebars. The rider employs various forms of control activity such as feedback, in which he operates on perceived errors between actual and desired motorcycle response, and preview, whereby he uses knowledge of the system future output to structure feedforward controls that enable that output to occur. Preview operation is fundamental to the guidance control to allow path following and feedback control can function in parallel to regulate the motion about the nominal path in response to random external disturbances. The rider uses motion and visual feedbacks to evaluate his condition in order to close the loop and apply one of the available control actions, which are steer torque, steer angle, rider lean, rider weight shifting laterally, and with better skilled riders throttle (engine torque) control. Steer torque to roll feedback is by far the most influential way to control the vehicle even for non-experienced riders, with also the possibility of rider lean angle to yaw rate or roll angle feedback being used for lighter motorcycles, mainly in parallel with steer torque.

The complexity involved in cornering motorcycle studies has been shown, and the necessity

of automated methods in the analysis of such systems has been demonstrated. Several multibody modelling tools exist which are capable of fulfilling this task. These can be employed in order to further advance knowledge and understanding of the subject.

Part II

Motorcycle Models

The use of automated methods for generating equations of motion and for the analysis of motorcycle dynamics is demonstrated in the following chapters. The multibody platform used is AUTOSIM. Three different motorcycle models are presented in order of complexity, one in each of the next three chapters. The first two models are reproductions of hand-derived models (Sharp, 1971, 1994*b*) and are presented in detail in a tutorial fashion in Chapters 3 and 4 respectively. This work is based on internal reports (Evangelou and Limebeer, 2000*a*,*b*). The third model is based on previous work by (Sharp and Limebeer, 2001) and an overview of that work is given in Chapter 5 together with some improvements. In Chapter 6 animation methods of the same model are presented, based on an internal report (Evangelou and Limebeer, 2001). All the computer files that will be mentioned are available for download from the website http://www.ee.ic.ac.uk/control/motorcycles/ and the various AUTOSIM commands used are explained in Appendix B. For further help with AUTOSIM the reference manual (Anon., 1998) can be consulted.

Chapter 3

The Sharp 1971 motorcycle model

3.1 Physical description of the model

The following assumptions are made regarding the representation of the vehicle (Sharp, 1971):

1. The vehicle consists of two rigid frames that are joined together via a conventional steering mechanism. This steering freedom is constrained by a linear steering damper.
2. The front frame consists of the front wheel, forks, handlebars and fittings.
3. The rear frame consists of the main structure, the engine-gearbox assembly, the petrol tank, seat, rear swinging arm, the rear wheel and a rigidly attached rider.
4. Each frame has a longitudinal plane of symmetry and the axis through the front frame mass centre parallel to the steering axis is a principal axis.
5. The road wheels are rigid discs each of which makes point contact with the road. They roll without longitudinal slip on a flat level road surface.
6. The axis of rotation of the engine flywheel is transverse.
7. The machine moves at constant forward speed with freedom to side slip, yaw, and roll; only small perturbations from straight running are considered.
8. The air through which the machine moves is stationary and the effects of aerodynamic side forces, yawing moments and rolling moments will be small compared with the tyre effects and are therefore neglected. The effects of drag, lift and pitching moment are to modify the vertical loading of the tyres and to make necessary a longitudinal force at the driving wheel sufficient to maintain the assumed constant forward speed. These effects are accounted for by variations in the coefficients relating tyre side forces to side-slip and camber angles.
9. Pneumatic trail of the tyres is not considered since, for the rear tyre, its effect will be very small, and for the front tyre it is small compared with the mechanical trail.

10. The drag force at the front tyre is small compared with the tyre side forces.

The motorcycle is represented diagrammatically in Figure 3.1 (Sharp, 1971):

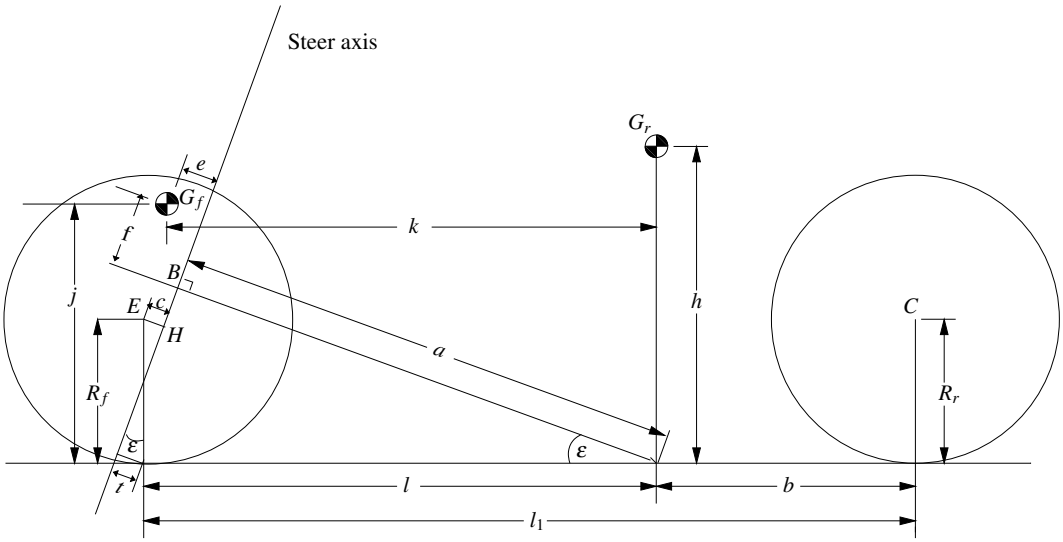

Figure 3.1: Diagrammatic representation of the motorcycle

3.2 Programming of the model

3.2.1 Body structure diagram

The multi-body system in Figure 3.1 is subdivided into its constituent bodies for the purpose of writing the AUTOSIM code. The bodies are arranged in a parent-child relationship as shown in Figure 3.2. The first body is the *Inertial Frame* and it has the *Yaw Frame* as its only child. The *Yaw Frame* has the *Inertial frame* as its parent and the *Rear Frame* as its only child. The *Rear Frame* has the *Yaw Frame* as its parent and the *Rear Wheel* and *Front Frame* as its children. The *Front Frame* has the *Front Wheel* as its only child. The road wheels have no children.

3.2.2 Program code

The same AUTOSIM code is used to generate the nonlinear and linearised models. The linear and nonlinear parts of the code are separated using a "linear" flag and the Lisp macros `unless` and `when`. The flag called `*linear*` is set to be true (`t`) or false (`nil`) at the beginning of the code thereby separating the linear and nonlinear parts of the code. The nonlinear part of the AUTOSIM code is then used to generate the FORTRAN file that is used to solve the nonlinear equations of motion, and the linear part is used to generate the symbolic representation of the linearised system matrices which are used to obtain root-locus plots.

AUTOSIM commands are used to describe the components of the motorcycle multi-body system in their parent-child relationship. The programming details are described next:

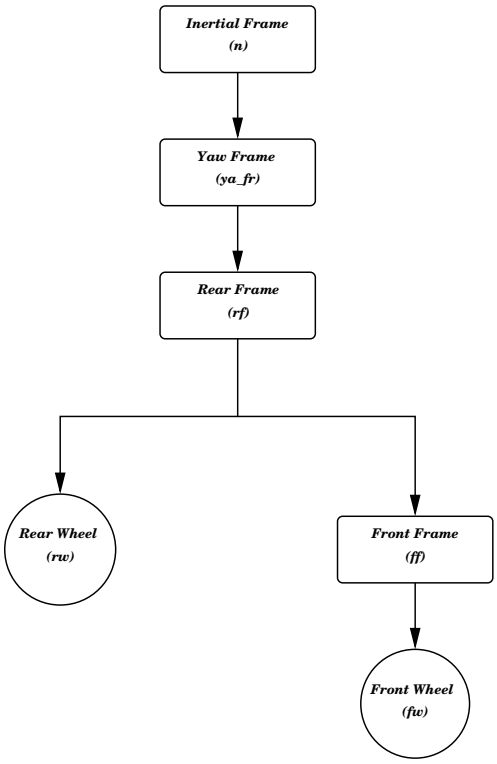

Figure 3.2: Body Structure Diagram of the motorcycle

- Set the flag for linear or nonlinear:

```
(defvar *linear*)
(setf *linear* t)
```

- A few preliminaries:

```
(reset)
(si)
(add-gravity)

(unless *linear* (setsym *multibody-system-name* "bk_71_ns"))
(when *linear* (setsym *multibody-system-name* "bk_71_ls"))
(setsym *double-precision* t)
```

The `reset` line sets various global variables used by AUTOSIM to store equations to their default values, `si` sets the units system to SI and `add-gravity` sets up a uniform gravitational field in the z-direction of the inertial frame. The next two lines name the system as `bk_71_ns` if the `*linear*` flag is set to `nil` and as `bk_71_ls` if the `*linear*` flag is set to `t`. The last line sets the `*double-precision*` variable to true so that all the FORTRAN floating-point declarations are made in double-precision.

- Various points in the motorcycle nominal configuration within the coordinate system of body *n* are defined:

```
(add-point Gr        :name "Rear frame centre of mass"
                     :body n :coordinates (0 0 -h))
(add-point rw_centre :name "Rear wheel centre point"
                     :body n :coordinates (-bb 0 -Rr))
(add-point ff_joint  :name "Front frame joint point with rear frame"
                     :body n :coordinates ("aa*cos(epsilon)"
                      0 "-aa*sin(epsilon)"))
(add-point Gf        :name "Front frame centre of mass"
                     :body n :coordinates (kk 0 -jj))
(add-point fw_centre :name "Front wheel centre point"
                     :body n :coordinates (ll 0 -Rf))
(add-point rwcpn     :name "Rear wheel ground contact point in n"
                     :body n :coordinates (-bb 0 0))
(add-point fwcpn     :name "Front wheel ground contact point in n"
                     :body n :coordinates (ll 0 0))
```

  Body *n* is the *Inertial Frame* in which all of the above points are defined. The coordinate system used to define the points is that associated with body *n*. The nominal configuration of the motorcycle is the upright position with zero roll, yaw and steer angles and with zero forward speed. In the above, it is usual to use "bb" to represent the distance "b" in Figure 3.1 and so on. The reason for this is that t, g etc. are reserved variables required by AUTOSIM; t is time and g is gravitational acceleration constant.

- The rear frame is built into the model next:

```
(add-body ya_fr :name "Yaw Frame"  :parent n
            :translate (x y)  :joint-coordinates (0 0 0)
            :body-rotation-axes z  :parent-rotation-axis z
            :reference-axis x  :mass 0
            :inertia-matrix 0)

(add-speed-constraint "tu(ya_fr,1) - vu" :u "tu(ya_fr,1)")

(add-body rf :name "Rear Frame"
             :parent ya_fr
             :body-rotation-axes x  :parent-rotation-axis x
             :reference-axis y  :cm-coordinates Gr
             :mass Mr
             :inertia-matrix ((Irx 0 Crxz)
                              (0 Iry 0)
                             (Crxz 0 Irz)))
```

This is done in two steps. Firstly, the *Yaw Frame* is introduced as a massless body with translational degrees of freedom along the x and y directions of body n (it is a child of n). The *Yaw Frame* has a further rotational degree of freedom in the z direction that describes the yawing motion of the motorcycle. The second body is the child of the *Yaw Frame* and is called the *Rear Frame*. This body possesses the mass and moments of inertia of the whole rear frame assembly and also a rotational degree of freedom in the x-direction of the *Yaw Frame* which is used to describe the rolling motion of the motorcycle. The `add-speed-constraint` command constrains the forward velocity of the *Yaw Frame*, and therefore of the motorcycle, to be equal to `vu`, which is the forward speed parameter defined at the end of the program.

- Add in the rear wheel:

```
(add-body rw :name "Rear Wheel"
             :parent rf
             :body-rotation-axes y
             :parent-rotation-axis y
             :reference-axis z
             :joint-coordinates rw_centre
             :mass 0
             :inertia-matrix (irwx irwy irwx))
```

The *Rear Wheel* is a child of the *Rear Frame*. Its mass is set to zero, because it is included in the mass of the *Rear Frame*, but its inertia matrix is inserted here. The `:joint-coordinates rw_centre` command line defines the coordinates of the joint of the rear wheel and the rear frame using the coordinates of a point defined above in n.

- Introduce an unspun ground contact point for the *Rear Wheel*:

```
(add-point rwcp :name "Rear wheel contact point"
                :body rf :coordinates rwcpn)
```

This point is fixed in the *Rear Frame*. It is introduced to assist with the calculation of the `vur` variable and the rear wheel side-slip angle.

- Define the velocity component of `rwcp` along the line of intersection of the *Rear Wheel* plane and the ground plane. This will be used to compute the angular velocity of the *Rear Wheel*:

```
(setsym vur "dot(vel(rwcp),[ya_frx])")
```

- Assume no longitudinal slip for the *Rear Wheel*:

```
(add-speed-constraint "ru(rw)*Rr + @vur" :u "ru(rw)")
```

The rotational speed of the *Rear Wheel* is constrained to be `-vur/Rr` which means that the wheel is not allowed to slip longitudinally. The effect of this (nonholonomic) constraint is to remove the rotational speed of the rear wheel as a freedom from the equations of motion.

- Define the steering and reference axis for the *Front Frame*:

```
(setsym steer_axis "sin(epsilon)*[rfx] + cos(epsilon)*[rfz]")
(setsym fw_reference "cos(epsilon)*[rfx] - sin(epsilon)*[rfz]")
```

These two axes are defined to assist the addition of the front frame assembly.

- Add in the *Front Frame*:

```
(add-body ff :name "Front Frame"
             :parent rf
             :body-rotation-axes z
             :parent-rotation-axis @steer_axis
             :reference-axis @fw_reference
             :joint-coordinates ff_joint
             :cm-coordinates Gf
             :mass Mf
             :inertia-matrix (Ifx Ify Ifz))
```

The *Front Frame* is a child of the *Rear Frame*. It has one degree of freedom, that is a steering freedom about the steering axis (`steer_axis`). The reference axis (`fw_reference`) is used to define the nominal configuration of the *Front Frame*.

- Add in the *Front Wheel*:

```
(add-body fw :name "Front Wheel"
             :parent ff
             :body-rotation-axes y
             :parent-rotation-axis y
             :reference-axis z
             :joint-coordinates fw_centre
             :mass 0
             :inertia-matrix (ifwx ifwy ifwx))
```

This body has the *Front Frame* as parent. Its mass is zero since this has been included in the mass of the *Front Frame*, but its moments of inertia are not and so they are inserted here.

- Introduce an unspun ground contact point for the *Front Wheel*:

```
(add-point fwcp :name "Front wheel contact point"
                :body ff :coordinates fwcpn)
```

This point is fixed in the *Front Frame*. It is introduced to assist with the calculation of the `vuf` variable and the *Front Wheel* side-slip angle.

- Define the velocity component of `fwcp` along the line of intersection of the *Front Wheel* plane and the ground plane:

```
(setsym fw_lat "dir(dplane([ffy],[nz]))")
(setsym fw_long "cross(@fw_lat,[nz])")
(setsym vuf "dot(vel(fwcp),@fw_long)")
```

  The second line, which makes use of the first, defines the direction of the line of intersection of the *Front Wheel* plane and the ground plane. The last line finds the velocity component of `fwcp` in the direction of `fw_long`.

- No longitudinal slip on the *Front Wheel*:

```
(add-speed-constraint "ru(fw)*Rf + @vuf" :u "ru(fw)")
```

  As with the *Rear Wheel*, it is assumed that the *Front Wheel* undergoes no longitudinal slip. Consequently, its angular velocity is set to `-vuf/Rf` and the rotational speed of this wheel as a freedom is eliminated from the equations of motion by AUTOSIM.

- Define the camber and side-slip angles:

```
(setsym phir "asin(dot([nz],[rfy]))")

(setsym phif "asin(dot([nz],[ffy]))")

(setsym alphar "asin(dot([ya_fry],dir(vel(rwcp))))")

(setsym alphaf "asin(dot(@fw_lat,dir(vel(fwcp))))")
```

  These angles are needed in the calculation of the side forces. The first line defines the *Rear Wheel* camber angle, the second line defines the *Front Wheel* camber angle and the third line defines the *Rear Wheel* side-slip angle by making use of the point `rwcp` defined above. The last line defines the *Front Wheel* side-slip angle via the point `fwcp`. Note that for the side-slip angles, positive lateral velocities give positive slip values and negative forces. As a consequence the signs of the side-slip angles in the side force expressions below are opposite to those in the original paper (Sharp, 1971).

- Introduce a steering head damping torque:

```
(add-moment sd :name "Steering Damping"
               :body1 ff :body2 rf
               :direction [ffz]
               :magnitude "-K*ru(ff)+st_tq")
```

This torque acts on the *Front Frame* with a positive magnitude and on the *Rear Frame* with negative magnitude in the z-direction of the *Front Frame*. Its magnitude is proportional to the rotation speed of the *Front Frame* relative to the *Rear Frame*. There is also a contribution from the rider (`st_tq`) which defaults to zero.

- Work out the tyre side forces and introduce a simple tyre relaxation model:

```
(add-state-variable Yr Yr_dot F)
(set-aux-state-deriv Yr_dot "(@vur/sigmar)*(-Cr1*@alphar+Cr2*@phir-Yr)")

(add-state-variable Yf Yf_dot F)
(set-aux-state-deriv Yf_dot "(@vuf/sigmaf)*(-Cf1*@alphaf+Cf2*@phif-Yf)")
```

The `add-state-variable` commands introduce two state variables, one for each of the two force expressions, that are used to describe the tyre relaxation property. The force equations are defined with the `set-aux-state-deriv` and use the values of the side-slip and camber angles defined above; the `set-aux-state-deriv` complements the `add-equation` command in earlier versions of AUTOSIM, overcoming a difficulty arising previously with added variables in forming the linear model. Notice the minus sign on the `Cr1*@alphar` and `Cf1*@alphaf` terms.

- Introduce the tyre side forces:

```
(add-line-force Yr2 :name "Rear Wheel Lateral Tyre Force"
                    :direction [ya_fry]
                    :point1 rwcp
                    :magnitude Yr)

(add-line-force Yf2 :name "Front Wheel Lateral Tyre Force"
                    :direction @fw_lat
                    :point1 fwcp
                    :magnitude Yf)
```

The direction of the two tyre side forces is in the ground plane and normal to the line of intersection of the ground plane and the wheel plane.

- Incorporate the normal tyre loads:

```
(setsym ground_vector "pos(fwcpn,rwcpn)")
(setsym Gr_vector     "pos(Gr,rwcpn)")
(setsym Gf_vector     "pos(Gf,rwcpn)")


(setsym Zf "-G*(Mf*dot(@Gf_vector,[nx])+Mr*dot(@Gr_vector,[nx]))
            /dot(@ground_vector,[nx])")
```

```
(add-line-force Zff :name "Vertical load on front wheel"
                    :direction [nz]
                    :point1 fwcp
                    :magnitude @Zf)
```

The first three lines define three vectors from the rear wheel ground contact point to three points in the nominal configuration. These points are the front wheel ground contact point, the rear frame centre of gravity and the front frame centre of gravity respectively. The next line calculates the magnitude of the normal force on the front wheel by projecting the three vectors onto the ground plane in the nominal configuration and taking moments about the rear wheel contact point. The `add-line-force` command introduces the normal force into the vehicle equations of motion. Note that only the front force is influential since the system has no heave freedom in body *n* and therefore the rear force is omitted.

- Derive the equations of motion of the system or the linearised equations:

```
(unless *linear* (dynamics))
(when *linear*
(add-variables dyvars real st_tq)
(linear :u st_tq)
)
```

If the `*linear*` flag is set to `nil` the full equations of motion are derived. Alternatively if the flag is set to `t` the linearised equations are derived with `st_tq` as the input. `st_tq` is defined as a real variable that is used as a steering torque input from the rider, and therefore the corresponding B-Matrix is also computed in the linearised equations.

- All the motorcycle parameters are introduced with their names and default values[1]:

```
;;Default values for masses
(set-names    Mf   "Mass of front frame"
              Mr   "Mass of rear frame")
(set-defaults Mf 30.6472 Mr 217.4492)

;;Default values for moments of inertia
(set-names    Ifx  "front frame inertia w.r.t. OX4 about mass centre"
              Ify  "front frame inertia w.r.t. OY4 about mass centre"
              Ifz  "front frame inertia w.r.t. OZ4 about mass centre"
              Irx  "rear frame inertia w.r.t. OX2 about mass centre"
              Iry  "rear frame inertia w.r.t. OY2 about mass centre"
```

[1] As can be seen from the sign of `Crxz`, AUTOSIM uses the opposite sign convention for products of inertia ($-\sum m_i x_i z_i$) as compared with (Sharp, 1971) ($\sum m_i x_i z_i$).

```
              Irz  "rear frame inertia w.r.t. OZ2 about mass centre"
              Crxz "rear frame inertia product w.r.t. mass centre"
              ifwx "front wheel camber inertia"
              ifwy "front wheel polar moment of inertia"
              irwx "rear wheel camber inertia"
              irwy "rear wheel polar inertia")
(set-defaults Ifx 1.2338 Ify 0 Ifz 0.4420 Irx 31.1838 Iry 0 Irz
              21.0694 Crxz -1.7354 ifwx 0 ifwy 0.7186 irwx 0 irwy 1.0508)

;;Geometric parameters
(set-names Rr    "Rear wheel radius"
           Rf    "Front wheel radius")
(set-defaults aa .9485 bb .4798  h 0.615696 Rf 0.30480 Rr 0.30480
              epsilon 471.5e-3 jj 0.46716 kk 0.853855 ll 0.934658)

;;Tyre parameters
(set-names    sigmar "rear tyre relaxation length"
              sigmaf "front tyre relaxation length"
              Cf1    "front tyre cornering stiffness"
              Cf2    "front tyre camber stiffness"
              Cr1    "rear tyre cornering stiffness"
              Cr2    "rear tyre camber stiffness")
(set-defaults sigmar 0.24384 sigmaf 0.24 Cf1 11174.38 Cf2 938.6124 Cr1
              15831.8556 Cr2 1326.6232)

;;Other parameters
(set-names    K "steering damping coefficient")
(set-defaults K 6.78 vu 6.1538)
(unless *linear* (set-defaults iprint 1 stopt 50 step 0.01 "rq(rf)"
                               0.005 epsdi 1e-7 st_tq 0))
```

The last line sets some default values relevant only to the nonlinear model.

- Write up files:

```
(unless *linear*
(write-to-file write-sim "bk_71_ns.f")
(write-to-file print-default-positions "positions.txt")
(write-to-file print-default-directions "directions.txt")
(write-to-file print-parameters "parameters.txt")
)
(when *linear*
(write-to-file write-matlab "bk_71_ls.m")
)
```

The FORTRAN file is written to `bk_71_ns.f` and the files `positions.txt`, `directions.txt`

and `parameters.txt` are used to store the default positions, directions and parameters if the `*linear*` flag is set to `nil`. This information is a useful debugging aid. If the linearised model is asked for, then the MATLAB^{TM} file `bk_71_ls.m` is written to disc.

3.3 Simulations and Results

The nonlinear code is used to generate the nonlinear equations of motion in the form of a FORTRAN code. The Fortran file is compiled and executed to generate time histories of the various dynamic variables (positions, velocities, accelerations, forces and so on). A typical plot of a time history is shown in Figure 3.3. In this case the forward speed is held constant at 20 ft/s (6.1538 m/s) and there is an initial non-zero roll angle of 0.005 rad.

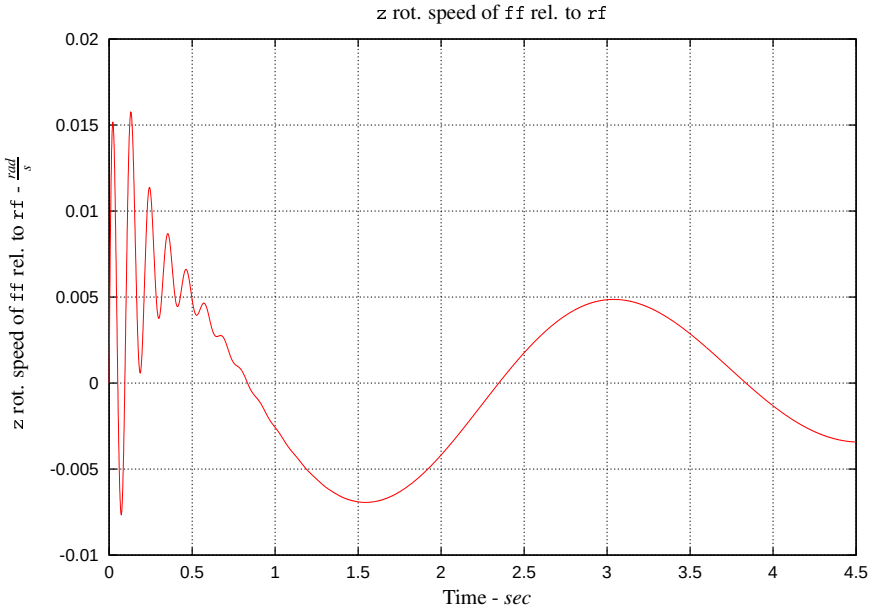

Figure 3.3: z rot. speed of `ff` rel. to `rf`

The z rotational speed of `ff` relative to `rf` undergoes an initial transient and then settles to zero, because the system is stable in its straight running configuration. It is easy to see that this transient has two different frequency components, one being fast and the other slow. The slow mode corresponds to the weave mode of the motorcycle and has a frequency of about 2.24 rad/s. The high frequency mode is the so called wobble mode which has a frequency of 58.18 rad/s.

The AUTOSIM code is used to generate the linearised equations of motion about straight running equilibrium conditions. In this equilibrium state the motorcycle is moving with constant forward speed and with zero roll, yaw and steer angles. The forward speed is varied in steps and the eigenvalues of the system for each equilibrium speed are calculated and plotted in Figure 3.4. The first part of Figure 3.4 is a plot of the real parts of the eigenvalues against forward speed - this agrees with Figure 5 in (Sharp, 1971). The second part of Figure 3.4 is the root-locus plot with forward speed the varied parameter. A detailed analysis of the weave, wobble and capsize modes is given in Appendix A.

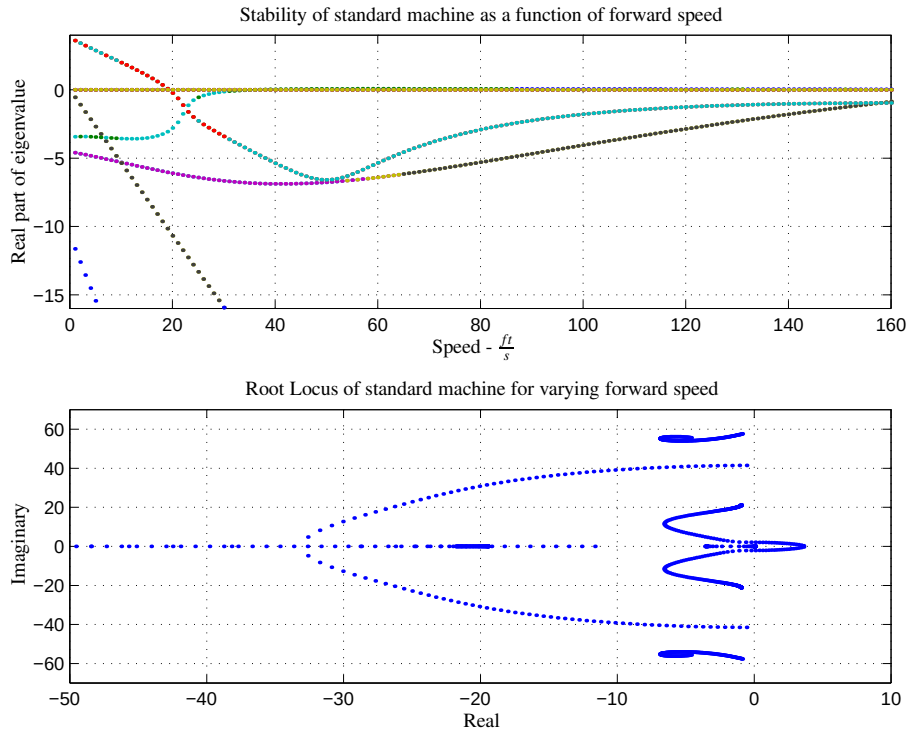

Figure 3.4: Stability and Root Locus plots

3.4 Conclusions

The aim of this Chapter is to demonstrate that the results presented in (Sharp, 1971) can be reproduced by the multi-body modelling code AUTOSIM. As is the case with many nonlinear systems, local stability is investigated via the eigenvalues of linearised models that are associated with equilibrium points of the nonlinear system. In the present case the linearisations were taken about constant-speed straight running conditions. AUTOSIM can be used to generate time histories from the nonlinear equations of motion, and most usefully, it can also be used to generate linearised state-space models in symbolic form. The linearised models can be imported into MATLAB^{TM} for evaluation. A typical local stability study will require time histories from the nonlinear model and the symbolic linearised equations of motion generated by the linear AUTOSIM code. The nonlinear equations are stored in the FORTRAN file `bk_71_ns.f` and the linearised equations of motion are stored in the MATLAB^{TM} file `bk_71_ls.m`. In order to construct the root-loci in Figure 3.4, two lines have to be removed from this code: the first line, which is a `clear` statement, and the line containing the `VU=80/13` statement. The modified version of the MATLAB^{TM} file is stored in `bk_71_ls.m` and the diagrams in Figure 3.4 may be generated using this file and the hand-written plotting codes `bk_71_results.m` and `bk_71_rootlocus.m`.

Chapter 4

The Sharp 1994 motorcycle model

4.1 Physical description of the model

The following assumptions are made regarding the vehicle under study (Sharp, 1994*b*):

1. The motorcycle is represented as an assembly of rigid bodies as follows:
   (a) Handlebars, front forks and front wheel.
   (b) Rear frame containing the engine with components rotating about transverse axes (giving rise to gyroscopic moments), the rider's legs and lower body.
   (c) The rear wheel assembly.
   (d) The rider's upper body.
2. The bodies are joined together as follows: Each of bodies (a), (c) and (d) are joined to the rear frame (b) as shown in Figure 4.1 (Sharp, 1994*b*). The joint between the front frame (a) and the rear frame (b) is the steer axis revolute joint. The damping and stiffness coefficients associated with this joint are used to represent the torques generated by the rider's arms. The housing of the steering head bearings is connected to the rear frame by two flexible mechanisms. One allows relative lateral translation, while the other allows relative rotation about an axis perpendicular to the steering axis. Appropriate stiffnesses and damping coefficients are associated with these mechanisms.
3. The joint between the rear frame (b) and the rear wheel assembly (c) is an inclined hinge. There are stiffness and damping coefficients associated with this hinge. The upper body of the rider (d) is connected to the rear frame (b) by a longitudinal hinge at saddle height. The rider's muscular activity in remaining upright is represented by a spring-damper system.
4. The following degrees of freedom are allowed:
   - Forward and lateral motion of the reference point O, Figure 4.1.
   - Yaw of the rear frame.
   - Roll of the rear frame.

- Lateral displacement of the steer axis relative to the rear frame.
- Twist displacement of the steer axis relative to the rear frame.
- Steering displacement of the front frame relative to the rear frame.
- Twist displacement of the rear wheel assembly relative to the rear frame.
- Roll displacement of the rider's upper body relative to the rear frame.

5. The tyre force and moment system is described as follows: side force and self aligning moments proportional to side-slip angle are generated. The constants of proportionality are functions of tyre load and these vary with speed since aerodynamic drag and lift forces and aerodynamic pitching moment influences are included in the model. The side force and aligning moment responses to side-slip are lagged, via a single time constant $\frac{\sigma}{u}$, in which σ is the tyre relaxation length and u the vehicle forward speed. The relaxation length σ varies with tyre load, in accordance with measured data.

6. Side forces, aligning moments and overturning moment responses proportional to camber angle are introduced. Again, the constants of proportionality depend on tyre load, but in this case the camber force system responds instantly to changes in camber angle. The overturning moment response, also instantaneous, is calculated from the radius of curvature of the tyre cross-section. The normal reaction between the tyre and the ground, in reality, moves around the cross-section as the camber angle changes. This effect is represented by a force and overturning moment at the theoretical centre of tyre/ground contact (as for an infinitely thin tyre). On this basis, the constant of proportionality between the overturning moment and the camber angle is proportional to load. These responses are not lagged, because they are geometrical in origin, rather than dependent on tyre distortions, that take time to build up.

The motorcycle is represented diagrammatically in Figure 4.1 (Sharp, 1994*b*).

4.2 Programming of the model

4.2.1 Body structure diagram

The multi-body system in Figure 4.1 is subdivided into its constituent bodies for the purpose of writing the AUTOSIM code – the bodies are arranged in the parent-child relationship shown in Figure 4.2. The first body is the *Inertial Frame* which has the *Yaw Frame* as its only child. The *Yaw Frame* has the *Inertial frame* as its parent and the *Rear Frame* as its only child. The *Rear Frame* has the *Yaw Frame* as its parent and the *Rider Upper Body*, *Engine Flywheel*, the *Rear Wheel* and *Steering Head* assemblies as its children. The *Rear Wheel Assembly* has the *Rear Wheel* as its only child. The *Steering Head Frame* has the *Front Frame* as its only child and the *Front Frame* has the *Front Wheel* as its only child. The road wheels, *Rider Upper Body* and *Engine Flywheel* have no children.

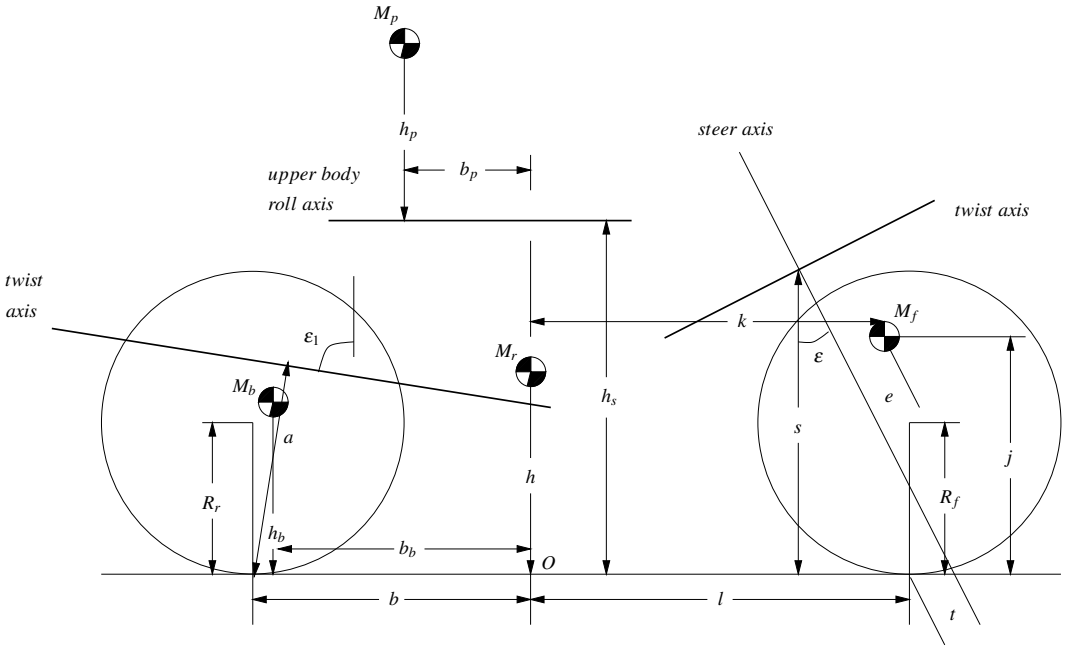

Figure 4.1: Diagrammatic representation of the motorcycle showing dimensions.

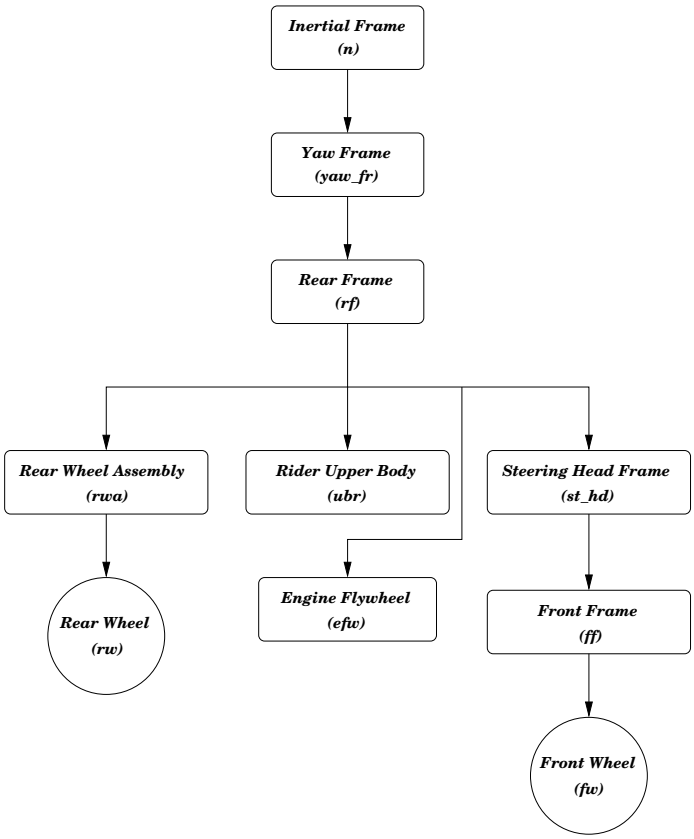

Figure 4.2: Body Structure Diagram of the motorcycle.

4.2.2 Program codes

The same AUTOSIM code is used to generate the nonlinear and linearised models. A flag called `*linear*` is set at the beginning of the code to either true (`t`) or false (`nil`) and the appropriate parts of the code are selected or deselected so as to provide the nonlinear and linearised models. Those parts of the code that are relevant to the nonlinear and linearised model building are separated via the use of the Lisp macros `unless` and `when`.

AUTOSIM commands are used to describe the components of the motorcycle multi-body system via their parent-child relationships. The nonlinear version of the AUTOSIM code is then used to generate the FORTRAN file that solves the nonlinear equations of motion, and the linear part is used to generate the symbolic representation of the linearised system matrices that are used to obtain root-locus plots. The programming details are described next:

- Set the flags:

```
(defvar *linear*)
(defvar *hands-on*)
(setf *linear* nil)
(setf *hands-on* nil)
```

  The `*linear*` flag is used to select nonlinear or linearised model building. The `*hands-on*` flag discriminates between the hands-off and hands-on cases.

- A few preliminaries:

```
(reset)
(si)
(add-gravity)

(unless *linear* (setsym *multibody-system-name* "bk_94_ns"))
(when *linear* (setsym *multibody-system-name* "bk_94_ls"))
(setsym *double-precision* t)
```

  The `reset` line sets various global variables used by AUTOSIM to store equations to their default values, `si` sets the units system to SI and `add-gravity` sets up a uniform gravitational field in the z-direction of the inertial frame. The next two lines name the system as `bk_94_ns` if the `*linear*` flag is set to `nil` and as `bk_94_ls` if the `*linear*` flag is set to `t`. The last line sets the `*double-precision*` variable to true so that all the FORTRAN floating-point declarations are made in double-precision.

- Some dimensions are computed here:

```
(setsym kk "ll+(ee+trail-jj*sin(epsilon))/cos(epsilon)")
(setsym whl_bs "bb+ll")
```

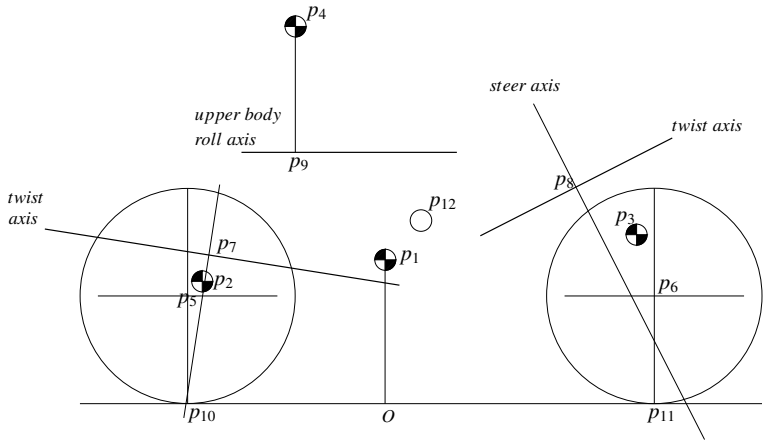

Figure 4.3: Diagrammatic representation of the motorcycle showing points.

- Various points in the motorcycle nominal configuration within the coordinate system of body *n* are defined (shown diagrammatically in Figure 4.3):

```
(add-point p1  :name "Rear Frame centre of mass"
               :body n :coordinates (0 0 -hh))
(add-point p2  :name "Rear Wheel Assembly centre of mass"
               :body n :coordinates (-bb_b 0 -hh_b))
(add-point p3  :name "Front Frame centre of mass"
               :body n :coordinates (@kk 0 -jj))
(add-point p4  :name "Rider centre of mass"
               :body n :coordinates (-bb_p 0 "-hh_s-hh_p"))
(add-point p5  :name "Rear Wheel centre point"
               :body n :coordinates (-bb 0 -Rr))
(add-point p6  :name "Front Wheel centre point"
               :body n :coordinates (ll 0 -Rf))
(add-point p7  :name "Rear Wheel Assembly joint with Rear Frame"
               :body n :coordinates ("-bb+aa*cos(epsilon1)" 0
                                     "-aa*sin(epsilon1)"))
(add-point p8  :name "Front Twist Frame joint with Rear Frame"
               :body n :coordinates
               ("ll+trail/cos(epsilon)-ss*tan(epsilon)" 0 -ss))
(add-point p9  :name "Rider joint with Rear Frame"
               :body n :coordinates (-bb_p 0 -hh_s))
(add-point p10 :name "Rear Wheel ground contact point in n"
               :body n :coordinates (-bb 0 0))
(add-point p11 :name "Front Wheel ground contact point in n"
               :body n :coordinates (ll 0 0))
(add-point p12 :name "Centre of pressure"
               :body n :coordinates ("@whl_bs/2-bb" 0 -hh_cp))
```

Body *n* is the *Inertial Frame* in which all of the above points are defined. The coordinate system used to define the points is that associated with body *n*. The nominal configuration of the motorcycle is the upright position with zero roll, yaw, steer and twist angles and with zero forward speed. In the above, it is usual to use "`bb`" to represent the distance "*b*" in Figure 4.1, or "`bb_b`" to represent "b_b" and so on. The reason for this is that `t`, `g` etc. are reserved variables required by AUTOSIM; `t` is time and `g` is acceleration due to gravity.

- The rear frame is introduced into the model next. This is done in two steps:

```
(add-body yaw_fr :name "Yaw Frame"
                 :translate (x y)
                 :body-rotation-axes z
                 :parent-rotation-axis z
                 :reference-axis x
                 :mass 0
                 :inertia-matrix 0)

(when *linear*
(add-speed-constraint "tu(yaw_fr,1) - vu" :u "tu(yaw_fr,1)")
)

(add-body rf    :name "Rear Frame"
                :parent yaw_fr
                :body-rotation-axes x
                :parent-rotation-axis x
                :reference-axis y
                :cm-coordinates p1
                :mass Mr
                :inertia-matrix ((Irx 0 Irxz)
                                 (0 0 0)
                                (Irxz 0 Irz)))
```

Firstly, the *Yaw Frame* is introduced as a massless body with translational freedoms in the *x* and *y* directions of body *n* (it is a child of *n*). Also, the *Yaw Frame* has a rotational degree of freedom in the *z*-direction (of body *n*) that describes the yawing motion of the motorcycle. The body named "Rear Frame" has the *Yaw Frame* as its parent and it has the mass and inertia properties[1] of the vehicle's entire rear frame assembly. It has one degree of rotational freedom around the *Yaw Frame's x*-axis and this freedom is used to model the rolling motion of the motorcycle. Unlike the "Sharp 1971" model (Sharp, 1971), we do not use an `add-speed-constraint` command to constrain the forward velocity of

[1] Note that the inertia matrices of the *Rear Frame* and *Rider Upper Body* have been interchanged as compared with reference (Sharp, 1994*b*). In addition, the reader should be warned that (Sharp, 1994*b*) and AUTOSIM use different sign conventions for the products of inertia. In AUTOSIM the product of inertia `Irxz` is of the form $-\sum m_i x_i z_i$.

the *Yaw Frame* unless the linear code has been selected. As will be explained later, the motorcycle speed is controlled using a feedback control system in the nonlinear case.

- Add in the rider upper body:

```
(add-body ubr   :name "Rider Upper Body"
                :parent rf
                :body-rotation-axes x
                :parent-rotation-axis x
                :reference-axis y
                :joint-coordinates p9
                :cm-coordinates p4
                :mass Mp
                :inertia-matrix ((Ipx 0 Ipxz)
                                 (0 0 0)
                                (Ipxz 0 Ipz)))
```

The *Rider Upper Body* is a child of the *Rear Frame*. It has the freedom to roll relative to the *Rear Frame* and it has a mass and inertia-matrix associated with it.

- Add the rear wheel assembly:

```
(setsym rear_twist "sin(epsilon1)*[rfx] + cos(epsilon1)*[rfz]")

(add-body rwa   :name "Rear Wheel Assembly"
                :parent rf
                :body-rotation-axes x
                :parent-rotation-axis @rear_twist
                :reference-axis y
                :joint-coordinates p7
                :cm-coordinates p2
                :mass Mb
                :inertia-matrix 0)
```

Before the *Rear Wheel Assembly* is included in the code, the direction vector about which the *Rear Wheel Assembly* twists relative to the *Rear Frame* is defined via the vector (`rear_twist`). The *Rear Wheel Assembly* is also a child of the *Rear Frame* and it only has mass associated with it.

- Add in the rear wheel:

```
(add-body rw    :name "Rear Wheel"
                :parent rwa
                :body-rotation-axes y
                :parent-rotation-axis y
                :reference-axis z
```

```
:joint-coordinates p5
:mass 0
:inertia-matrix ((irwx 0 0)
                 (0 irwy 0)
                 (0 0 irwx)))
```

The *Rear Wheel* is a child of the *Rear Wheel Assembly*. Its mass is set to zero, because it has already been included in the mass of the *Rear Wheel Assembly*; the *Rear Wheel* does however have inertia properties. The `:joint-coordinates p5` command line defines the coordinates of the wheel spin axis. The point `p5` has already been defined in body *n*.

- Introduce an unspun ground contact point for the *Rear Wheel*:

```
(add-point rwcp :name "Rear wheel contact point"
                :body rwa :coordinates p10)
```

This point is fixed in the *Rear Frame* and is introduced to assist with the calculation of the `vur` variable and the rear wheel side-slip angle. It is also used as the point of application of the rear tyre forces.

- Define the velocity component of `rwcp` along the line of intersection of the *Rear Wheel* plane and the ground plane. This will be used to compute the angular velocity of the *Rear Wheel* as follows:

```
(setsym rw_lat "dir(dplane([rway],[nz]))")
(setsym rw_long "cross(@rw_lat,[nz])")
(setsym vur "dot(vel(rwcp),@rw_long)")
```

The second line, which makes use of the first, defines the direction of the line of intersection of the *Rear Wheel* plane and the ground plane. The last line finds the velocity component of `rwcp` in the direction of `rw_long`. The reader is referred to Figure 4.4 for a diagrammatic representation of the various vector quantities being used.

- Assume no longitudinal slip for the *Rear Wheel*:

```
(add-speed-constraint "ru(rw)*Rr + @vur" :u "ru(rw)")
```

The rotational speed of the *Rear Wheel* is constrained to be `-vur/Rr` which means that the wheel is not allowed to slip longitudinally. The effect of this (nonholonomic) constraint is to remove the rotational speed of the rear wheel degree of freedom from the equations of motion.

- Define the front twist axis for the *Front Frame*:

```
(setsym front_twist "cos(epsilon)*[rfx] - sin(epsilon)*[rfz]")
```

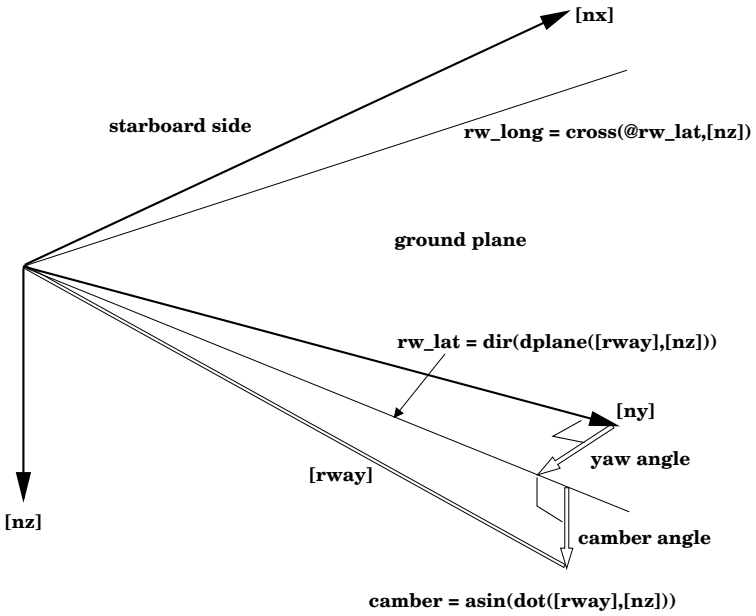

Figure 4.4: Wheel camber and yaw angles.

This axis is used to assist with the addition of the front frame assembly, which is introduced into the model in two steps.

- Add in the front frame assembly:

```
(add-body st_hd :name "Steering Head Frame"
                :parent rf
                :translate y
                :body-rotation-axes x
                :parent-rotation-axis @front_twist
                :reference-axis y
                :joint-coordinates p8
                :mass 0
                :inertia-matrix 0)


(add-body ff    :name "Front Frame"
                :parent st_hd
                :body-rotation-axes z
                :parent-rotation-axis z
                :reference-axis x
                :cm-coordinates p3
                :mass Mf
                :inertia-matrix ((Ifx 0 Ifxz)
                                 (0 0 0)
                                (Ifxz 0 Ifz)))
```

To begin, the *Steering Head Frame* is used to represent lateral displacements and rotational twist freedoms between the *Front Frame* and the *Rear Frame*. The *Front Frame* is then added as a child of the *Steering Head Frame*. The steering freedom, the mass and the inertia-matrix of the front frame assembly are also included at this point.

- Add in the *Front Wheel*:

```
(add-body fw   :name "Front Wheel"
               :parent ff
               :body-rotation-axes y
               :parent-rotation-axis y
               :reference-axis z
               :joint-coordinates p6
               :mass 0
               :inertia-matrix (0 ifwy 0))
```

This body has the *Front Frame* as its parent. Its mass and x and z inertias are zero since these have been included in the *Front Frame* description. The spin inertia of the *Front Wheel* is included so that angular momentum (gyroscopic) effects are correctly represented.

- Introduce an unspun ground contact point for the *Front Wheel*:

```
(add-point fwcp :name "Front wheel contact point"
                :body ff :coordinates p11)
```

This point is fixed in the *Front Frame*. It is introduced to assist with the calculation of the `vuf` variable and the *Front Wheel* side-slip angle. It is also used as the point of application of the front tyre forces.

- Define the velocity component of `fwcp` along the line of intersection of the *Front Wheel* plane and the ground plane:

```
(setsym fw_lat "dir(dplane([ffy],[nz]))")
(setsym fw_long "cross(@fw_lat,[nz])")
(setsym vuf "dot(vel(fwcp),@fw_long)")
```

The second line, which makes use of the first, defines the direction of the line of intersection of the *Front Wheel* plane and the ground plane. The last line finds the velocity component of `fwcp` in the direction of `fw_long`.

- No longitudinal slip on the *Front Wheel*:

```
(add-speed-constraint "ru(fw)*Rf + @vuf" :u "ru(fw)")
```

As with the *Rear Wheel*, it is assumed that the *Front Wheel* undergoes no longitudinal slip. Consequently, its angular velocity is set to `-vuf/Rf` and the rotational speed of the wheel degree of freedom is eliminated from the equations of motion by AUTOSIM.

- Add in the engine flywheel:

```
(add-body efw   :name "Engine flywheel"
                :parent rf
                :body-rotation-axes y
                :parent-rotation-axis y
                :reference-axis z
                :mass 0
                :inertia-matrix (0 iry 0))
```

The *Engine Flywheel* is a child of the *Rear Frame* and is located at its origin with freedom to rotate about the `y`-axis of the *Rear Frame*. The *Engine Flywheel* has a spin inertia associated with it so that the associated angular momentum effects associated with the spinning engine can be reproduced in the model.

- The *Engine Flywheel* is assumed to rotate at the same speed as the *Rear Wheel* – Its inertia is adjusted to make this accurate:

```
(add-speed-constraint "ru(efw)*Rr + @vur" :u "ru(efw)")
```

The *Engine Flywheel* rotates with an angular speed of `-vur/Rr` and consequently this freedom is eliminated from the equations of motion.

- Define the camber and side-slip angles:

```
(setsym phir "asin(dot([nz],[rwy]))")
(setsym phif "asin(dot([nz],[fwy]))")
(setsym alphar "asin(dot(@rw_lat,dir(vel(rwcp))))")
(setsym alphaf "asin(dot(@fw_lat,dir(vel(fwcp))))")
```

These angles are needed in the calculation of the tyre side forces and moments. The first line defines the *Rear Wheel* camber angle, the second line defines the *Front Wheel* camber angle and the third defines the *Rear Wheel* side-slip angle by making use of the point `rwcp` defined above. The last line defines the *Front Wheel* side-slip angle via the point `fwcp`. Note that for the side-slip angles, positive lateral velocities give positive slip values and negative forces.

- Add the driving torque:

```
(unless *linear*
```

```
(add-state-variable D_tqi D_tqip "F*l")
(set-aux-state-deriv D_tqip "vu-tu(yaw_fr,1)")
(setsym D_tq "kp*(vu-tu(yaw_fr,1))+ki*D_tqi")

(add-moment Dr_mom        :name "Rear wheel drive torque"
                          :body1 rw     :body2 rf
                          :direction [rwy]
                          :magnitude -@D_tq)
)
```

Unlike the "Sharp 1971" model (Sharp, 1971), this code uses a PI control loop to maintain a constant forward velocity for the *Yaw Frame* for the nonlinear case. This controller is shown in Figure 4.5. The first two lines define the integral part of the control loop. All

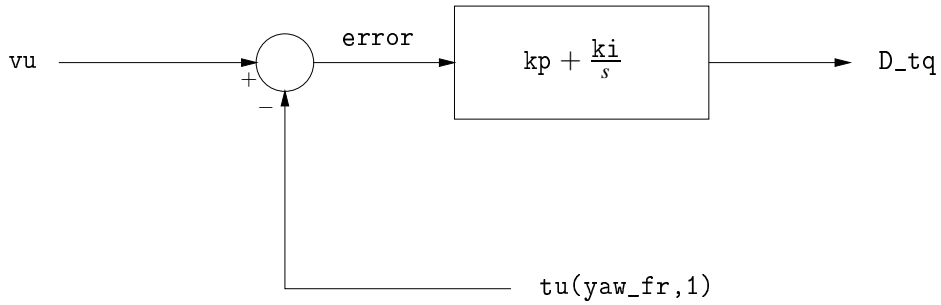

Figure 4.5: Control loop on the forward speed.

the contributions are added on the last line. The drive torque is then applied to the *Rear Wheel* with the reaction coming from the *Rear Frame*. Strictly, this is representative of a shaft driven motorcycle, but this assumption does not make any difference here due to the absence of rear suspension freedom. If the `*linear*` flag is set to `t`, then no driving torque is added and the `add-speed-constraint` command discussed earlier is used. When present, the drive torque changes with forward speed (to maintain speed) to counterbalance the change in aerodynamic resistance (see below). The implied longitudinal rear tyre force would slightly alter the behaviour of the tyre in respect of lateral force and its value would therefore need to be tracked through simulation runs for importation into the stability analysis via the linear model. To avoid this complication the speed constraint is used in the linear model, treating the influence of the drive thrust as negligible.

- Introduce various damping and stiffness forces and moments:

```
(add-moment ubr_tq      :name "Rider Upper Body Damping and Stiffness"
                        :body1 ubr      :body2 rf
                        :direction [ubrx]
                        :magnitude "-k_zita*rq(ubr) - D_zita*ru(ubr)")
```

```
(add-moment rwa_tq      :name "Rear Twist Damping and Stiffness"
                        :body1 rwa      :body2 rf
                        :direction [rwax]
                        :magnitude "-k_lamda*rq(rwa) - D_lamda*ru(rwa)")

(add-line-force st_hd_f :name "Steering Head Lateral Stiffness"
                        :direction [st_hdy]
                        :point1 st_hd0   :point2 st_hdj
                        :magnitude "-k_v*tq(st_hd) - D_v*tu(st_hd)")

(add-moment st_hd_tq    :name "Front Twist Torque"
                        :body1 st_hd     :body2 rf
                        :direction [st_hdx]
                        :magnitude "-k_gamma*rq(st_hd) - D_gamma*ru(st_hd)")

(add-moment steer_torq  :name "Steering Damping and Stiffness"
                        :body1 ff       :body2 st_hd
                        :direction [ffz]
                        :magnitude "-k_steer*rq(ff)-D_steer*ru(ff)+rid_tq")
```

All the above moments are generated by torsional springs and dampers except for the last one which includes an external torque input from the rider – this defaults to zero. The first one is the moment between the *Rider Upper Body* and the *Rear Frame*. The second is between the *Rear Wheel Assembly* and the *Rear Frame*. The third moment is between the *Steering Head Frame* and the *Rear Frame* and the final one is between the *Front Frame* and the *Steering Head Frame*. The `add-line-force` command introduces a lateral force between the *Steering Head Frame* and the *Rear Frame* via a spring and damper. Appropriate values for the spring and damper constants are given at the end of the program listing.

- Introduce the aerodynamic drag and lift forces:

```
(add-point p13 :name "Centre of Pressure in rf" :body rf :coordinates p12)

(add-line-force drag    :name "Aerodynamic Drag"
                        :direction [rfx]
                        :point1 p13
                        :magnitude "-Dc*(tu(yaw_fr,1)**2)")

(add-line-force lift    :name "Aerodynamic Lift"
                        :direction [rfz]
                        :point1 p13
                        :magnitude "-Lc*(tu(yaw_fr,1)**2)")
```

The point `p13` is used to define the centre of pressure which is a point attached on the

Rear Frame. The aerodynamic drag and lift forces are both applied here. These forces are proportional to the square of the forward speed (`tu(yaw_fr,1)**2`).

- Work out the normal tyre loads:

```
(setsym Zf "((Mf*(bb+@kk)+Mr*bb+Mb*(bb-bb_b)+Mp*(bb-bb_p))*G
-(vu**2)*(Dc*hh_cp+Lc*@whl_bs/2))/@whl_bs")
(setsym Zr "(Mf+Mr+Mp+Mb)*G-Lc*vu**2-@Zf")
```

The purpose of the above is to compute the normal tyre loads under a steady speed condition. This is done by taking moments about the rear wheel ground contact point.

- Calculate tyre parameters:

```
(setsym Cfvr "-92.9+23.129*@Zr-(4.663/1000)*@Zr**2-(6.457*10**(-7))*@Zr**3
+(1.887*10**(-10))*@Zr**4")
(setsym Cfvf "-300+28.577*@Zf-0.0143*@Zf**2+(1.431*10**(-6))*@Zf**3
+(3.347*10**(-10))*@Zf**4")
(setsym Cmvr "9+0.3573*@Zr + (3.378*10**(-5))*@Zr**2")
(setsym Cmvf "-0.281+0.2442*@Zf+(8.575*10**(-5))*@Zf**2")
(setsym Cr1 "27.38+0.9727*@Zr-(4*10**(-6))*@Zr**2")
(setsym Cf1 "-13.25+1.302*@Zf-(1.39*10**(-4))*@Zf**2")
(setsym Cr2 "2.056+0.01282*@Zr+(4.928*10**(-6))*@Zr**2")
(setsym Cf2 "2.788+0.0165*@Zf+(3.9*10**(-6))*@Zf**2")
(setsym Cr3 "-0.07*@Zr")
(setsym Cf3 "-0.06*@Zf")
(setsym sigmar "0.03594+(1.941*10**(-4))*@Zr-(5.667*10**(-8))*@Zr**2
+(5.728*10**(-12))*@Zr**3")
(setsym sigmaf "0.1012+(1.297*10**(-4))*@Zf-(3.267*10**(-8))*@Zf**2")
```

Since aerodynamics effects are included, the tyre loads will vary with forward speed as will the various tyre parameters[2].

- Introduce a simple tyre relaxation model:

```
(add-state-variable Yr Yr_dot F)
(set-aux-state-deriv Yr_dot "(@vur/@sigmar)*( -@Cfvr*@alphar - Yr)")

(add-state-variable Yf Yf_dot F)
(set-aux-state-deriv Yf_dot "(@vuf/@sigmaf)*( -@Cfvf*@alphaf - Yf)")

(add-state-variable Mzr Mzr_dot "F*l")
(set-aux-state-deriv Mzr_dot "(@vur/@sigmar)*( @Cmvr*@alphar - Mzr)")

(add-state-variable Mzf Mzf_dot "F*l")
(set-aux-state-deriv Mzf_dot "(@vuf/@sigmaf)*( @Cmvf*@alphaf - Mzf)")
```

[2]Note that the polynomial expressions used here are corrected so that they fi t the graphs given in (Sharp, 1994*b*).

The `add-state-variable` commands introduce four state variables, one for each of the tyre force expressions and one for each of the tyre moment expressions. These states are used to describe the tyre relaxation properties. The force and moment equations are defined with the `set-aux-state-deriv` expressions and use the values of the side-slip and tyre parameters defined above. Notice the minus sign on the `Cr1*@alphar` and `Cf1*@alphaf` terms.

- Introduce the tyre side forces and moments:

```
(add-line-force Yrt      :name "Total Rear Lateral Force"
                         :direction @rw_lat
                         :point1 rwcp
                         :magnitude "@Cr1*@phir + Yr")

(add-line-force Yft      :name "Total Front Lateral Force"
                         :direction @fw_lat
                         :point1 fwcp
                         :magnitude "@Cf1*@phif + Yf")

(add-moment Mzrt         :name "Total Rear Aligning Moment"
                         :body1 rwa
                         :direction [nz]
                         :magnitude "@Cr2*@phir + Mzr")

(add-moment Mzft         :name "Total Front Aligning Moment"
                         :body1 ff
                         :direction [nz]
                         :magnitude "@Cf2*@phif + Mzf")

(add-moment Mxr          :name "Rear Righting Moment"
                         :body1 rwa
                         :direction @rw_long
                         :magnitude "@Cr3*@phir")

(add-moment Mxf          :name "Front Righting Moment"
                         :body1 ff
                         :direction @fw_long
                         :magnitude "@Cf3*@phif")
```

The two forces are the tyre side forces and their directions are in the ground plane and normal to the line of intersection of the ground plane and the wheel plane. The tyre models include side forces due to camber and are introduced without relaxation, because these forces are produced by geometric effects. Next, the aligning moments are introduced with terms due to side-slip and terms due to camber. As with the side forces, relaxation effects

are only associated with the side-slip components. The direction of these moments is the z-axis of the inertial frame. Finally, we introduce the front and rear tyre overturning moments. These moments are applied in the `fw_long` and `rw_long` directions respectively. Since these moments are purely geometric in character, they do not have relaxation effects associated with them.

- Incorporate the longitudinal and normal tyre loads:

```
(setsym Xr "-(Crr1 + Crr2*@vur**2)*@Zr")
(setsym Xf "-(Crr1 + Crr2*@vuf**2)*@Zf")

(add-line-force Xrr     :name "Rear Longitudinal Force"
                        :direction @rw_long
                        :point1 rwcp
                        :magnitude @Xr)

(add-line-force Xff     :name "Front Longitudinal Force"
                        :direction @fw_long
                        :point1 fwcp
                        :magnitude @Xf)

(add-line-force Wr      :name "Rear Vertical Force"
                        :direction [nz]
                        :point1 rwcp
                        :magnitude "-@Zr")

(add-line-force Wf      :name "Front Vertical Force"
                        :direction [nz]
                        :point1 fwcp
                        :magnitude "-@Zf")
```

The two longitudinal forces represent the rolling resistance to the forward motion of the motorcycle wheels and have a magnitude that depends on the forward speed of the vehicle. These forces are proportional to the normal tyre loads as defined in the two `setsym` expressions. The normal tyre forces are introduced into the vehicle equations of motion by the last two commands.

- Derive the equations of motion of the system or the linearised equations:

```
(unless *linear* (dynamics))
(when *linear*
(add-variables dyvars real rid_tq)
(linear :u rid_tq)
)
```

If the `*linear*` flag is set to `nil` the full equations of motion are derived; otherwise the linearised equations are computed with `rid_tq` as the input. `rid_tq` is defined as a real variable that is used as a steering torque input from the rider. The corresponding B-Matrix is computed in the linearised equations.

- All the motorcycle parameters are introduced with their names and default values[3]:

```
;;; Default values for masses:
(set-names      Mf      "Mass of Front Frame"
                Mr      "Mass of Rear Frame"
                Mb      "Mass of Rear Wheel Assembly"
                Mp      "Mass of Upper Body of Rider")
(set-defaults   Mf 40.59 Mr 170.3 Mb 25.0 Mp 50.0)

;;; Default values for moments of inertia:
(set-names      Ifx     "front frame inertia about x-axis"
                Ifz     "front frame inertia about z-axis"
                Ifxz    "front frame inertia product"
                Ipx     "rear frame inertia about x-axis"
                Ipz     "rear frame inertia about z-axis"
                Ipxz    "rear frame inertia product"
                Irx     "rider upper body inertia about x-axis"
                Irz     "rider upper body inertia about z-axis"
                Irxz    "rider upper body inertia product"
                irwx    "rear wheel inertia about x-axis"
                irwy    "rear wheel spin inertia"
                ifwy    "front wheel spin inertia"
                iry     "effective engine flywheel inertia")
(set-defaults   Ifx 3.97 Ifxz 0 Ipx 1.96 Ipz 0.55 Ipxz 0.26 Irx 7.43
                Irz 11.63 Irxz 7.4 irwx 0.4 irwy 0.65 ifwy 0.58 iry 0.41)

;;; Geometric parameters:
(set-names      Rr      "Rear wheel radius"
                Rf      "Front wheel radius"
                hh_cp   "Centre of pressure height")
(set-defaults   aa 0.527 bb 0.628 bb_b 0.62 bb_p 0.28 ee 0.049 hh 0.438
                hh_b 0.33 hh_p 0.4 hh_s 0.8 jj 0.527 ll 0.807
                Rf 0.336 Rr 0.321 ss 0.77 trail 0.094
                epsilon 0.47 epsilon1 1.435 hh_cp 0.33)

;;; Frame flexibility and rider parameters:
(set-names      k_v     "steering head lateral stifness coefficient"
                D_v     "steering head lateral damping coefficient"
```

[3]It can be seen from the signs of `Ipxz` and `Irxz` that AUTOSIM uses a negative sign convention ($-\sum m_i x_i z_i$), as compared with (Sharp, 1994*b*), for products of inertia.

```
                k_lamda "rear wheel assembly twist stiffness coefficient"
                D_lamda "rear wheel assembly twist damping coefficient"
                k_gamma "steering head torsional stiffness coefficient"
                D_gamma "steering head torsional damping coefficient"
                k_zita  "rider upper body restraint stiffness coefficient"
                D_zita  "rider upper body restraint damping coefficient"
                k_steer "steer stiffness coefficient"
                D_steer "steer damping coefficient")
(set-defaults   k_v "1.04*(10**6)" D_v 456 k_lamda 46000 D_lamda 17.7
                k_gamma 61200 D_gamma 44.1 k_zita 10000 D_zita 156)

(unless *hands-on* (set-defaults Ifz 0.71 k_steer 0.0 D_steer 1.0))
(when *hands-on* (set-defaults Ifz 0.91 k_steer 50.0 D_steer 6.0))

;;; Tyre parameters:
(set-names      @Cfvf   "Front Tyre Cornering Stiffness"
                @Cfvr   "Rear Tyre Cornering Stiffness"
                @Cmvf   "Front Tyre Aligning Moment Stiffness"
                @Cmvr   "Rear Tyre Aligning Moment Stiffness"
                @Cf1    "Front Tyre Camber Stiffness"
                @Cr1    "Rear Tyre Camber Stiffness"
                @Cf2    "Front Tyre Aligning Moment Camber Coefficient"
                @Cr2    "Rear Tyre Aligning Moment Camber Coefficient"
                @Cf3    "Front Tyre Overturning Moment Coefficient"
                @Cr3    "Rear Tyre Overturning Moment Coefficient"
                Crr1    "Tyre rolling resistance coefficient 1"
                Crr2    "Tyre rolling resistance coefficient 2")
(set-defaults   Crr1 0.018 Crr2 "6.8*10**(-6)")

;;; Other parameters:
(set-names      Dc      "Aerodynamic Drag Coefficient"
                Lc      "Aerodynamic Lift Coefficient")
(set-defaults   Dc 0.377 Lc 0.05 vu 53.5)
(unless *linear* (set-defaults step 0.001 stopt 20 iprint 10 rid_tq 0
                      ki 300 kp 300 "tu(yaw_fr,1)" vu "rq(rf)" 0.005))
```

The `*hands-on*` flag is used to choose the appropriate values for the parameters corresponding to the hands-off and hands-on cases. Strictly speaking, for the hands-on case, the reaction to the steering restraint torque (`steer_tq`) comes from both the *Steering Head* (`st_hd`) and the *Rider Upper Body* (`ubr`) and not only from the *Steering Head* as in the hands-off case, but this is neglected. The last line sets some default values relevant only to the nonlinear model.

- Write up files:

```
(unless *linear*
(write-to-file write-sim "bk_94_ns.f")
(write-to-file print-default-positions "positions.txt")
(write-to-file print-default-directions "directions.txt")
(write-to-file print-parameters "parameters.txt")
)
(when *linear*
(write-to-file write-matlab "bk_94_ls.m")
)
```

The FORTRAN file is written to `bk_94_ns.f` and the files `positions.txt`, `directions.txt` and `parameters.txt` are used to store the default positions, directions and parameters if the `*linear*` flag is set to `nil`. This information is useful as a debugging aid. If the linearised model is asked for, then the MATLAB^{TM} file `bk_94_ls.m` is written.

4.3 Simulations and Results

The nonlinear code is used to generate the nonlinear equations of motion in the form of a FORTRAN code which is compiled to produce an executable program. This program can then be used to generate time histories of the various dynamic variables (positions, velocities, accelerations, forces and so on). A typical plot of a time history for the hands-off case is shown in Figure 4.6. In this case the forward speed is held constant at 53.5 m/s and there is an initial non-zero roll angle of 0.005 rad.

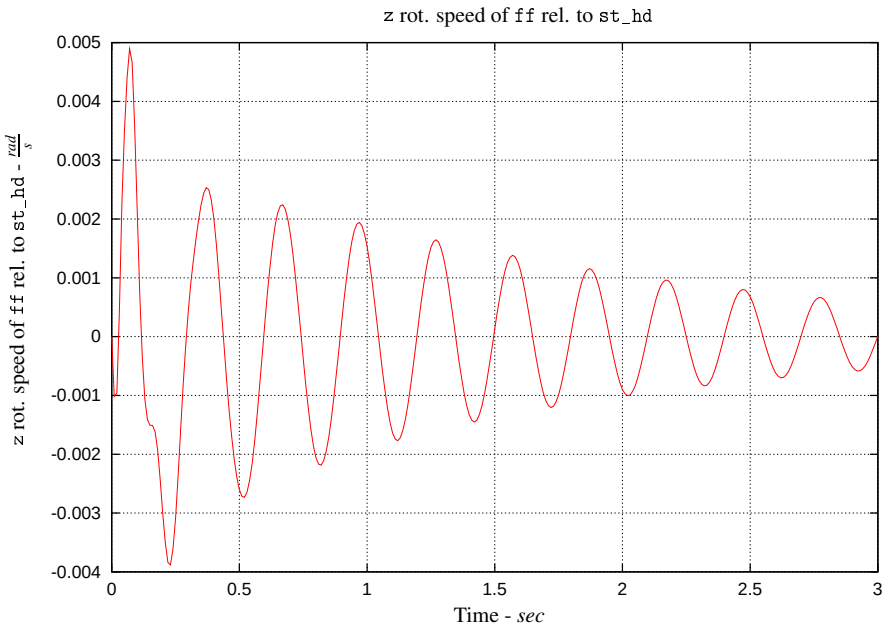

Figure 4.6: z rot. speed of `ff` rel. to `st_hd`.

The z-rotational speed of `ff` relative to `st_hd` undergoes an initial transient and then settles

to zero, because the system is stable in the straight running configuration for this value of forward speed. This transient has a slow frequency component that corresponds to the weave mode of the motorcycle with a frequency of about 22.85 rad/s. The initial part of the transient suggests also the presence of a higher frequency mode that corresponds to the so called wobble mode. A detailed discussion of these modes is given in Appendix A.

The linear code is used to generate the linearised equations of motion about straight running equilibrium conditions. In the equilibrium state, the motorcycle is moving with constant forward speed and with zero roll, yaw, steer and twist angles. Figure 4.7 shows root-locus plots in which speed is the varied parameter.

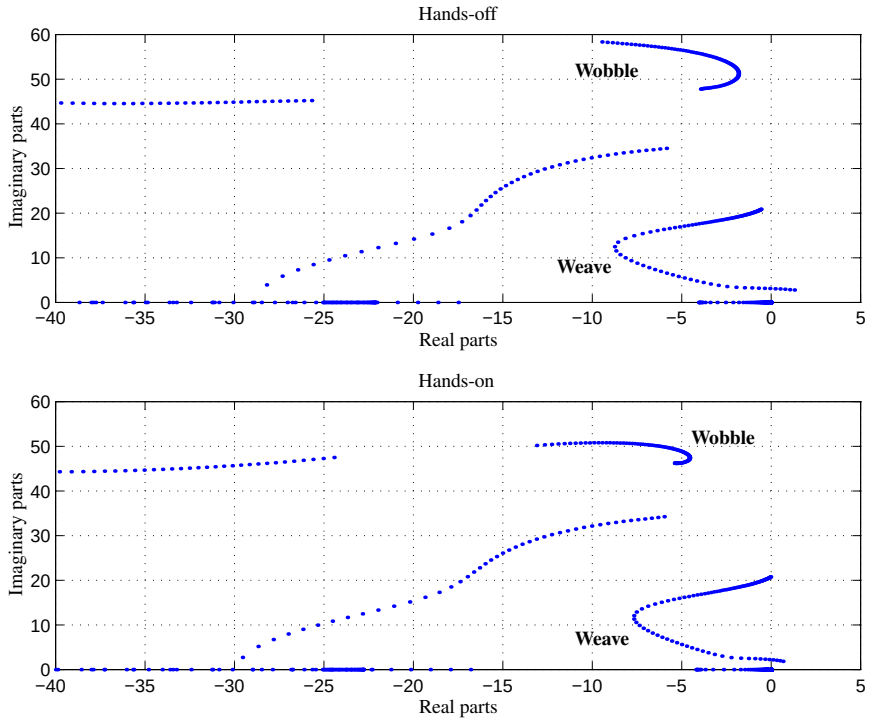

Figure 4.7: Root-loci for the weave and wobble modes of baseline machine and rider for the speed range 5 - 53.5 m/s.

The first part of Figure 4.7 is a plot for the hands-off case, while the second part of Figure 4.7 is a root-locus plot for the hands-on case. These figures agree with Figures 3 and 4 in the original paper (Sharp, 1994*b*).

4.4 Conclusions

The aim of this Chapter is to demonstrate that the results presented in (Sharp, 1994*b*) can be reproduced by the multi-body modelling code AUTOSIM. As is the case with many nonlinear systems, local stability is investigated via the eigenvalues of linearised models that are associated with equilibrium points. In the present case the linearisations were taken about constant-speed

straight running conditions. AUTOSIM can be used to generate time histories from the nonlinear equations of motion, and most usefully, it can be used to generate linearised state-space models in symbolic form. The linearised models can be imported into MATLAB^{TM} for evaluation. A typical local stability study will require time histories from the nonlinear model and the symbolic linearised equations of motion generated by the linear AUTOSIM code. The nonlinear equations are stored in the FORTRAN file `bk_94_ns.f` and the linearised equations of motion are stored in the MATLAB^{TM} file `bk_94_ls.m`. In order to construct the root-loci in Figure 4.7, two lines have to be removed from this code: the first line which is a `clear` statement and second a line containing the `VU=53.5` statement. The modified version of the MATLAB^{TM} file is stored in `bk_94_ls.m` and the diagrams in Figure 4.7 may be generated using this file and the hand-written plotting code `bk_94_rootlocus.m`.

Chapter 5

The 'SL2001" motorcycle model

5.1 The Mathematical Model

The basic components of the vehicle are:

(a) separate bodies for the front and rear frame that are joined by an inclined steering axis;

(b) a rear frame that is allowed longitudinal, lateral and heave translational freedoms, as well as yaw, pitch and roll angular freedoms;

(c) a swinging arm and its associated rear suspension system;

(d) telescopic front forks and the associated front suspension system;

(e) spinning road wheels;

(f) twist and steer freedoms for the rear frame relative to the front frame;

(g) longitudinal tyre forces proportional to and opposed to the longitudinal slip as defined in (Pacejka and Sharp, 1991)[1];

(h) lateral tyre forces and moments decoupled from the longitudinal tyre forces, and computed using the empirical expressions given in (Koenen, 1983);

(i) first order lags to represent tyre relaxation effects, whereby the tyre forces and moments do not respond immediately to changes in the tyre slip (dynamic tyres)[2];

(j) overturning moments due to camber assumed to be instantaneous functions of the tyre contact geometry (Sharp and Limebeer, 2001; Sharp *et al.*, 1999).

[1]Checks are made to ensure that these longitudinal tyre forces do not exceed 80% of the normal tyre load. If this fi gure is exceeded by either tyre at any point during a simulation run the results are deemed invalid, because they lie outside the tyre model's intended operating regime.

[2]Relaxation effects are associated with the lateral force systems, but not with the longitudinal ones. The wheel aligning moments due to side-slip include relaxation effects, while those due to camber are assumed instantaneous.

(k) simple in-plane aerodynamic effects, so that the tyre loads respond properly to changes in speed;

(l) a freedom that allows the rider's body to roll with respect to the motorcycle's rear frame.

The road is assumed to be flat, or regularly profiled, and the motorcycle can travel anywhere in the horizontal plane.

Figure 5.1 shows the machine in its nominal configuration in static equilibrium with the key modelling points labelled as $p_1, \cdots, p_{14}$. The child-parent structure used here is very similar to that employed in (Sharp and Limebeer, 2001) as shown in Figure 5.2.

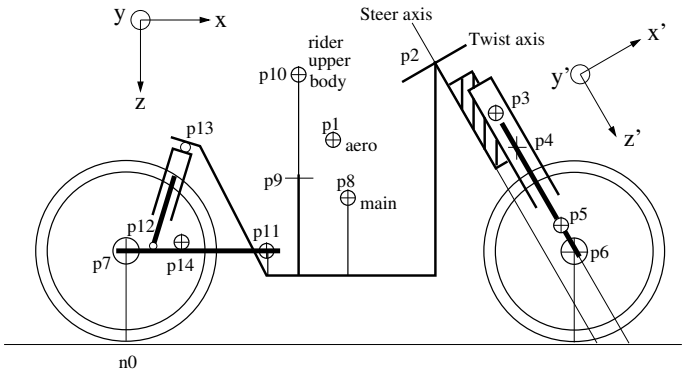

Figure 5.1: Motorcycle model in its nominal confi guration.

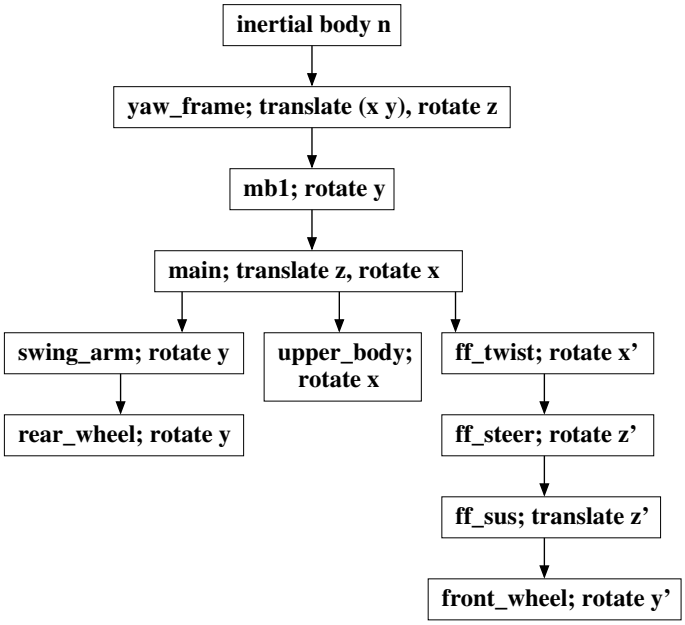

Figure 5.2: Body structure diagram showing the freedoms and the parent/child relationships.

The symbolic multibody modelling package AUTOSIM (Anon., 1998) is used to convert this conceptual model into a FORTRAN (or C) code that is used to produce the nonlinear simulation

results, and a MATLAB M-file for the linearised model based studies.

5.1.1 Various geometric details

5.1.1.1 Tyre loading

Each wheel-tyre combination is treated as a thin disc with a radial flexibility. The massless outer ring of the tyre can translate from contact point to wheel centre, with a spring force restraint used to represent the tyre wall compliance. The tyre loading is illustrated in Figure 5.3.

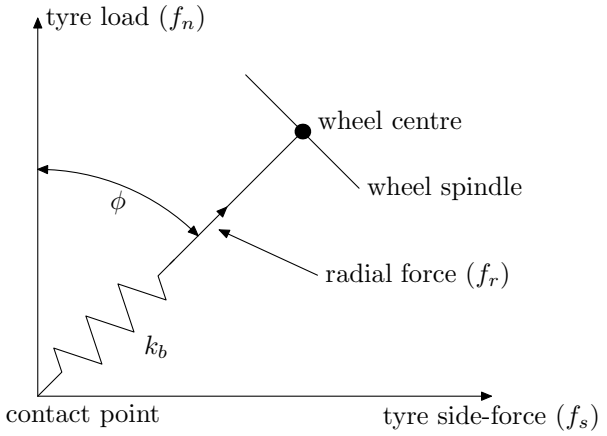

Figure 5.3: The tyre loading showing a radial deformation of the structure. View from rear.

5.1.1.2 Tyre contact point geometry and road forcing

In order to introduce road forcing into the model, it is necessary to examine the road wheel ground contact geometry in some detail. The complex dynamic geometry associated with the migration of the tyre contact points (especially that of the front tyre) is an outstanding feature of this model (Sharp and Limebeer, 2001; Sharp *et al.*, 1999). It will be assumed that the road undulation amplitudes are small compared to the wheel radii and that their wavelengths are long.

The front road wheel ground contact geometry is shown in detail in Figure 5.4.

A vector along the line of intersection between the ground and wheel planes can be calculated via a cross product between vectors that are normal to these planes. Since the wheel spindle unit vector `[fwy]` is perpendicular to the wheel plane, and `[yaw_frz]` is a unit vector that is normal to the ground plane, we can use `cross([fwy],[yaw_frz])` to generate the plane-intersection vector. Appendix B contains a brief description of the AUTOSIM instructions used here. The vector pointing from the wheel centre to the ground contact point must be perpendicular to both the wheel spindle vector and the plane intersection vector. This vector is computed using the vector triple product `cross(cross([fwy],[yaw_frz]),[fwy])`. To ensure that the triple product is a unit vector, we divide it by the sine of the angle between `[yaw_frz]` and `[fwy]` as follows:

```
cross(cross([fwy],[yaw_frz]),[fwy])/sqrt(1-dot([fwy],[yaw_frz])**2)
```

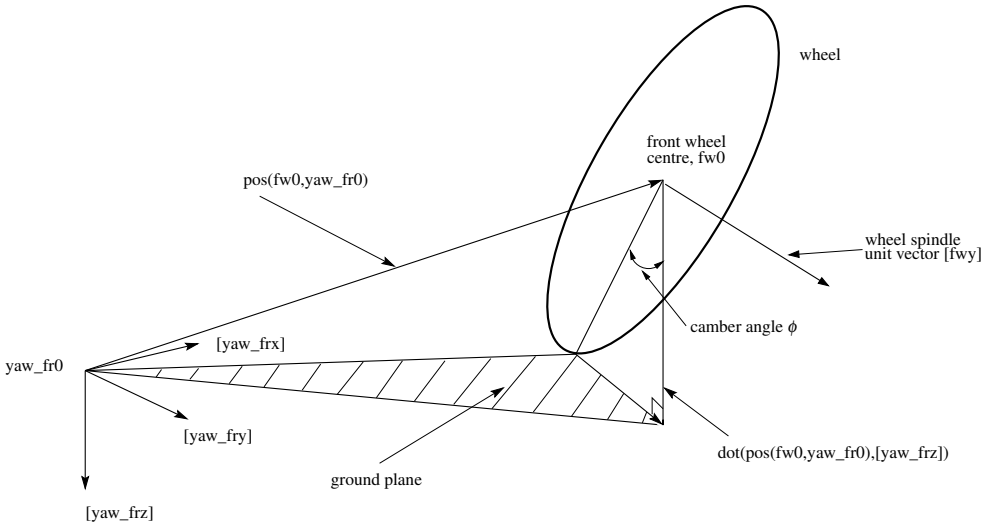

Figure 5.4: Wheel and tyre geometry, showing the migration of the ground contact point.

Note that `[fwy]` is always perpendicular to `cross([fwy],[yaw_frz])` and consequently there is no need for a second normalisation term. The vertical component of the vector joining the origin of the yaw frame axis system `yaw_fr0` to the front wheel centre `fw0` is the height from the ground of the wheel centre in the case of a smooth road and is computed as follows:

```
dot(pos(fw0,yaw_fr0),[yaw_frz]).
```

In the case of a profiled road, the height from the ground of the front wheel centre is adjusted via a front wheel road height variable `uf`:

```
dot(pos(yaw_fr0,fw0),[yaw_frz])-uf.
```

Dividing the height by the cosine of the camber angle gives the distance from wheel centre to the ground contact point:

```
dot(pos(yaw_fr0,fw0),[yaw_frz])-uf)/sqrt(1-dot([fwy],[yaw_frz])**2)
```

In the nominal condition, this distance is the wheel radius, so the tyre radial deflection from the nominal can be found via a tyre deflection calculation and this deflection is converted into a force change via the tyre carcass radial stiffness. Combining this with the unit vector defined above via the vector triple product, one obtains a vector that points from the wheel spindle axis to the ground contact point:

```
cross(cross([fwy],[yaw_frz]),[fwy])*(dot(pos(yaw_fr0,fw0),[yaw_frz])-uf)
/(1-dot([fwy],[yaw_frz])**2).
```

The contact point can now be defined via the coordinates of this vector as a moving point on the tyre circumference. This point is used to calculate the side-slip angle and it is the point of application of the load and the sideforce. A parallel set of arguments apply to the rear road wheel.

5.1.1.3 Overturning moment

In the case of the real tyre, the contact point moves round the sidewall as the wheel cambers, giving rise to an overturning moment. This effect is not reproduced in the thin disc tyre assumed, so the overturning moment is calculated separately and added. This calculation is illustrated in Figure 5.5.

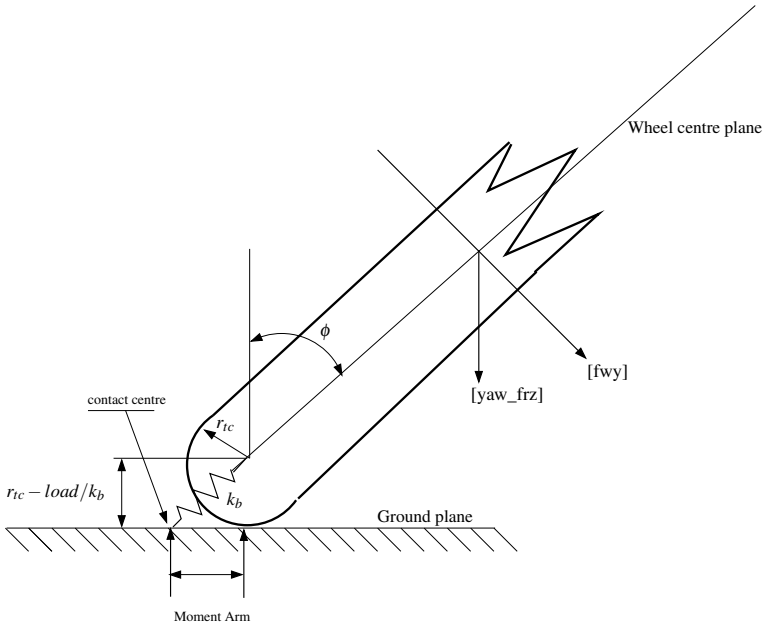

Figure 5.5: Wheel geometry showing how overturning moment is calculated.

5.1.2 Drive, braking and steer controller moments

The drive and braking moments are generated using proportional plus integral control signals based on speed error, the difference between the actual speed and a speed reference signal. In most cases the speed reference is a simple ramp function of the form:

$$v_{ref} = v_i + at.$$

where v_i is the initial speed demand and a is the target acceleration (or deceleration). When the applied wheel moment is a (negative) drive moment, it is applied to the rear wheel alone from the main frame. In the case of a (positive) braking moment, it is split in the ratio $(1-\lambda) : \lambda$ between the rear and front wheels respectively. The constant λ is given by $\lambda = 0.9$ for predominantly front wheel braking and $\lambda = 0.1$ for predominantly rear wheel braking. In order to implement these ideas, the driving/braking moment applied to the rear wheel is computed via,

$$M_{rear} = min(drive, drive * (1-\lambda)),$$

while that applied to the front wheel is

$$M_{front} = max(0.0, drive * \lambda).$$

drive is the total applied wheel moment. The control gains were found by simple trial and error techniques, to obtain good performance at constant or varying speed (up to ± 5 m/s^2) conditions.

Cornering manoeuvres can be enforced via a lean angle controller. The lean angle controller has proportional-integral-derivative terms which operate on the error between a reference lean angle and the actual lean angle to produce a steering torque. This controller is also tuned by trial.

The drive and steering torque controllers are not intended to replicate any active rider control actions, because the aim is to characterise the properties of the machine in isolation. The purpose of the feedback controls is simply to facilitate the solution of the equations of motion, in particular, to find equilibrium (trim) states.

5.1.3 Machine parameters

The main part of the model is intended to represent Koenen's motorcycle (Koenen, 1983). The machine and machine parameters are based on a large touring motorcycle of an early 1980's design; some of its basic parameters are given in Table 5.1. A complete set of parameters can be obtained from the web site http://www.ee.ic.ac.uk/control/motorcycles/.

Total mass	235 *kg* (518 *lbs*)
Maximum engine power	65 *kW* (87 *bhp*)
Steering head angle	30^o
Steering offset	0.0659 *m*
Mechanical trail	0.0924 *m*

Table 5.1: Machine parameters

More modern aerodynamic data for drag, lift and pitching moment (Knight, 2000) have been used, since Koenen's data gives unrealistic machine attitudes at high speeds (Sharp and Limebeer, 2001).

5.2 Model Validation

The model validation processes used here are an evolution of those described elsewhere (Sharp and Limebeer, 2001). To maximise their effectiveness, they were designed to be substantially independent of the motorcycle model itself. Since only the updates to the checks from earlier work (Sharp and Limebeer, 2001) are described, it is suggested that the interested reader consults this paper as well as the modelling code that is located at the website
http://www.ee.ic.ac.uk/control/motorcycles.

The underlying principles behind the checks are that under equilibrium conditions:

- the external forces acting on the motorcycle-rider system must match the sum of the inertial and gravitational forces,

- the external moments acting on the motorcycle-rider system must sum to zero and
- the power supply and dissipation must be equal.

5.2.1 The force balance

The force balance check ensures that under equilibrium cornering conditions the sum of the external forces is equal to the sum of the inertial and gravitational forces. To check the balance, the force error

$$\boldsymbol{F}_{error} = \sum_i \boldsymbol{F}_i^{ext} + \left(\sum_j m_j\right)(\boldsymbol{v} \times \boldsymbol{\omega} + \boldsymbol{g})$$

must be computed. The first sum contains the external forces, while the second sum contains the centripetal and gravitational forces. The $\boldsymbol{F}_i^{ext}$'s include: (i) The aerodynamic lift and drag forces, (ii) the front and rear wheel normal loads, (iii) the tyre side forces, and (iv) the longitudinal driving and braking forces that act on the wheels at the ground contact points. In the second term, the m_j's are the machine's constituent masses, $\boldsymbol{v}$ is the velocity of the mass centre of the main body, $\boldsymbol{\omega}$ is the main body yaw rate vector, and $\boldsymbol{g}$ is the gravitational acceleration vector. In the author's experience, one should achieve $|\boldsymbol{F}_{error}| < 4N$, although many of the constituent forces have magnitudes of several thousands of Newtons.

5.2.2 The moment balance

In a similar way, it is possible to check that under equilibrium cornering conditions a moment error vector is zero. We compute:

$$\boldsymbol{M}_{error} = \sum_i \boldsymbol{l}_i \times m_i(\boldsymbol{v} \times \boldsymbol{\omega} + \boldsymbol{g}) + \sum_j \boldsymbol{l}_j \times \boldsymbol{F}_j + \sum_k \boldsymbol{M}_k.$$

The reference point for all the moment calculations is the rear-wheel ground contact point. The $\boldsymbol{l}_i$'s are moment arm vectors that point from the reference point to the appropriate mass centres and $m_i(\boldsymbol{v} \times \boldsymbol{\omega} + \boldsymbol{g})$ are the corresponding inertial and gravitational forces. The index i ranges over each of the constituent masses. The second term contains all the external force-induced moments including: (i) the aerodynamic lift and drag forces, (ii) the front wheel normal load, (iii) the front wheel lateral tyre forces and the (iv) the front tyre longitudinal force. The $\boldsymbol{l}_j$'s are moment arms that point from the reference point to the points of application of the various forces. The third term contains the gyroscopic moments due to the rates of change of angular momentum of the spinning road wheels under cornering, and the tyre moments. In the author's experience, one should achieve $|\boldsymbol{M}_{error}| < 5Nm$, although some of the constituent moments have magnitudes of several thousand Newton-metres.

5.2.3 The power audit

This check is based on a "conservation of power" audit. The power source is the engine and the power developed at the rear wheel is simply

$$P_{rear} = M_{rear}\omega_{rear}.$$

where ω_{rear} is the angular speed of the rear wheel. The most important dissipators are the aerodynamic forces and are given by

$$P_{aero} = -\text{dot}((\boldsymbol{F}_{drag} + \boldsymbol{F}_{lift}), \boldsymbol{v}_{main})$$

where dot$(\cdot,\cdot)$ represents a dot product between the relevant vectors. v_{main} is the velocity of the rear frame assembly. Not surprisingly, a reliable checking process necessitates the inclusion of other effects to do with the tyre forces and moments. The tyres dissipate power via the longitudinal and lateral slip forces and this power dissipation is, in each case, computed via a dot product of the form $\boldsymbol{F} \cdot \boldsymbol{v}$ in which $\boldsymbol{F}$ is the force applied to the tread base material and $\boldsymbol{v}$ is the corresponding velocity[3]. The longitudinal component of this velocity is the machine velocity multiplied by the tyre's longitudinal slip, while the lateral component is the machine velocity multiplied by the tangent of the tyre side-slip angle. The remaining dissipation effects are associated with the tyres' aligning moments. These dissipation effects can be computed using expressions of the form $\boldsymbol{M} \cdot \boldsymbol{\omega}$ in which the $\boldsymbol{M}$'s are the aligning moments and the $\boldsymbol{\omega}$'s are the wheel's angular velocity vectors. The experience has been that the power checksum error should be no more than 100 W even if the power produced by the engine could reach 65 kW. Checks that achieve higher accuracy (smaller error in the checksum) will be described later.

5.3 Conclusions

The model presented here is believed to be the most comprehensive motorcycle model in the public domain. The basis of this model has been described elsewhere (Sharp and Limebeer, 2001), and it is suggested that this paper is consulted in conjunction with the current Chapter for completeness. For further details, the reader is also referred to the AUTOSIM code that can be found at the website: http://www.ee.ic.ac.uk/control/motorcycles/. This code contains much fine detail that is only discussed briefly here. The code also contains a complete list of the motorcycle parameters, most of which are the same as those in (Sharp and Limebeer, 2001). The symbolic multibody modelling tool AUTOSIM (Anon., 1998) can be used to obtain the full nonlinear model in a FORTRAN (or C) code that is used to produce the nonlinear simulation results. The small perturbation linearised model can also be obtained as a MATLAB M-file, containing the state space matrices in symbolic form, for the investigation of the local stability of the open loop system via eigenvalue type studies. The complexity of the model allows to some extent general equilibrium conditions to be considered such as steady cornering, whereby the equilibrium states are obtained from nonlinear simulations of the closed loop system. The drive and steering controllers are not connected to the rider control actions in that case but merely they provide the solving algorithm for the nonlinear equations of motion. Both the symbolic state space matrices and equilibrium states are required to quantify the system eigenvalues associated with some operating condition. The present model is the one that will be used in subsequent chapters.

[3]The required velocity is that of a material point of the tyre that is currently the nominal contact point. This material point changes continuously as the wheel rotates.

Chapter 6

Animation of the ‘SL2001” motorcycle model

Animations are a valuable aid in the visualisation of complicated motions. A methodology for fulfilling animation tasks in connection with AUTOSIM will be described next. The motorcycle under study is that presented in the previous chapter.

6.1 Program codes

As shown in Figure 6.1, two files are required to run the animation: the parsfile and the simulation file. The first file is a keyword-based text file that contains the definitions of all the parts of the model, their shape information and other information such as program settings. Typically,

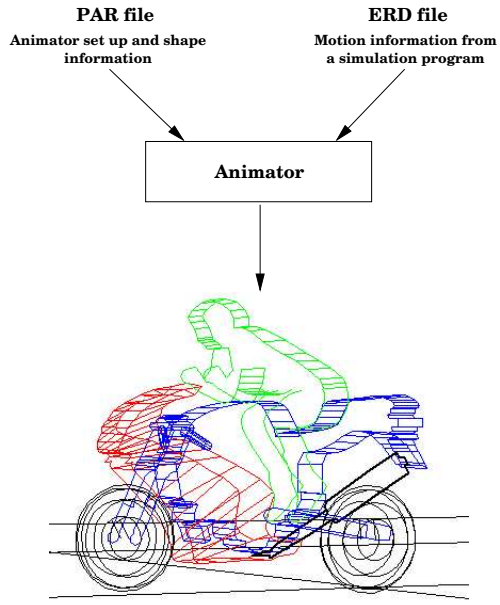

Figure 6.1: Animator input fi les.

this file has the extension PAR. The simulation file, which is an ERD file generated by AUTOSIM, contains the simulation responses in global coordinates[1]. In general, the motion of each body requires three translational data sequences and three rotational data sequences. These responses are used by the animator to drive the various parts of the motorcycle as defined in the parsfile.

6.1.1 Parsfile

The animator creates images that are based on a set of visible objects that include a grid and wire-frame shapes that are defined via a sequence of connected lines. Some of the wire-frame objects are organised into groups that move together. A group of points and objects that maintain a fixed relationship to each other (i.e. that constitute a rigid body) is called a reference frame. Although a reference frame might move and rotate, the spatial relationships between the objects in the reference frame do not change relative to each other. In the animator all motions are associated with reference frames and their movement is defined by up to six variables from the ERD file (three translational freedoms and three rotations (Euler angles) in global coordinates). The reference frames that are used to define the motorcycle model are shown in Figure 6.2. Each reference frame has associated with it a group of shapes that are used to build up a detailed

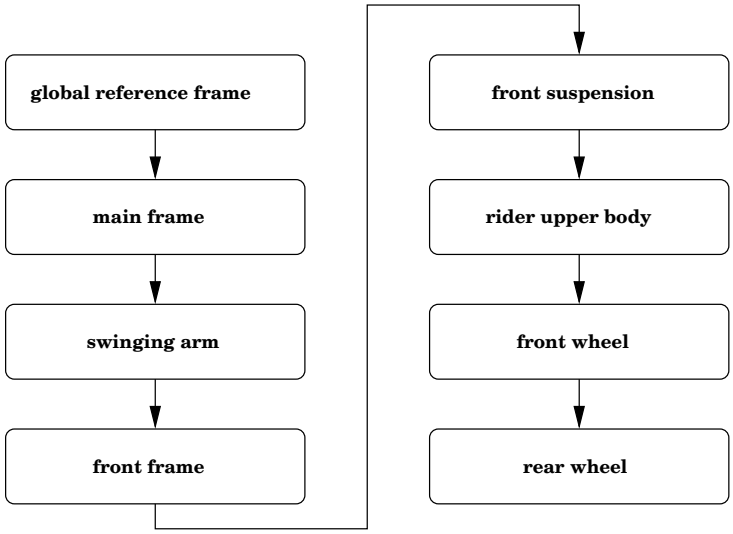

Figure 6.2: Reference Frames of the motorcycle.

visual representation of the motorcycle. As the inputs to the animator are processed, each shape is moved along with its particular reference frame. As the animator is reading input data, the active reference frame and its associated shapes are moved with that frame.

A shape is a set of points connected by straight lines and each point is defined by a set of

[1]The body of the simulation responses in reality is stored in a separate BIN file, also generated by AUTOSIM. Both the ERD and the BIN files are needed by the animator, and when an ERD file is mentioned subsequently both of these files are implied.

three coordinates (X-Y-Z). The animator starts with the first point and draws connecting lines to each of the following points in the list. All the coordinates are assumed to be in a local coordinate system that is associated with the active reference frame. Figure 6.3 shows the shapes associated with each reference frame.

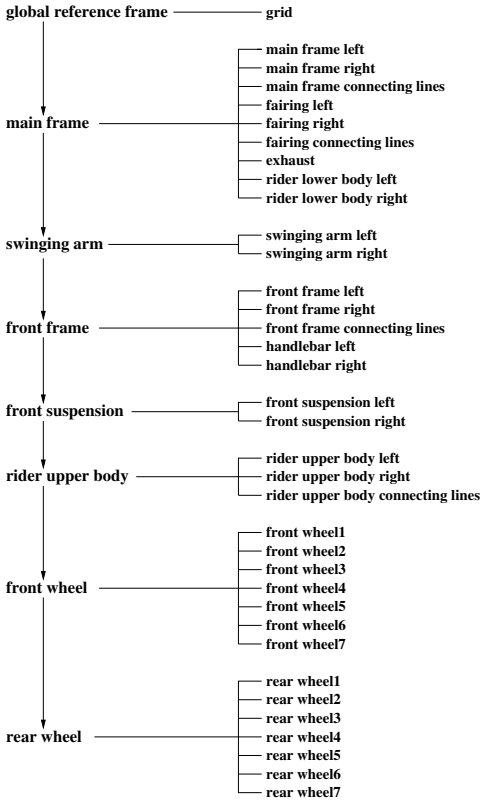

Figure 6.3: Groups of shapes.

The axis orientation used by the animator follows the ISO 8855 standard instead of SAE J670e used by AUTOSIM. ISO 8855 has X pointing forwards, Z pointing upwards and Y pointing towards the left-hand side of the vehicle. In contrast, SAE J670e has Z pointing downwards, X pointing forwards and Y pointing towards the right-hand ride on the vehicle. All coordinates in the output file are in SI units if units have been set to "SI" in the AUTOSIM LISP code. Both variable and static coordinates can be converted using scale factors. All animator Euler angles must be expressed in degrees and so scale factors are used to convert the Euler angles generated by AUTOSIM to degrees, since the variables in the ERD file are in radians. If, however, `(si)` is replaced by `(mks)` in the AUTOSIM code angles will be in degrees.

The parsfile commands[2] are described next and it is recommended that the reader studies these in conjunction with the motorcycle parsfile `bk_sl2001.par`.

- Add the 2D ground-plane grid:

[2]Typically, each line in the parsfile starts with a keyword followed by the associated value.

Keyword	Value	Description
`add_grid`	<none>	tells animator to draw a reference grid
`set_interval_x` `set_interval_y`	numbers	spacing used for drawing the grid lines
`set_color`	color name	color used for the grid lines

`set_min_x`
`set_max_x`
`set_min_y`
`set_max_y`
	numbers	size of the grid in the X and Y directions

Table 6.1: Keywords for describing the grid

A grid fixed in the global reference frame is drawn. Table 6.1 lists the keywords for describing the grid.

- Specify the camera settings:

  The camera point determines the location of the observer and the look point determines the point that the camera is aimed at. Both of these points are shown in Figure 6.4. At each

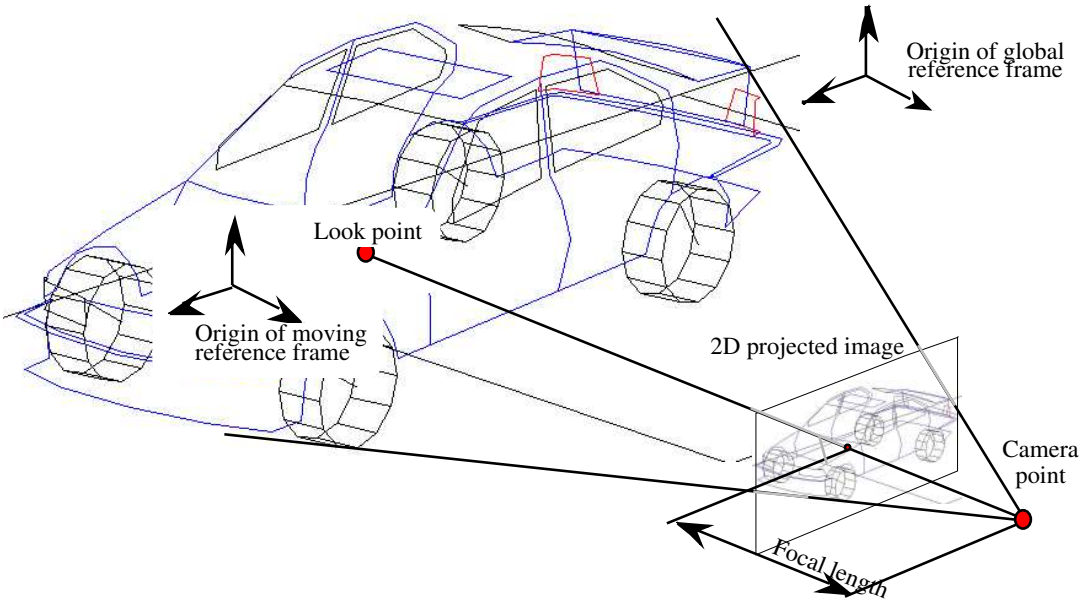

Figure 6.4: Geometry of the camera point and the look point (Anon., 1997*a*).

time instant, the animator generates a 2D image based on the relationships between the location and orientation of the simulated vehicle and the camera and look points. Table 6.2 lists the keywords that are used to specify the camera settings.

- All the reference frames with all the shapes associated with them as shown in Figure 6.3 are added by making use of the keywords in Table 6.3.

Keyword	Value	Description
set_camera_reference_frame	name of reference frame	reference frame in which the camera is situated
set_camera_x set_camera_y set_camera_z	numbers	coordinates of the camera location in its reference frame
set_lookpoint_reference_frame	name of reference frame	reference frame in which the look point is situated
set_lookpoint_x set_lookpoint_y set_lookpoint_z	numbers	coordinates of the look point in its reference frame
set_focal_length	number	focal length of camera (distance from point of viewer to 2D image on screen)
set_use_cpu_clock	on or off	option to slow animation down to real time by using the clock
set_superimpose	on or off	option to superimpose all images–don't erase between animation frames

Table 6.2: Keywords for the animator camera settings

The keyword add_reference_frame has three effects:

(a) It starts the scope of a new reference frame.

(b) It ends the scope of the previous one.

(c) It assigns a name to the new frame that can be used with the set_camera_reference_frame and set_lookpoint_reference_frame keywords. Each reference frame must have a unique name.

All of the keywords shown in Table 6.3 are repeated several times in the parsile. Each time the value associated with the keyword is applied, the current reference frame is affected.

The position of a reference frame is defined by six variables: the three coordinates (X, Y, and Z), and three Euler angles. The animator reads the six variables from the output files generated by the simulation. The six keywords used to specify the ERD file short names determine how the three coordinates and the three Euler angles are defined. After reading the six variables, each coordinate and Euler angle is calculated via a relationship of the form:

$$\text{coordinate} = C_o + C^*SF_c$$

$$\text{angle} = A_o + A^*SF_a$$

where C and A are the translation and angle variables obtained from the ERD file. The constants C_o and A_o are offsets while SF_a and SF_c are scale factors (gains). The offsets

Keyword	Value	Description
add_reference_frame	name of new reference frame	gives name to new reference frame and starts its scope
set_x_name set_y_name set_z_name	names of variables in ERD file	specifies the variables to be read from the ERD file and associated with X,Y,Z coordinates of the reference frame
set_pitch_name set_roll_name set_yaw_name	names of variables in ERD file	specifies the variables to be read from the ERD file and associated with Euler angles
set_scale_var_x set_scale_var_y set_scale_var_z set_scale_var_roll set_scale_var_pitch set_scale_var_yaw	numbers	scale factors for data read from the ERD file
set_offset_var_x set_offset_var_y set_offset_var_z set_offset_var_roll set_offset_var_pitch set_offset_var_yaw	numbers	offsets added to coordinates and Euler angles
set_euler_angles	yaw_pitch_roll or yaw_roll_pitch	sequence of rotation by Euler angles used to define orientation of the reference frame

Table 6.3: Keywords associated with reference frames

and scale factors are specified by the keywords shown in Table 6.3. The scale factors are often used to convert angles from radians to degrees. The keyword `set_euler_angles` is used to specify the type of transformation used. There are two options: `yaw_roll_pitch` is used for rolling-wheel reference frames and `yaw_pitch_roll` is used for all the other vehicle reference frames.

Within the scope of a particular moving frame, the associated parts (shapes) are specified. A part is a set of points connected by straight lines. Each point is defined by a set of three coordinates (X-Y-Z). The animator starts with the first point and draws a connecting line to the second point and so on to the last point in the list. All the coordinates are assumed to be in a local coordinate system associated with the active reference frame. The keyword `add_part` has the effect of starting the scope of a new object. It also has the effect of ending the scope of the previous object. However, it does not affect the scope of the current moving reference frame. All the keywords relevant to shapes are defined in Table 6.4. The list of coordinates begins with a line containing the keyword `set_coordinates`. Each following line contains X, Y, and Z coordinates, separated by

Keyword	Value	Description
`add_part`	name of part	starts scope for new part
`set_color`	color name	color used for lines drawn to connect the points in this part
`set_line_width`	integer	sets thickness of lines drawn for this part
`set_coordinates` `end_coordinates`	list of coordinates: 3 numbers per line	coordinates of the points making up the shape

`set_scale_x`
`set_scale_y`
`set_scale_z`
	numbers	scale factors applied to all coordinates in the part

`set_offset_x`
`set_offset_y`
`set_offset_z`
	numbers	offsets added to all points in the part

Table 6.4: Keywords for describing parts

white space, until the list ends with a line containing the keyword `end_coordinates`. The listed coordinates for the part are transformed by the equations:

$$x_{new} = x_o + s_x\, x$$

$$y_{new} = y_o + s_y\, y$$

$$z_{new} = z_o + s_z\, z$$

where x_o, y_o, and z_o are offsets and s_x, s_y, and s_z are scale factors specified with the keywords `set_offset_x`, `set_offset_y`, `set_offset_z`, `set_scale_x`, `set_scale_y` and `set_scale_z`.

6.1.2 Example reference frame

The purpose of this section is to show how each motorcycle component is inserted one-by-one into the animation. The front wheel is used to explain the procedure. The remaining components are added in a similar manner using the ideas of reference frames, shapes and global coordinates.

To begin, it should be noted that each of the wheels is made up of a number of parts that are assembled using the `add_part` keyword. As indicated in Figure 6.3, the wheels are made up of seven circles of different diameters in parallel planes. The diameters are chosen to correctly represent the tyre cross-sectional profiling. In the parsfile given here, the first part is the central circle. Copies of this circle are then scaled and shifted to generate the other six. These seven parts can then be grouped together under the front wheel reference frame to form the front wheel. The origin of this reference frame is at the centre of the detached wheel as shown in Figure 6.5. The shapes that make up the front wheel are designed so that the centre of the wheel is at the centre of the reference frame. The reason for this is that all the Euler angles of the reference frame are defined as rotations about axes through the origin of the current reference frame. It is

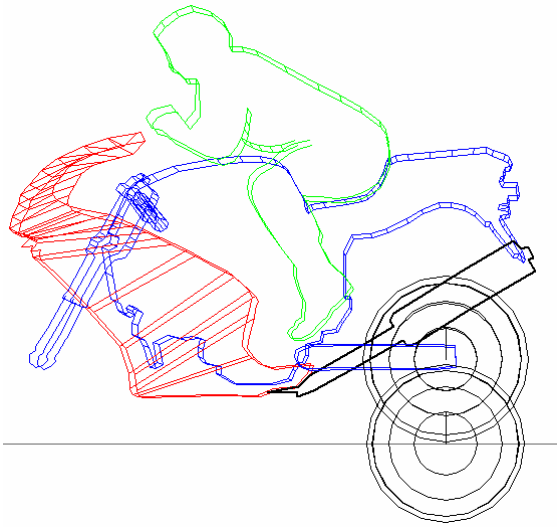

Figure 6.5: Front wheel example.

essential that this setup is made precisely compatible with the AUTOSIM code that will be used to generate the data that drives the animation. For example, this means that if the front wheel is to be designed to rest on the ground plane in the nominal configuration, in the same way that the rear wheel does in Figure 6.5, then the pitch rotation will rotate the wheel around the ground contact point and not the wheel hub. Any yawing rotation must occur around the wheel centre. Once all the reference frame constituent parts have been designed with the same considerations in mind, appropriate output variables in the ERD file are linked to the reference frame in order that it is driven properly. In the present case each reference frame uses the AUTOSIM origin of the relevant body as its (0,0,0) point, because this makes it easy to link to the driving variables that are stored in the ERD file. Obviously, the final aim is to create an image of the motorcycle that has all its components correctly dimensioned and correctly placed in relation to each other through the motion being studied. In the case of the front wheel, the output variables are `fw_xo`, `fw_yo` and `fw_zo` for the translational movements, while `fw_rol`, `fw_pit` and `fw_yaw` are used for the roll, pitch and yaw rotations respectively. These variables are calculated by the simulation programme that is derived from the AUTOSIM lisp code. The lisp commands that are used to find the animator driving variables in global coordinates are discussed next.

6.1.3 Lisp code

The following lisp instructions must be added to `bk_sl2001.lsp` code that describes the "SL2001" model. These commands are used to calculate the output variables needed by the animator:

- Main frame:

```
(setsym main_x "dot(pos(yaw_fr0,n0),[nx])")
(setsym main_y "-dot(pos(yaw_fr0,n0),[ny])")
```

```
(setsym main_z "-dot(pos(main0,n0),[nz])")

(setsym main_yaw   "-rq(yaw_fr)")
(setsym main_pit   "-rq(mb1)")
(setsym main_rol   "rq(main)")

(add-out "@main_x" "main_x")
(add-out "@main_y" "main_y")
(add-out "@main_z" "main_z")

(add-out "@main_yaw"  "main_yaw")
(add-out "@main_pit"  "main_pit")
(add-out "@main_rol"  "main_rol")
```

The `setsym` commands define the global variables required by the animator and the `add-out` commands add them to the output variables that are stored in the ERD file. The first three lines take the projections of the position vector between the origin of the `yaw_frame` (or `main`) and the origin of the inertial frame in the three standard directions. These projections are used to calculate the three translational coordinates in the global reference frame `n`. The next three lines define the global angles of rotation of the main frame. The y-component and z-component of position and two of the angles of rotation have minus signs, because the orientations of the axes in the animator and AUTOSIM follow different standards. Note that some of the variables are already calculated by AUTOSIM as standard outputs. However, these variables have been redefined for completeness. The remaining bodies are treated in much the same way.

- Swinging arm:

```
(setsym swg_arm_x "dot(pos(swg_arm0,n0),[nx])")
(setsym swg_arm_y "-dot(pos(swg_arm0,n0),[ny])")
(setsym swg_arm_z "-dot(pos(swg_arm0,n0),[nz])")

(setsym swg_arm_yaw   "-euler(swg_arm,1,n)")
(setsym swg_arm_pitch "-euler(swg_arm,2,n)")
(setsym swg_arm_roll  "euler(swg_arm,3,n)")

(add-out "@swg_arm_x" "sa_x")
(add-out "@swg_arm_y" "sa_y")
(add-out "@swg_arm_z" "sa_z")

(add-out "@swg_arm_roll"  "sa_rol")
(add-out "@swg_arm_pitch" "sa_pit")
(add-out "@swg_arm_yaw"   "sa_yaw")
```

AUTOSIM uses the `yaw_pitch_roll` convention when calculating Euler angles via the `euler` command.

- Rider upper body:

```
(setsym ubr_x "dot(pos(ubr0,n0),[nx])")
(setsym ubr_y "-dot(pos(ubr0,n0),[ny])")
(setsym ubr_z "-dot(pos(ubr0,n0),[nz])")

(setsym ubr_rol "rq(main)+rq(ubr)")

(add-out "@ubr_x" "ubr_x")
(add-out "@ubr_y" "ubr_y")
(add-out "@ubr_z" "ubr_z")

(add-out "@ubr_rol" "ubr_rol")
```

  In the case of the rider's upper body it is only necessary to calculate the roll angle, because the pitch and yaw angles for this body are the same as those used for the main frame. We observe that the roll angle is the sum of the roll angle of the main frame and the roll angle of the rider's upper body with respect to the main frame. It is possible to simply sum up these angles, because the series of Euler angles used is `yaw_pitch_roll` and roll is the last rotation.

- Front frame:

```
(setsym ff_x "dot(pos(ff_str0,n0),[nx])")
(setsym ff_y "-dot(pos(ff_str0,n0),[ny])")
(setsym ff_z "-dot(pos(ff_str0,n0),[nz])")

(setsym ff_yaw "-euler(ff_str,1,n)")
(setsym ff_pit "-euler(ff_str,2,n)")
(setsym ff_rol "euler(ff_str,3,n)")

(add-out "@ff_x" "ff_x")
(add-out "@ff_y" "ff_y")
(add-out "@ff_z" "ff_z")

(add-out "@ff_yaw" "ff_yaw")
(add-out "@ff_pit" "ff_pit")
(add-out "@ff_rol" "ff_rol")
```

  The front frame variables are calculated as before.

- Front suspension:

```
(setsym ff_sus_x "dot(pos(ff_sus0,n0),[nx])")
(setsym ff_sus_y "-dot(pos(ff_sus0,n0),[ny])")
(setsym ff_sus_z "-dot(pos(ff_sus0,n0),[nz])")

(add-out "@ff_sus_x" "ffsu_x")
(add-out "@ff_sus_y" "ffsu_y")
(add-out "@ff_sus_z" "ffsu_z")
```

It is not necessary to calculate the Euler angles of the front suspension because they are the same as those of the front frame.

- Rear wheel:

```
(setsym rw_xo "dot(pos(rw0,n0),[nx])")
(setsym rw_yo "-dot(pos(rw0,n0),[ny])")
(setsym rw_zo "-dot(pos(rw0,n0),[nz])")

(setsym rwlong   "cross([swg_army],[nz])")
(setsym rw_rol   "angle(dplane([swg_army],[nz]),[swg_army],@rwlong)")
(setsym rw_pit_i "angle(@rwlong,[swg_armx],[swg_army])")
(setsym rw_pit   "-(-@rw_pit_i+rq(rw))")

(add-out "@rw_xo" "rw_xo")
(add-out "@rw_yo" "rw_yo")
(add-out "@rw_zo" "rw_zo")

(add-out "@rw_rol" "rw_rol")
(add-out "@rw_pit" "rw_pit")
```

It will be noted that the scheme here is different from the previous one used to calculate the Euler angles, since these now involve angles that are outside the range $\pm\pi$. In particular, the pitch angle of the wheel undergoes angular wind-up (it keeps rotating in one direction and consequently the pitch angle continues to grow). It can be seen that roll angle is calculated from first principles (it is different from the roll angle of the main frame since the series of rotations for the wheels is `yaw_roll_pitch`.). The quantity -`rw_pit_i` is the initial pitch angle of the wheel produced by the rotation of the swinging arm. The pitch angle of the wheel is consequently the sum of this angle and `rq(rw)`. The negative sign is required because AUTOSIM and the animator use different standards. The yaw angle of the wheel need not be calculated because it is the same as that of the main frame.

- Front wheel:

```
(setsym fw_xo "dot(pos(fw0,n0),[nx])")
(setsym fw_yo "-dot(pos(fw0,n0),[ny])")
(setsym fw_zo "-dot(pos(fw0,n0),[nz])")
```

```
(setsym fwlong   "cross([ff_susy],[nz])")
(setsym fw_rol   "angle(dplane([ff_susy],[nz]),[ff_susy],@fwlong)")
(setsym fw_pit_i "angle(@fwlong,[ff_susx],[ff_susy])")
(setsym fw_pit   "-(-@fw_pit_i+rq(fw))")

(add-out "@fw_xo" "fw_xo")
(add-out "@fw_yo" "fw_yo")
(add-out "@fw_zo" "fw_zo")

(add-out "@fw_rol" "fw_rol")
(add-out "@fw_pit" "fw_pit")
```

6.1.4 Running the animator

To run the animator the following items are needed:

- The animator executable file `animator.exe` (this can be downloaded from the author's website http://www.ee.ic.ac.uk/control/motorcycles).
- The parsile `bk_sl2001.par` (this can be downloaded from the same website).
- The simulation files `example.erd` and `example.bin`. These files can be downloaded from the above website, or they can be generated by patching the Lisp code `bk_sl2001.lsp`. The instructions that generate the required data in global coordinates should be placed just before the `(finish)` command. A new data file must be generated by loading the modified AUTOSIM code and running the associated simulation file.

The animation can be run as follows:

- Start the animator by running the executable file `animator.exe`.
- Go to the *file* roll-down menu in the animator window, click on *Open Parsfile* and select the parsfile `bk_sl2001.par`.
- Find and select the ERD file (`example.erd`) in the same window.
- After all the files are loaded the animation can be started by going to the *Animation* roll-down menu and clicking on *Start From Beginning*.

Part III

Results

The theoretical techniques that have been presented will now be employed for the investigation of the stability of motorcycles under acceleration and deceleration, and the effects on motorcycle stability from road forcing. These issues are treated in Chapters 7 and 8 respectively. The work presented was also covered in (Limebeer *et al.*, 2001) and (Limebeer *et al.*, 2002).

Chapter 7

The stability of motorcycles under acceleration and braking

The dynamic properties of single-track vehicles under acceleration and deceleration have not received much attention in the literature, and as far the present author is aware, the only work in this area is that given in (Sharp, 1976*b*). The analysis techniques employed in that study were introduced earlier in the context of the jack-knifing of articulated vehicles (Hales, 1965), but by contemporary standards these are simplistic because they only consider the 'inertial effects' of acceleration. Also, the vehicle model used was simple and the absence of a suspension system meant that the effects of acceleration on the tyre loads were not treated accurately. A further weakness was that the influence of load on the tyre shear forces was not known with any precision.

In the present chapter an attempt is made to evaluate the dynamic behaviour of motorcycles under acceleration and deceleration using modern theoretical techniques. The main focus is on the behaviour of the wobble and weave modes and the motorcycle model employed is the one described in Chapter 5.

7.1 Stability/instability of time varying systems

Mathematical models of motorcycles under acceleration and deceleration are time varying systems and special methods are required to examine their dynamic stability properties. The purpose of this short section is to review briefly some of the stability/instability properties of time-varying systems.

It is well known that the nth-order order differential equation:

$$\dot{\boldsymbol{x}}(t) = \boldsymbol{A}\boldsymbol{x}(t) \qquad \boldsymbol{x}(0) = \boldsymbol{x}_o,$$

has solution:

$$\boldsymbol{x}(t) = \sum_{i=1}^{n} w_i e^{\lambda_i t} v_i^* \boldsymbol{x}_o$$

in which the λ_i's are the eigenvalues of the constant matrix $\boldsymbol{A}$ ($\boldsymbol{A}$ is assumed to be diagonalisable) (Strang, 1988), and the w_i's and v_i's are the corresponding eigenvectors and dual eigenvectors respectively. These solutions will vanish asymptotically if $Re(\lambda_i) < 0$. In other words, for an arbitrary $\boldsymbol{x_o}$ the solutions of this equation converge to zero *if* (*and only if*) all the eigenvalues of $\boldsymbol{A}$ have negative real parts. In general, the stability properties of linear time varying systems cannot be tested using the eigenvalues in this way. For example, the matrix

$$\boldsymbol{A}(t) = \begin{bmatrix} -1 & e^{2t} \\ 0 & -1 \end{bmatrix}$$

has both its eigenvalues at -1 for all t, but the corresponding system $\dot{\boldsymbol{x}}(t) = \boldsymbol{A}(t)\boldsymbol{x}(t)$ is unstable in the sense that for some initial conditions $\lim_{t\to\infty}\boldsymbol{x}(t)$ is unbounded (Kailath, 1980). Therefore, in general, there is no significance to the concept of a 'mode', or a 'time varying natural frequency' in the case of time-variant linear systems. Consider:

$$\dot{\boldsymbol{x}}(t) = \boldsymbol{A}(t)\boldsymbol{x}(t), \qquad \boldsymbol{x}_o = \boldsymbol{x}(0).$$

Provided $\dot{\boldsymbol{A}}(t)$ is small enough for all $t \geq 0$, it would be expected intuitively that the time-varying system will be stable provided that for each frozen time $\bar{t}$, the (frozen-time) system $\boldsymbol{A}(\bar{t})$ is stable. It is known (Desoer, 1969) that if the eigenvalues of $\boldsymbol{A}(t)$ have real parts that are sufficiently negative for all $t \geq 0$, and $\sup_{t\geq 0}\|\dot{\boldsymbol{A}}(t)\|$ is sufficiently small, then the solutions of $\dot{\boldsymbol{x}}(t) = \boldsymbol{A}(t)\boldsymbol{x}(t)$ go to zero as $t \to \infty$.

There might also be trouble when predicting instability using the frozen-time eigenvalues of $\boldsymbol{A}(t)$. If $\boldsymbol{A}(t)$ has at least one frozen-time eigenvalue with positive real part, the solutions of $\dot{\boldsymbol{x}}(t) = \boldsymbol{A}(t)\boldsymbol{x}(t)$ may be stable. One would expect that if $\boldsymbol{A}(t)$ has eigenvalues in the right half plane, then the system $\dot{\boldsymbol{x}}(t) = \boldsymbol{A}(t)\boldsymbol{x}(t)$ will have unbounded solutions if $\sup_{t\geq 0}\|\dot{\boldsymbol{A}}(t)\|$ is sufficiently small. This is indeed the case provided no eigenvalue crosses the imaginary axis (Skoog and Lau, 1972) as time changes. If eigenvalues are allowed to cross the imaginary axis, then even though there is always an eigenvalue with positive real part, the system can be asymptotically stable for arbitrarily small $\sup_{t\geq 0}\|\dot{\boldsymbol{A}}(t)\|$. Consider the matrix (Skoog and Lau, 1972)

$$\boldsymbol{A}(t) = \begin{bmatrix} -1 + \alpha\cos\omega t\sin\omega t & \alpha\cos^2\omega t + \omega \\ -\alpha\sin^2\omega t - \omega & -1 - \alpha\cos\omega t\sin\omega t \end{bmatrix}.$$

The corresponding transition matrix $\phi(t,t_0)$ is given by

$$\boldsymbol{\Phi}(t,t_o) = e^{-(t-t_0)}\begin{bmatrix} \cos\omega t & \sin\omega t \\ -\sin\omega t & \cos\omega t \end{bmatrix}\begin{bmatrix} 1 & \alpha(t-t_0) \\ 0 & 1 \end{bmatrix}\begin{bmatrix} \cos\omega t_0 & -\sin\omega t_0 \\ \sin\omega t_0 & \cos\omega t_0 \end{bmatrix}$$

and so with this $\boldsymbol{A}(t)$ all the corresponding equation solutions are exponentially bounded. It is easy to check that the eigenvalues of $\boldsymbol{A}(t)$ are time independent and given by

$$\lambda = -1 \pm \sqrt{-\alpha\omega - \omega^2}.$$

Setting $\omega = 1$ and $\alpha = -5$ the eigenvalues of $\boldsymbol{A}(t)$ are at $+1$ and -3 for all time. Note, however, that for any $\alpha < -2$, if

$$0 < \omega < -\frac{\alpha}{2} - \frac{1}{2}\sqrt{\alpha^2 - 4}$$

or

$$\omega > -\frac{\alpha}{2} + \frac{1}{2}\sqrt{\alpha^2 - 4},$$

then the eigenvalues of $\boldsymbol{A}(t)$ have negative real parts. Thus when $\boldsymbol{A}(t)$ is varying either slowly or rapidly, the eigenvalues of $\boldsymbol{A}(t)$ correctly predict the stability properties of the system. When ω lies between the aforementioned limits,

$$-\frac{\alpha}{2} - \frac{1}{2}\sqrt{\alpha^2 - 4} < \omega < -\frac{\alpha}{2} + \frac{1}{2}\sqrt{\alpha^2 - 4}$$

they do not.

The idea of a 'mode' will be used for the linear time varying systems and the eigenvalues of frozen-time linearised models will be used to infer stability properties, but it is recognised that this must be done with due caution.

7.2 Results

Root-loci and nonlinear simulation results are presented that show the effects of acceleration and deceleration on motorcycle stability. The main emphasis will be on the weave and wobble modes, as these are the dominant ones under the acceleration/deceleration conditions of interest here. The nonlinear simulation results come directly from the FORTRAN simulation codes generated by AUTOSIM. The root-locus plots are generated via the eigenvalues of frozen-time symbolic linearised state-space models (also generated by AUTOSIM). The evaluation of the linearised state-space model matrices requires information about the frozen-time values of the various model states—this information is provided by the nonlinear simulation codes. In order to generate a root-locus plot, the nonlinear simulation model is accelerated/decelerated over the speed range of interest. These data had to be checked to ensure: (a) that the rear wheel did not leave the ground (thereby indicating a stoppie), (b) that the front wheel did not leave the ground (thereby indicating a wheelie), (c) that the tyres did not undergo longitudinal saturation; and (d) that the engine power did not exceed 65 kW. The saturation condition was checked via the negativity, or otherwise, of the test force:

$$F_{check} = 0.8F_{load} + |F_{long}| \tag{7.1}$$

in which F_{load} is the tyre normal load and is always negative, while F_{long} is the tyre longitudinal force and can be positive or negative. If $F_{check} \geq 0$, the tyre was deemed to have saturated and the associated simulation data was disregarded. The root-locus plots that correspond to the constant-speed cases were generated by accelerating the machine very gradually over the speed range of interest.

7.2.1 Straight running on an incline

The results in this chapter begin by building on the intuitive ideas in (Hales, 1965) and (Sharp, 1976*b*). To do this, the stability properties of the machine on inclined surfaces are studied at constant speed. The idea is that ascending/descending inclined running surfaces generates gravitational forces that mimic the inertial forces associated with acceleration/deceleration conditions, respectively. It should also be noted that the constant-speed condition means that there is no temporal variation in the aerodynamic loading as the speed changes and that the associated linearised models are time-invariant. There is therefore no need to consider the complications associated with the stability testing, via the eigenvalues of frozen-time linearised models, of time-varying systems. Figure 7.1 shows root-locus plots for the cases of straight running, at constant speed, on both level and inclined smooth surfaces. The speed ranges associated with the various cases are dictated by the limiting conditions referred to above. The first thing to note is that the wobble mode is destabilised significantly on downhill (as opposed to uphill) inclinations. It can also be seen that the wobble mode is marginally more stable under rear-wheel-dominated braking. It is common experience that one should use rear-wheel-dominated braking on down-hill slopes at very low speeds, especially in slippery road conditions. Figure 7.1 also shows that inclined road surfaces have very little influence on the weave mode. At very low speeds, the weave mode forms at higher than usual speed under front-wheel dominated braking. Intuitively, this makes the machine harder to control under these conditions, because it tends to just 'fall over', rather than undergo an unstable low frequency oscillation. This could be the reason for the rider training advice that at very low speed the machine should be controlled by alternating the throttle and rear brake.

7.2.2 Acceleration studies

Figures 7.2, 7.3 and 7.4 consider the effects of acceleration on motorcycle stability. As expected, the general trends follow those associated with the results obtained for constant speeds on ascending slopes. The reason for this is that the inertial forces act in the same direction in the acceleration case as the gravity forces do in the uphill case. Figure 7.2 shows that the weave mode is hardly affected by the acceleration, while the wobble mode is substantially more heavily damped. These effects probably account for the good 'feel' associated with powerful machines under firm acceleration.

Figure 7.3 shows the effect of speed on the aerodynamic drag, the tyre loads, the drive torque and the rear tyre saturation. The aerodynamic drag increases quadratically with speed as does the required drive moment. The aerodynamic drag also tends to load the rear wheel, while correspondingly lightening the normal load on the front tyre. Also, as expected, the increased drive torque and longitudinal tyre force bring the rear tyre closer to saturation.

In Section 7.1 the reader was reminded that the stability of linear time-varying systems cannot be tested using the frozen-time eigenvalues of $\boldsymbol{A}(t)$ alone. With that warning in mind, the transient behaviour of the machine was examined with the nonlinear simulation model and

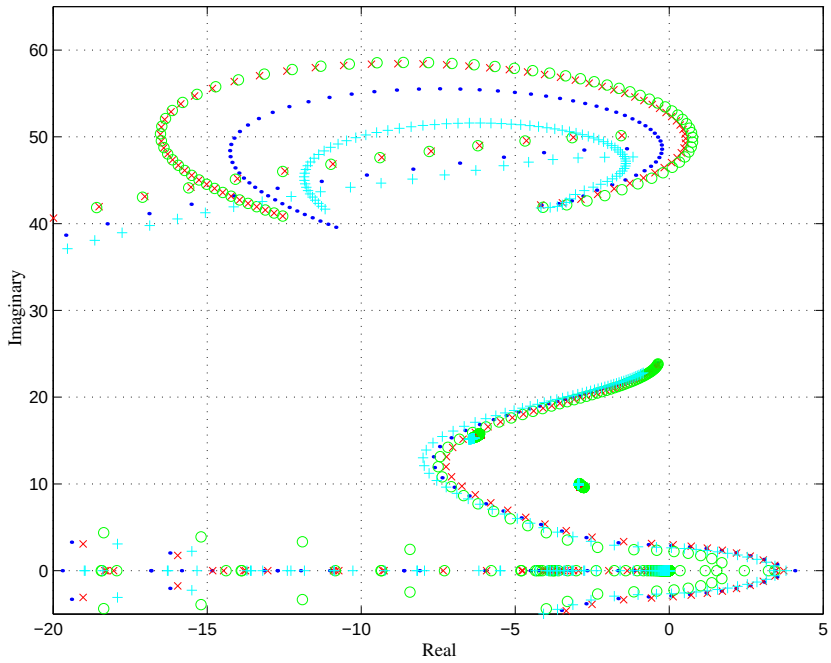

Plot symbol	Inclination angle (rad)	Front brake (%)	Rear Brake (%)	Speed range (m/s)
·	0	–	–	0.1–67.9
×	-0.2	10	90	0.06–70.0
o	-0.2	90	10	0.06–70.0
+	0.2	–	–	0.02–53.0

Figure 7.1: Root-loci for straight running on level and inclined smooth surfaces. Positive inclination angles correspond to the uphill case, whereas negative ones correspond to the downhill case.

compared with the outcomes predicted by the results given in Figure 7.2. By re-examining that plot it can be seen that the weave mode of the frozen-time model is unstable at time t_1, neutrally stable at t_2 and stable at t_3. The goal is to check that the nonlinear simulation model reproduces, qualitatively, that same behaviour. Given the approximations involved, it is unrealistic to expect exact quantitative agreement. Figure 7.4 shows the response of the nonlinear model to a steering angle offset of 0.1 rad at the unstable initial time t_1. This plot shows that an unstable behaviour builds up, and then decays over the time interval t_1 to t_2. The temporary growth appears to be dominated by the weave mode, and as predicted by the frozen-time model, the oscillations die out by the time t_2 is reached. As far as the weave mode is concerned, in this case the frozen-time linear model appears to be pessimistic in its predictions.

7.2.3 Deceleration studies

It has already been seen that downhill running tends to destabilise the wobble mode, while the weave mode remains relatively unaffected. One expects to see these trends reproduced in the

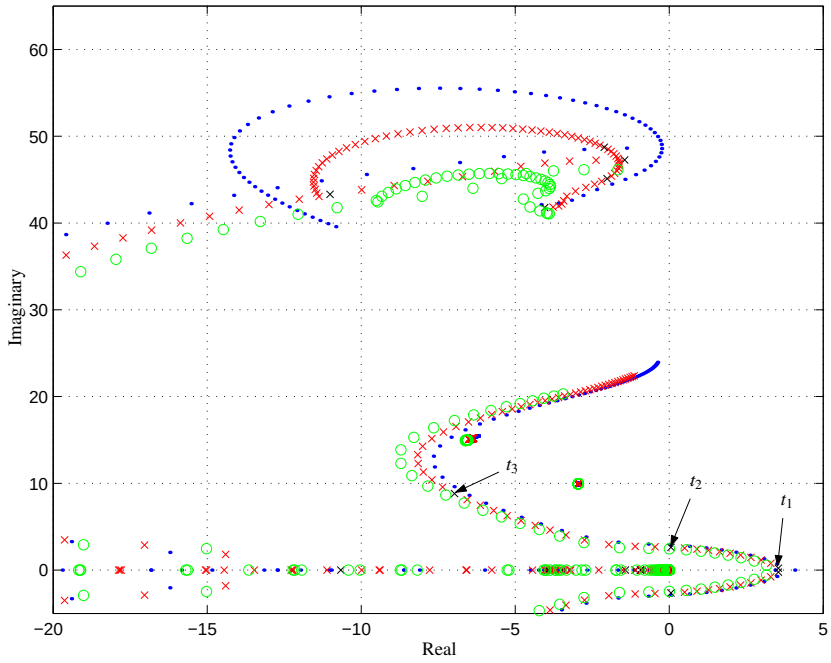

Plot symbol	Acceleration (m/s^2)	Speed range (m/s)
·	0	0.1–67.9
×	2.5	0.25–48.8
o	5.0	0.5–33.25

Figure 7.2: Root-loci for constant speed and steady acceleration on a level surface.

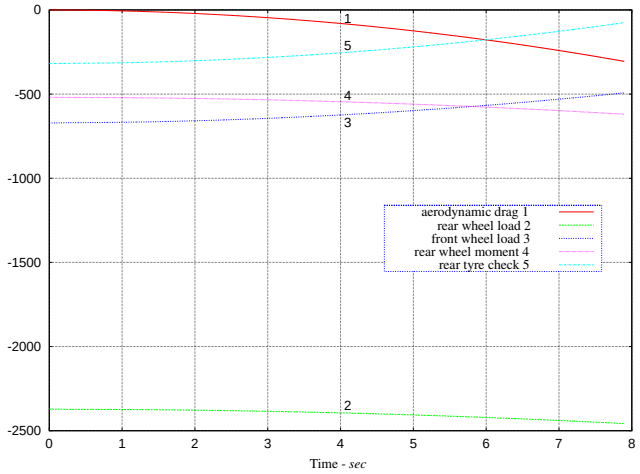

Figure 7.3: The wheel loads, the rear wheel drive moment, the aerodynamic drag and the rear wheel longitudinal tyre force check for the 5 m/s^2 acceleration case. All the forces are given in N, while the moment has units of Nm. The tyre force-check curve is also given in N.

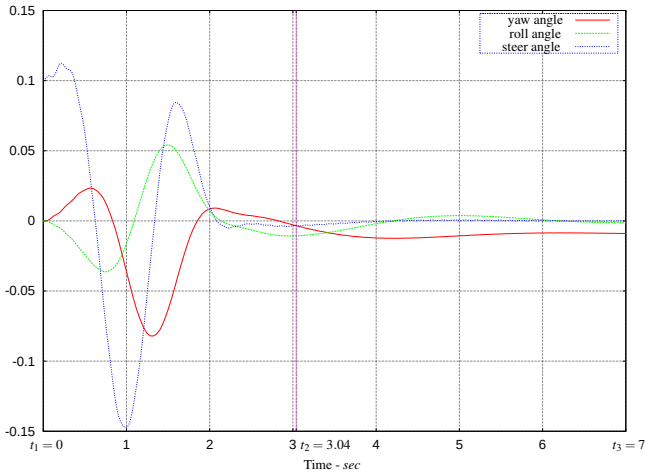

Figure 7.4: Transient response of the weave mode for the 2.5 m/s^2 acceleration case. The initial speed is 0.25 m/s and the initial steer angle offset is 0.1 rad; the speed at t_2 is 7.85 m/s, while that at t_3 is 17.75 m/s. The time origin corresponds to the point t_1 in Figure 7.2, and the other two time-marker points are labelled as t_2 and t_3.

deceleration studies, because the inertial forces in deceleration are equivalent to the gravitational forces in the downhill case. Figure 7.5 shows that these expectations are substantially true. It can be seen from this figure that the wobble mode becomes significantly less stable under braking and the effects become exaggerated as the deceleration rate increases. This figure also shows that the weave mode remains relatively unaffected by braking—as with the downhill case, the weave mode is affected most at very low speed. Figure 7.6 shows the anticipated changes in the wheel loads and wheel drive moments under braking. As expected, the bulk of the motorcycle's weight is carried by the front wheel, as is the bulk of the braking torque (under front-wheel-dominated braking). Note how the braking moment increases as the speed drops. This is explained by the fact that the aerodynamic drag does most of the high-speed braking, but this task is then taken over by the brakes as the aerodynamic drag reduces. Figure 7.7 is used to check the stability interpretations being given to the root-loci in Figure 7.5. As the speed decreases, the 2.5 m/s^2 wobble mode moves through the time markers t_1, t_2, t_3 and t_4 in that order. On the basis of the frozen-time root-locus analysis, the wobble mode is deemed unstable at t_1, neutrally stable at t_2 and stable at times t_3 and t_4. Figure 7.7 shows the response of the nonlinear model to a steer angle offset of 0.0001 rad applied at time t_1. As expected, the oscillations grow until t_3 and decay thereafter. This figure is therefore in qualitative agreement with Figure 7.5[1]. Figure 7.8 shows the response of the nonlinear simulation model to a small roll angle offset of 0.0005 rad that is applied at t_1 in Figure 7.5. The yaw angle, roll angle and steering head twist angle all show

[1]The author's supervisor has repeatedly noted a marked steering shimmy at about 60 mile/h under fi rm braking—this was not caused by disk run out! At the time he was riding a Kawasaki ZX-9R on Snetterton race track in Norfolk and was braking down from about 140 mile/h. This anecdotal evidence is in broad agreement with the theoretical results presented here.

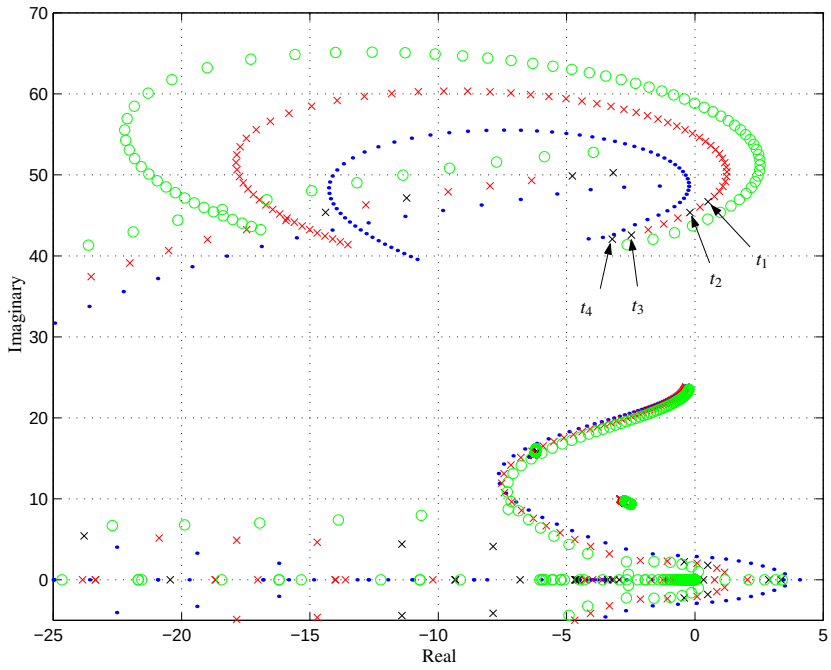

Plot symbol	Deceleration (m/s^2)	Front brake (%)	Rear brake (%)	Speed range (m/s)
·	0	–	–	0.1–67.9
×	2.5	90	10	70.0–0.126
o	5	90	10	70.0–0.8

Figure 7.5: Root-loci for constant speed straight running and steady rates of deceleration. A level surface is used throughout. Note the four time markers labelled t_1 to t_4.

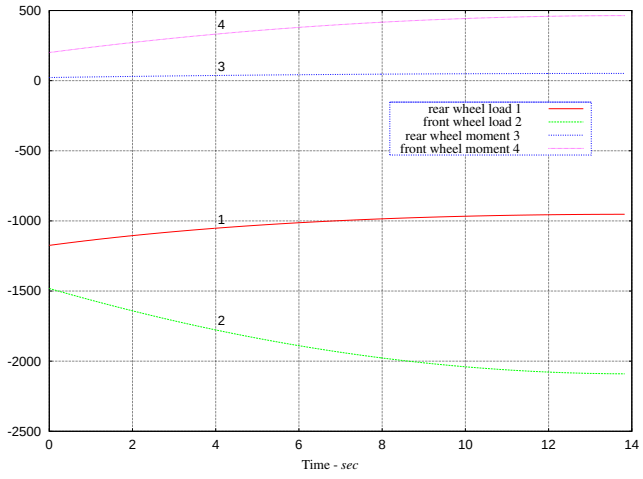

Figure 7.6: The normal wheel loads and drive/braking moments in the 5 m/s^2 deceleration case. The braking strategy is 90 per cent on the front wheel and 10 per cent on the rear. All the forces are given in N, while the moments have units of Nm.

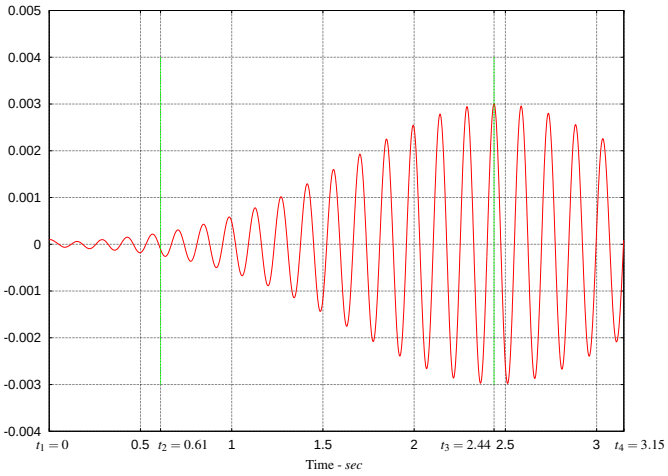

Figure 7.7: Transient response of the steering angle in the 2.5 m/s^2 deceleration case. The initial speed is 8 m/s and the initial steer angle offset is 0.0001 rad; the speed at t_1 is 8 m/s; the speed at t_2 is 6.48 m/s; the speed at t_3 is 1.9 m/s, while that at t_4 is 0.13 m/s. The time origin corresponds to the point t_1 in Figure 7.5 while the other three time-marker points are labelled t_2, t_3 and t_4.

clear evidence of both the wobble and weave modes. The high-frequency components have a frequency of roughly 7 Hz, or 44 rad/s, while the low frequency component is of the order 2 rad/s. By the time t_4 is reached, the wobble component appears to be dying out—this is most evident in the steering head twist angle. Again, these responses are all in qualitative agreement with the frozen-time linear model eigenvalue analysis. A similar set of conclusions can be drawn from Figure 7.9. The only difference between Figures 7.8 and 7.9 is the braking strategy. The first figure employs correct front-wheel-dominated braking, while the second plot corresponds to incorrect rear wheel braking. Figure 7.10 shows the wobble mode eigenvector components corresponding to the yaw, roll and twist angles. These plots show that the twist and yaw angle components are almost in phase, while the roll angle is almost in exact antiphase with the other two signals. These conclusions are in exact agreement with the phasing conclusions one derives from Figure 7.8 at times t_3 and t_4.

7.2.4 Braking strategies

Every serious motorcyclist knows that the correct use of the brakes is a vital constituent of competent and safe riding. In particular, excessive use of the rear brake should never be made when travelling at speed, especially if heavy braking is required in an emergency situation. This error is even more likely to end in mishap if one makes excessive use of the rear brake when banked over under cornering. In cases of mishap, the rear tyre ‘lets go’ and the rear end of the machine slides away, resulting in a loss of control. The question is whether this is simply a matter of rear tyre saturation, or if there is a stability issue associated with these incidents as

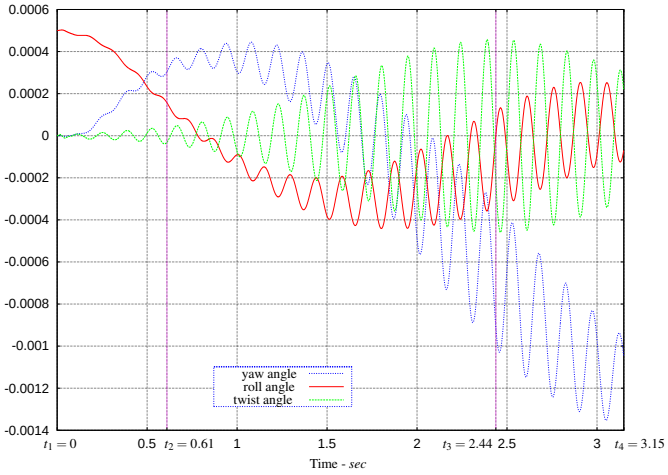

Figure 7.8: Transient behaviour of the weave and wobble modes for the 2.5 m/s^2 deceleration case with braking 90 per cent on the front and 10 per cent on the rear wheel. The initial roll angle offset is 0.0005 rad. The time labels t_1, t_2, t_3 and t_4 can be identified in Figure 7.5.

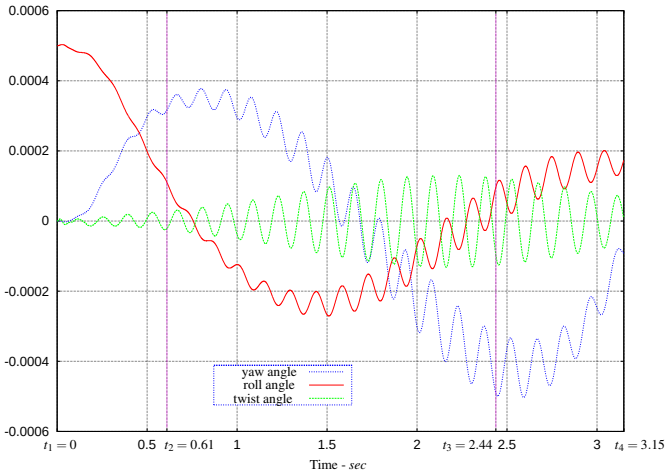

Figure 7.9: Transient behaviour of the weave and wobble modes for the 2.5 m/s^2 deceleration case with braking 10 per cent on the front and 90 per cent on the rear. The initial roll angle offset is 0.0005 rad. The time labels t_1, t_2, t_3 and t_4 can be identified in Figure 7.5.

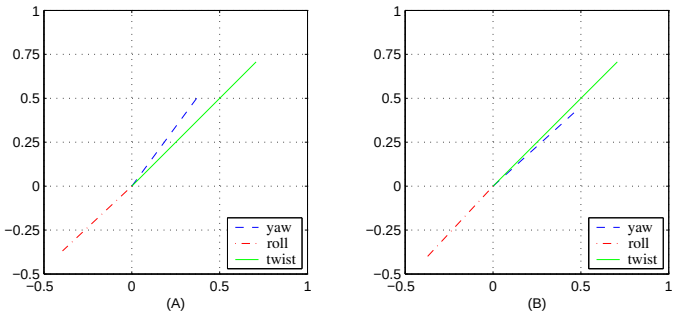

Figure 7.10: Wobble mode eigenvector components for the yaw, roll and twist angles at times (A) t_3 and (B) t_4 identified in Figure 7.5.

well.

Figure 7.11 shows a pair of root-locus plots for the 2.5 m/s^2 deceleration case. In one case, the front brake produces the bulk of the retarding moment, while in the other case, the rear brake is used. It can be seen from this plot that braking using the front wheel has a marginally greater destabilising effect on the wobble mode, while rear-wheel braking is to be preferred at very low speeds. The greater destabilising effect of front braking is obvious if Figures 7.8 and 7.9 are compared. In Figure 7.8, the amplitudes of the wobble mode components are bigger than those in Figure 7.9. The conclusion here is that the change in the braking strategy does not have a significant impact on the small amplitude machine stability.

Figure 7.12 examines the nonlinear system behaviour under more severe rear wheel braking at a deceleration rate of 5 m/s^2. It is clear from curves 1 and 2 that there is a significant load transfer from the rear tyre onto the front tyre and that this effect becomes exaggerated at lower speeds, owing to the reducing effects of aerodynamic loading.

Curves 3 and 4 show the longitudinal tyre-loading tests that are based on equation (7.1); the reader will recall that a tyre is deemed to have begun sliding if the associated tyre check quantity goes positive. The front tyre-check curve is seen to go more and more negative as the speed reduces—the front tyre performs its task easily under these conditions. This reduction is attributable to the fact that the front tyre load increases as the effects of aerodynamic braking reduce. The rear tyre-check curve is both more interesting and more alarming. First, it has a kink at just under 1s, and then goes positive at 8s, thereby indicating an impending mishap. The reason for the kink is as follows: at very high speed, even under deceleration, the machine has to be driven in order to overcome the effects of aerodynamic drag. At the kink, the need to drive the machine disappears and mild braking begins. Obviously, as the effects of aerodynamic drag reduce, it becomes necessary to apply increasing levels of braking moment in order to sustain the predetermined rate of deceleration. In other words, the reducing effect of aerodynamic drag acts to undermine the rear tyre in two ways. Firstly, as this drag reduces, the brakes (especially the rear brake) have to work harder. Secondly, as the drag reduces the normal load on the rear tyre reduces causing it to saturate. The strong well known message is that heavy braking must be done on the front brake. Under extreme track conditions, the rear brake should be used to do

little more than remove the angular momentum from the rear wheel. After all, the rear tyre may become airborne in a stoppie.

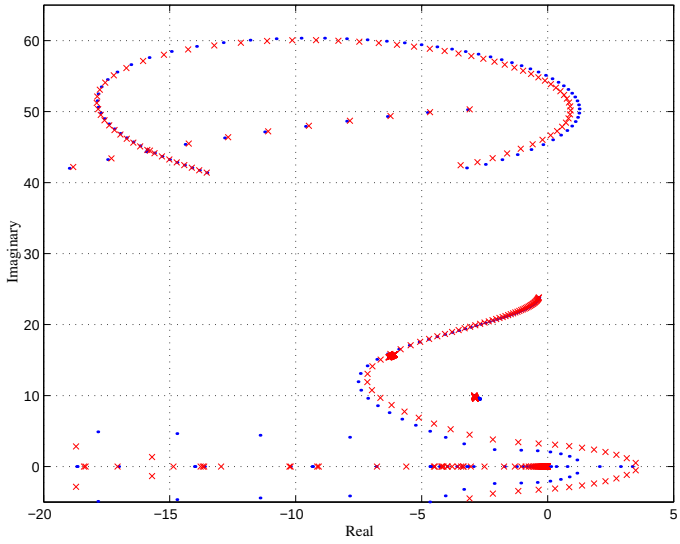

Plot symbol	Deceleration (m/s^2)	Front brake (%)	Rear brake (%)	Speed range (m/s)
·	2.5	90	10	70.0–0.126
×	2.5	10	90	70.0–0.175

Figure 7.11: Root-loci for different braking conditions at a deceleration of 2.5 m/s^2.

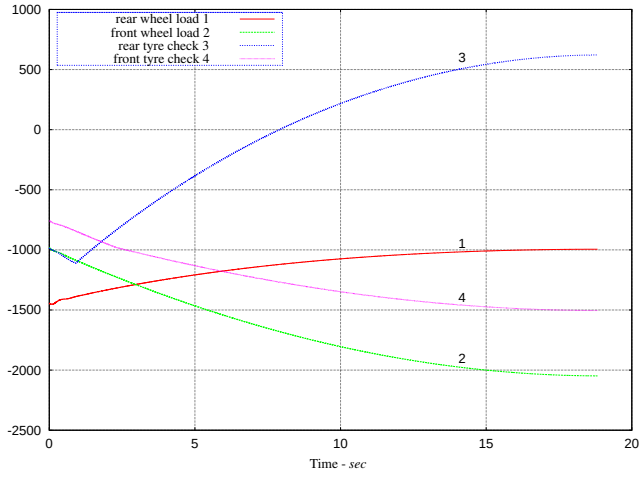

Figure 7.12: Normal wheel loads and longitudinal force checks in the 5 m/s^2 deceleration case with 90 per cent of the braking on the rear wheel and 10 per cent on the front wheel. All the curves are given in N.

7.3 Conclusions

The results presented here show that the wobble mode of a motorcycle is significantly destabilised when the machine is descending an incline, or braking on a level surface. These findings have been substantiated by the author's supervisor on his own machine. Conversely, the wobble mode damping is substantially increased when the machine is ascending an incline at constant speed or accelerating on a level surface. This probably accounts for the stable 'feel' of the machine under acceleration. There is still a discrepancy with respect to the most problematic running condition of the Suzuki TL 1000, which was famously prone to wobble under mild acceleration (Farr, 1997*b*; Anon., 1997*c*). Except at very low speeds, inclines, acceleration and deceleration appear to have very little effect on the damping or frequency of the weave mode.

It was claimed in (Sharp, 1976*b*) that acceleration can introduce a large reduction in weave mode damping and that the weave and wobble modes can lose their identities due to a narrowing of the frequency gap between these modes. Neither of these effects were observed in this study and this discrepancy was attributed to the relative simplicity of the model employed in (Sharp, 1976*b*) as well as on differing parameters.

A review of the known results on the stability of linear time varying systems reinforces the idea that extreme care has to be taken when testing the stability of these systems via the eigenvalues of frozen-time models. This situation is especially problematic when the frozen-time eigenvalues cross the imaginary axis, or are close to it as time varies. In the present work, the conclusions drawn from linearised frozen-time models were verified against nonlinear simulations. In the context, the frozen-time models have been found to predict the behaviour quite accurately.

The known problems to do with rear tyre adhesion in heavy rear-wheel-dominated braking situations have been exposed by the nonlinear simulations. The analysis has quantified the transfer of normal tyre loading to the front tyre under heavy braking. This means that, if an attempt is made to slow the machine using rear-wheel-dominated braking, it is very likely that the rear tyre will go into a slide, causing an irrecoverable loss of control. The aerodynamic drag acts to reduce these difficulties at high speeds.

Chapter 8

Motorcycle steering oscillations due to road profiling

8.1 Introduction

The previous chapter has shown that acceleration or deceleration can have an impact on the stability of motorcycles. A source of even greater concern which can potentially endanger the rider is the one described in this chapter. That is that there is a clear possibility for the lightly damped modes of motorcycles to be excited by regular road surface undulations. The motivation to study this issue is reinforced by a number of rider-loss-of-control incidents that have been reported in the popular motorcycle press and involve no other road users. It is believed that road forcing induced oscillations are strongly related to the causes of such accidents. These reports are mainly non-technical and are based on anecdotal evidence, yet there is a compelling level of consistency between them as we will see below.

One example of a loss-of-control event occurred during police motorcycle training and the circumstances of this incident are summarised in the following extract from (Anon., 1993*a*): "... there is a specific section of road which can cause severe handling difficulties for motorcycles being ridden at high speed... this section of road has a series of small undulations in it at the beginning of a large sweeping right hand bend...".

Another well-publicised event occurred at a relatively low speed under apparently benign circumstances (Cutts, 1993): "... we were approaching a village at no more than 65/70 mph, on a smooth road, on a constant or trailing throttle when, for no apparent reason, the bike went wildly out of control...". This incident and some of the associated background are described in (Evans, 1993; Raymond, 1993; Anon., 1993*b*,*c*).

A high profile fatal accident occurred, when according to an eye witness, the machine being ridden went into a violent "tank slapper"[1] at about 60 mph as the rider was going around a gentle corner (Duke, 1997). The offending machine model (Suzuki TL 1000) was subsequently recalled in the U.S. (Anon., 1997*c*) as well as in the U.K. (Farr, 1997*b*). In their recall state-

[1] This expression is used to describe an oscillation that causes the handle bars to swing from lock to lock.

ment, the manufacturers said: "... the front wheel may oscillate, causing the handlebars to move rapidly from side to side when accelerating from a corner and/or (accelerating) over a rough road surface, commonly known as tank slapping...". There was further speculation as to the possible causes of the difficulty and various tests were performed on the machine that involved changing tyres, fitting a steering damper and changing the rear damper unit (Anon., 1997*b*). Tyre changes did not seem to make a significant difference, but a steering damper and, strangely enough, a new rear damper unit were reported to make a large improvement. One article claimed that riders who weigh over 95 kg had not experienced the instability phenomena (Farr, 1997*a*).

A remarkable video tape of a weave-type instability was taken during the 1999 Formula One Isle of Man TT race (Duke Marketing Ltd, 1999). Paul Orritt can be seen exiting the gentle left-hand bend at the top of Bray Hill on a Honda Fireblade at approximately 150 mph when for no apparent reason his machine went into an uncontrollable 2-3 Hz oscillation. His motorcycle subsequently ran wide and crashed. "It just wouldn't come out of the tank slapper," he recalled. "I was no longer in control ... the trouble began immediately after I ran over a couple of bumps in the freshly laid road surface..." (Farrar, 2002). Another case of weave-type instability was captured on video during the South African 250cc GP in April 2002. Casey Stoner can be seen hitting a very small bump while exiting a corner, and subsequently undergoing an unstable oscillation before falling on the road. His attempt to control the vehicle by using the brakes is clear.

In technical terms, the mechanism by which an undulating road can influence the lateral motions of a motorcycle is provided by the coupling terms between in-plane and out-of-plane motions under cornering. A signal transmission path thus exists whereby steering oscillations can be produced by road profiling. It is the author's belief that the theory and results presented here, provide an explanation for most of the behavioural problems described above.

In every case it will be assumed that the machine is operating in the neighbourhood of an equilibrium cornering condition and the attention will be on quantifying the steering response of the machine to regular road undulations through theoretical analysis. The associated design parameter sensitivity problem is also studied. The machine condition of interest involves cornering and consequently an elaborate mathematical model of the system is needed. The existing state-of-the-art model in Chapter 5 is used with particular employment of the road forcing mechanism described there. The full nonlinear model is linearised for small perturbations about an equilibrium cornering state that is found from a simulation of the motorcycle-rider system on a smooth road. The linear, small perturbation, uncontrolled model is then subjected to sinusoidal road displacement forcing and the frequency responses are computed. The responses to forcing from both the front and rear wheels are considered. When studying the combined effects of front and rear wheel road forcing, a wheelbase travel time delay is introduced into the model that ensures that the two road wheel inputs are correctly phased.

8.1.1 Linearised models and Frequency response calculations

The preparation of linearised models involves a two-step procedure as usual. In the first, AUTOSIM is used to compute, symbolically, the linearised equations of motion. In the second, the nonlinear simulation code is used to find the equilibrium state associated with the steady-state cornering condition being studied, via the use of drive and steering controllers. The drive torque is controlled so that the machine maintains a preset speed, while the steering torque is adjusted to maintain a desired roll angle.

A number of Bode (frequency response) plots will be presented that were calculated using the linearised models. In the current case, two inputs u_f and u_r are used. These represent changes in the road height at the front and rear wheels' ground contact points respectively. The steering angle δ was the only output. Let us now suppose that the state-space model, generated by AUTOSIM, that corresponds to a given cornering trim condition is:

$$\begin{aligned} \dot{x} &= Ax + Bu \\ \delta &= Cx \end{aligned}$$

in which

$$u = \begin{bmatrix} u_f \\ u_r \end{bmatrix}.$$

The transfer functions that relate the front and rear road disturbance input to the steering angle are given by:

$$\begin{bmatrix} g_f & g_r \end{bmatrix} = C(sI - A)^{-1}B$$

in which s is the usual Laplace transform complex variable. One can study separately the influences of the front and rear road-wheel disturbances using $g_f(s)$ and $g_r(s)$ independently. In the case of studies of the combined influence of both wheels, the transfer function

$$g(s) = g_f(s) + e^{-s\tau} g_r(s)$$

is used, in which τ is the wheelbase filtering time delay given by w_b/v. The constant w_b is the machine wheelbase and v its forward speed. All computations and plot outputs were computed using MATLAB (The Mathworks Inc., 2000) M-files.

8.2 Results

8.2.1 Introductory comments

Straight running root-loci of the type presented in Figure 8.1 are well known from earlier chapters.

This plot shows that the wobble mode is lightly damped at 13 m/s and that the associated resonant frequency is approximately 48 rad/s (7.6 Hz). This diagram also shows that the weave mode becomes lightly damped at high speeds and that the resonant frequency of this mode is approximately 22 rad/s (3.5 Hz) at a machine speed of 40 m/s. It should also be noted that the front

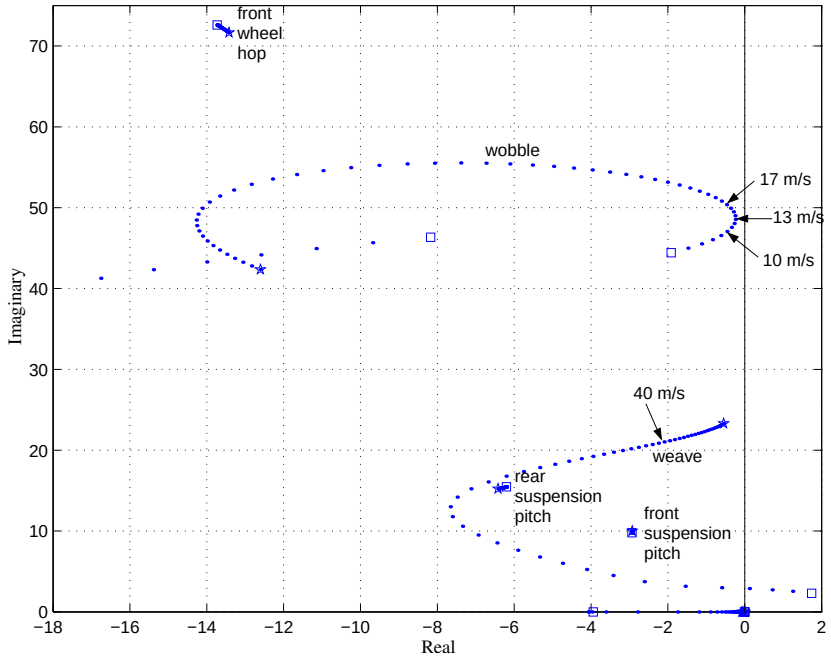

Figure 8.1: Straight running root-locus with speed the varied parameter. The speed is increased from 5 m/s (□) to 60 m/s (⋆).

wheel hop mode[2], the rear suspension bounce (pitch) mode[3] and the front suspension bounce (pitch) mode[4] are relatively insensitive to variations in the machine speed. This observation reinforces the notion that the in-plane and out-of-plane dynamics are decoupled from each other under straight running conditions. We should also observe that in-plane disturbances such as sinusoidal road undulations will not couple at first-order level into out-of-plane freedoms such as the roll and steering angles.

Let us now contrast Figures 8.1 and 8.2 with the help of Figures 8.3 and 8.4. Figure 8.2 shows the behaviour of the important machine modes under cornering at different speeds at a fixed roll angle—in this case 30 deg. Figures 8.3 and 8.4 show the effect of varying the machine roll angle at two constant speed values 13 m/s and 40 m/s. When one compares these plots, it can be seen that:

(a) cornering increases the damping of the wobble mode, while the speed for minimum damping remains at approximately 13 m/s. The associated resonant frequency of this mode is essentially unaffected.

(b) cornering reduces the damping of the front wheel hop mode and it is least damped at

[2]This mode is associated with an oscillation that involves the compression and expansion of the fork legs and the tyre carcass.

[3]This mode is associated with an oscillatory motion of the swinging arm. This movement results in the pitching, and to a lesser extent, the heaving of the machine's main body.

[4]This mode is dominated by a pitching motion that hinges around the rear wheel ground contact point and involves the oscillatory compression and expansion of the fork leg assemblies. When this mode is excited there is also a discernible heaving of the machine's main body.

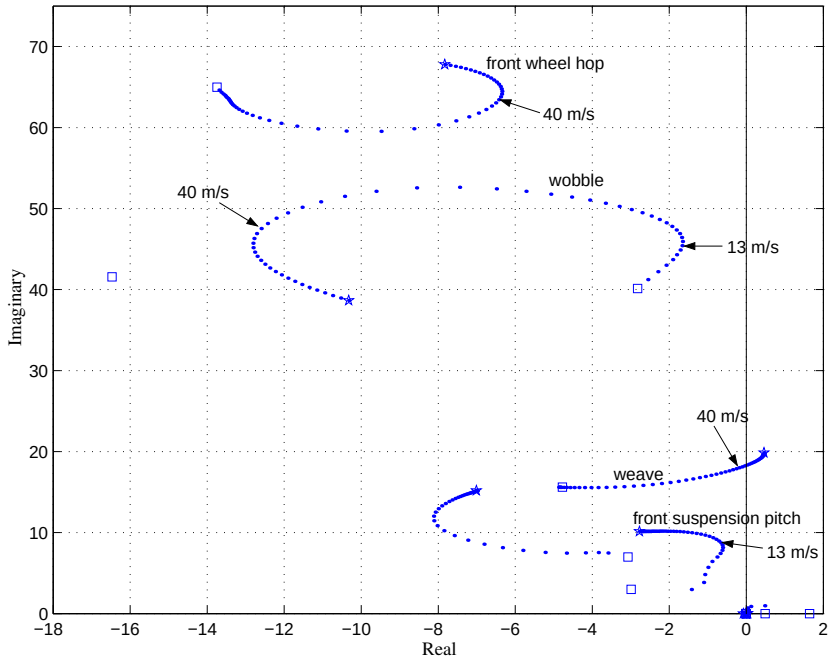

Figure 8.2: Root-locus for a fi xed roll angle of 30 deg. The speed is increased from 6 m/s (□) to 60 m/s (⋆).

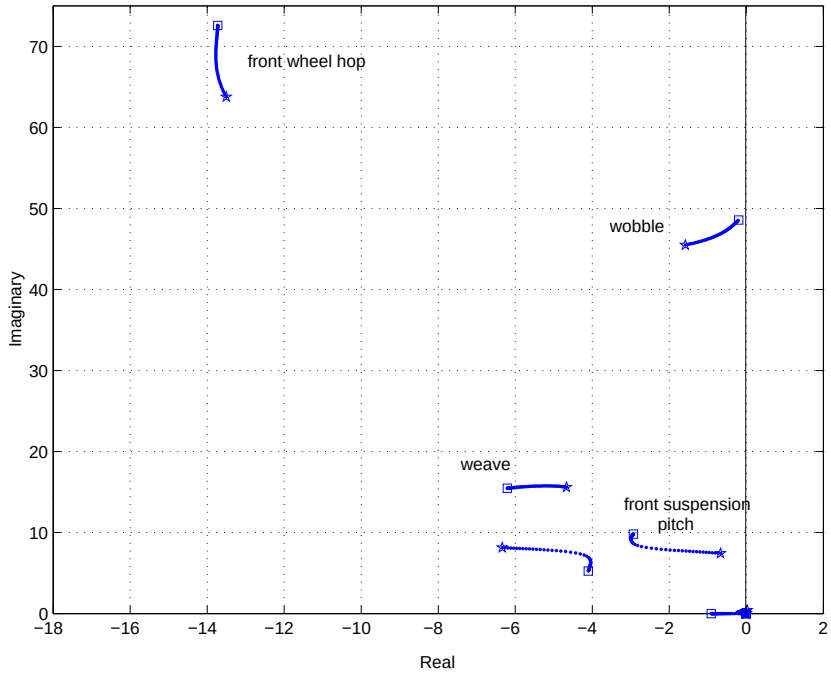

Figure 8.3: Root-locus for a fi xed speed of 13 m/s. The roll angle in increased from 0 (□) to 30 deg (⋆).

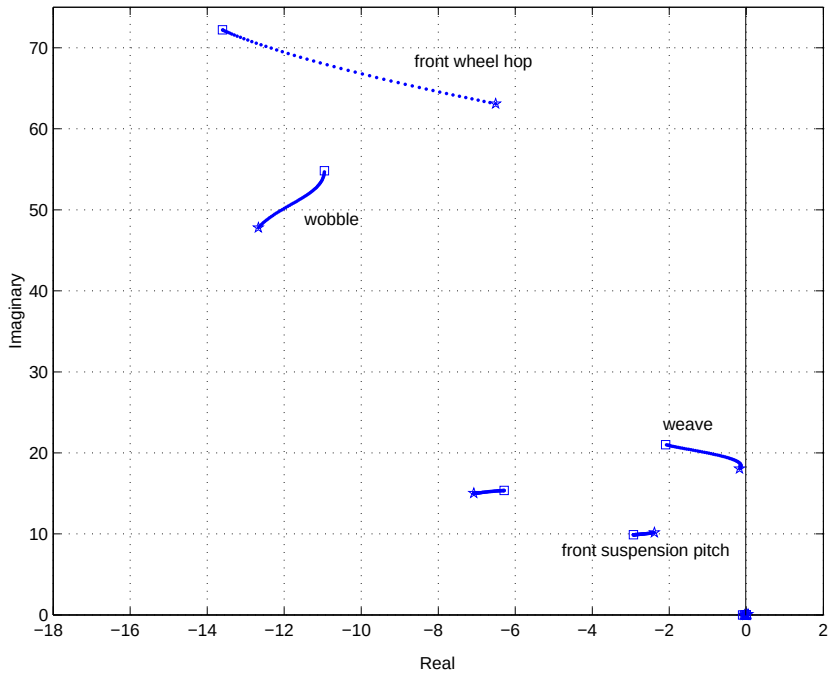

Figure 8.4: Root-locus for a fi xed speed of 40 m/s. The roll angle in increased from 0 (□) to 30 deg (⋆).

approximately 40 m/s with an associated resonant frequency of approximately 63 rad/s (10 Hz). This figure is lower than the straight running figure of 73 rad/s (11.6 Hz).

(c) cornering tends to reduce the damping of the weave mode and in the present case this mode becomes unstable at high speed; the weave mode is lightly damped at 40 m/s.

(d) cornering has a destabilising effect on the front suspension pitch mode and it becomes particularly lightly damped at 13 m/s and 30 deg of roll angle. The resonant frequency of this mode is approximately 8 rad/s (1.27 Hz) under these conditions.

Since road forcing signals will couple into out-of-plane freedoms under cornering, these observations lead to the following hypotheses:

(a) The wobble and front suspension pitch modes are exposed to resonant forcing due to road profiling at speeds of the order 13 m/s, and

(b) the weave and front wheel hop modes are similarly vulnerable at high speeds.

(c) Since the coupling between road disturbances and the out-of-plane dynamics increases with roll angle, we expect to find an increase in the vulnerability of the front wheel hop mode, the weave mode and the front suspension pitch mode with roll angle. All three modal damping factors decrease with increasing roll angle.

(d) The vulnerability of the wobble mode is expected to reach a peak at some worst-case value of roll angle. This is suggested because the interplane coupling increases with roll angle,

while the damping of the wobble mode also increases with roll angle.

It is the business of the remainder of this chapter to investigate these conjectures.

8.2.2 Individual wheel contributions

Figure 8.5 shows Bode plots of $g_f(s)$ and $e^{-s\tau}g_r(s)$ at the relatively low speed of 13 m/s, a roll angle of 30 deg and with nominal parameter values. It is clear from these plots that the resonant peaks for both the wobble and front suspension pitch modes are front-wheel-input dominated. The difference between the front and rear wheel excited resonant peaks for the wobble mode is 12 dB, while that for the front suspension pitch mode is approximately 5 dB. It is concluded, therefore, that difficulties with either of these modes will almost certainly be ameliorated via adjustments to the front of the machine.

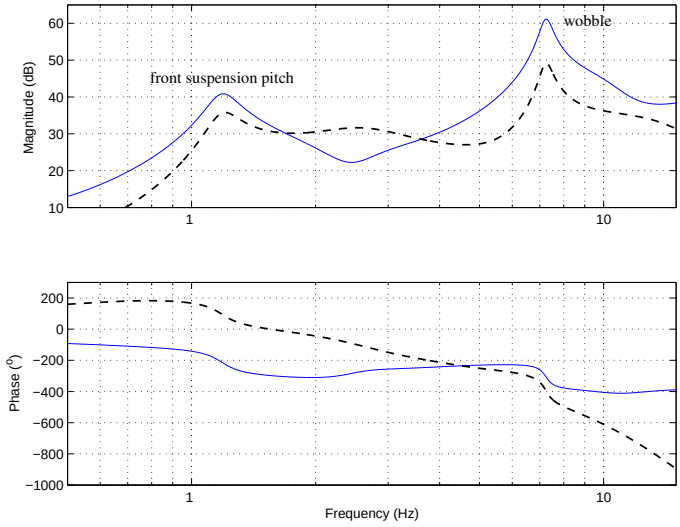

Figure 8.5: Frequency response for $g_f(s)$ (solid), and $e^{-s\tau}g_r(s)$ (dashed) (0 dB=1 deg/m). The steady-state conditions are a 30 deg roll angle and a forward speed of 13 m/s.

The situation at higher speeds is quite different as is shown in Figure 8.6. At 40 m/s and 30 deg of roll, we see that there are resonance peaks associated with the weave and the front wheel hop modes. In the case of the weave mode, the front and rear wheel forcing signals are making equal contributions and their combined effect is a large one. Resonance difficulties with this mode are likely to be more difficult to isolate and prevent, because the problem involves potentially the geometry and parameters of the whole machine as well as the properties of both tyres. The excitation of the front wheel hop mode is due almost entirely to front wheel forcing and is consequently a problem that can be isolated and tackled at the front of the bike.

At the weave mode peak, the frequency responses $g_f(s)$ and $e^{-s\tau}g_r(s)$ have a phase angle difference of approximately 56 deg. As the motorcycle speed changes, the phase shift $e^{-s\tau}$ associated with the wheelbase travel time changes. In principle, therefore, changing the speed will influence the maximum gain, not only through affecting the modal damping factor, but

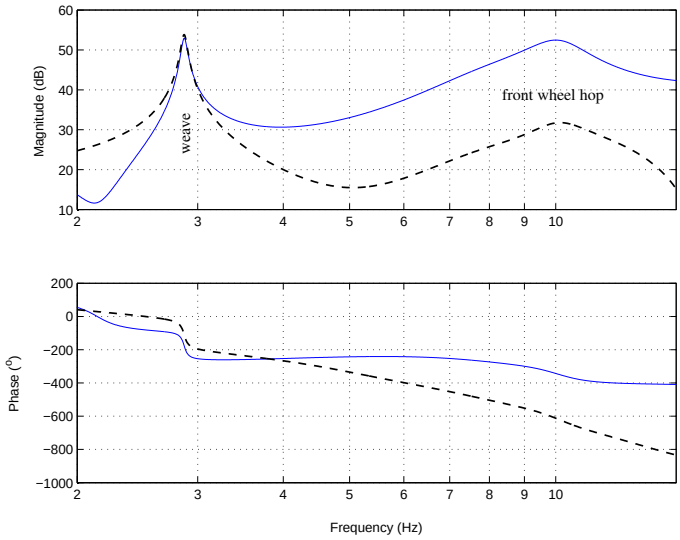

Figure 8.6: Frequency response for $g_f(s)$ (solid), and $e^{-s\tau}g_r(s)$ (dashed) (0 dB=1 deg/m). The steady-state conditions are a 30 deg roll angle and a forward speed of 40 m/s.

also through influencing the phase angle. However, changing the speed from 38 to 42 m/s only changes the phase lag, at the weave mode frequency of 18 rad/s (2.86 Hz), by about 4 deg. Quantitatively, therefore, the reinforcement/cancellation issue is a small one.

8.2.3 Low-speed forced oscillations

The root-loci presented in Figure 8.3 suggest that road forcing effects may cause the wobble and front suspension pitch modes to resonate at low speeds in response to regular road profiling. The investigation of this possibility is started by referring to Figure 8.7 that shows a frequency response plot that relates the vehicle's steer angle to road forcing inputs. The road profile input is in meters, while the output is in degrees. If the vehicle is travelling at 13 m/s, road undulations with a wavelength of 1.8 m, will generate a road forcing signal with a frequency of 45.4 rad/s (7.22 Hz). Since the transfer function gain is approximately 62 dB at this frequency, Figure 8.7 indicates that one can expect ± 1.28 deg of steering movement for sustained road undulations with amplitude ± 1 mm. If we assume that the steering head mechanism can move through approximately ± 20 deg from lock to lock, the linear model would suggest that road undulations of ± 15 mm will produce a sustained "tank slapping" action[5]. This figure also shows that road undulations could excite the front suspension pitch mode, but the gain is only approximately 44 dB in this case.

Immediately, it is of interest to consider the influences of design and/or suspension parameter changes on the resonant peaks. Figure 8.7 also shows the effect of changing the steering damper setting by ± 1.5 Nms/rad around the nominal value of 7.4 Nms/rad. Decreasing the steering damper setting causes the road forcing gain to increase to 66 dB, while increasing it reduces the gain to 58 dB.

[5]Note that this is only an estimate from a linearised model—see Section 8.2.6 for more on nonlinear effects.

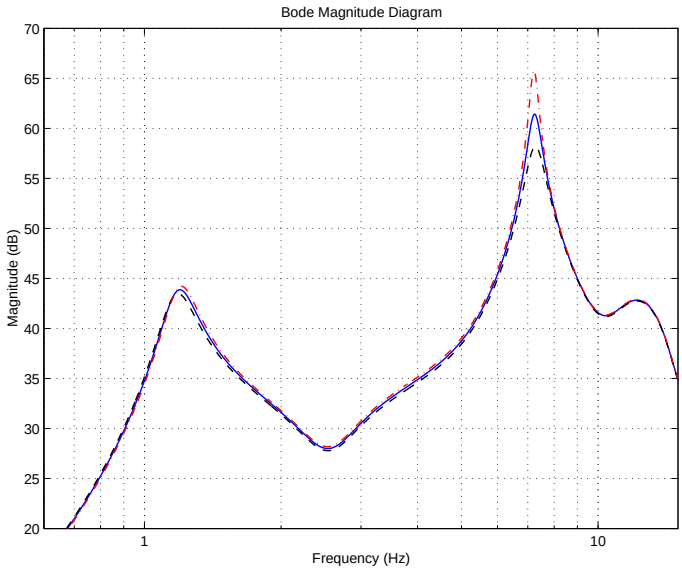

Figure 8.7: Bode magnitude plot of $g(s)$ (0 dB=1 deg/m). Nominal state: 13 m/s, 30 deg roll angle. The solid curve represents the nominal case, the dashed one shows the effect of an increase of 20 % in the steering damper setting, while the dot-dash curve shows the effect of a 20 % reduction in the steering damping.

The root-loci presented in Figure 8.3 demonstrate an increase in the wobble mode damping with increased roll angle. As a consequence, it was predicted that a reduction in roll angle could lead to an increase (rather than a decrease) in the wobble mode peak gain despite an accompanying reduction in the coupling between the in-plane and out-of-plane dynamics. Figures 8.7 and 8.8 shows that the peak wobble mode gain for the 15 deg and 30 deg roll angle cases are roughly equal at 62 dB for the nominal value of steering damping. An increase of 20% in the steering damping decreases the peak wobble mode gain to approximately 55 dB (rather than 58 dB in the case of 30 deg of roll). When the steering damping is decreased by 20%, the peak wobble mode gain increases to 83 dB which is substantially higher than the peak gain achieved at 30 deg of roll angle.

Figure 8.9 shows that changing the rear damper setting has little impact on the susceptibility of the wobble and front suspension pitch modes to road forcing. This result casts doubt on the suspected contributions of the rear damper to the wobble mode instability associated with the Suzuki TL1000 (Anon., 1997*b*).

As one would expect, the damping of the front suspension pitch mode, and consequently the road forcing gain associated with that mode, is influenced by changes in the front suspension damper setting. Figure 8.10 shows the effect of changing this damper setting by $\pm$220 Ns/m about a nominal setting of 550 Ns/m. Although the wobble mode gain is relatively unaffected by these changes, the impact on the pitch mode is significant and it can be seen that a reduction of 220 Ns/m leads to a gain increase of 8 dB over the nominal value.

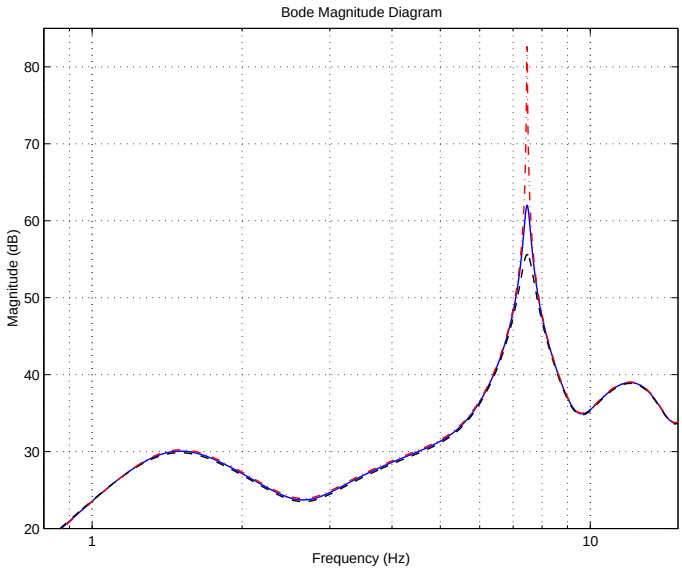

Figure 8.8: Bode magnitude plot of $g(s)$ (0 dB=1 deg/m). Nominal state: 13 m/s, 15 deg roll angle. The solid curve represents the nominal case, the dashed one shows the effect of an increase of 20% in the steering damping, while the dot-dash curve shows the effect of a 20% decrease.

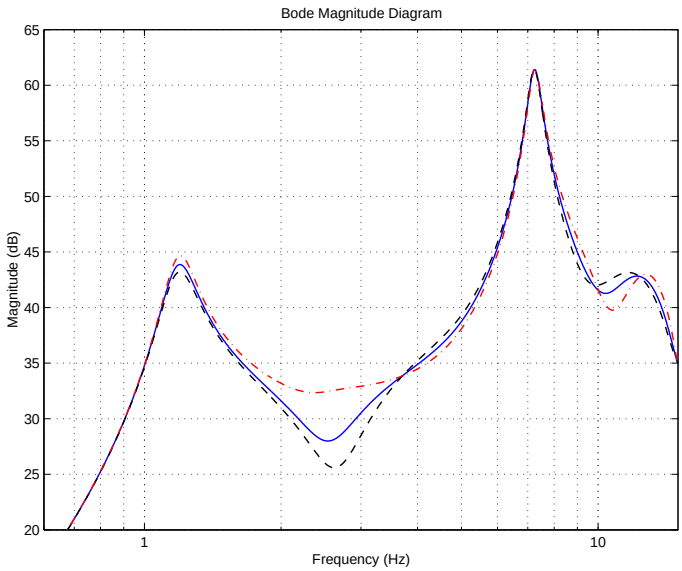

Figure 8.9: Bode magnitude plot of $g(s)$ (0 dB=1 deg/m). Nominal state: 13 m/s, 30 deg roll angle. The solid curve represents the nominal case, the dashed one shows the effect of an increase of 40% in the rear damper setting, and the dot-dash curve shows the effect of a 40% decrease.

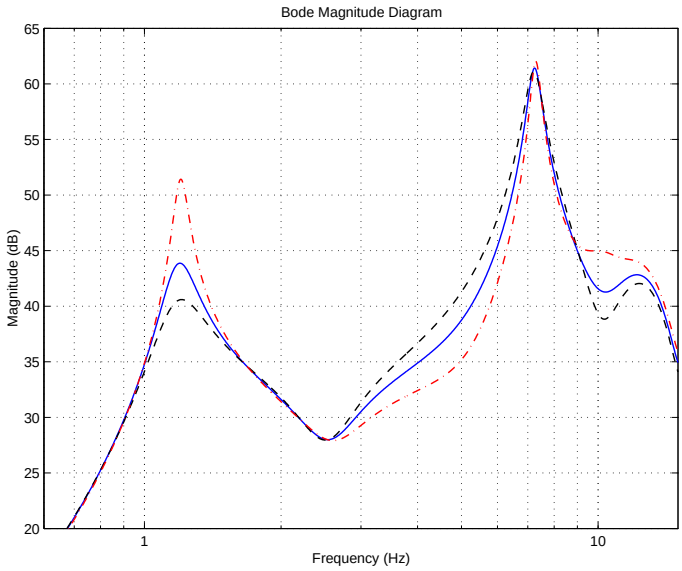

Figure 8.10: Bode magnitude plot of $g(s)$ (0 dB=1 deg/m). Nominal state: 13 m/s, 30 deg roll angle. The solid curve represents the nominal case, the dashed one shows the effect of an increase of 40% in the front damper setting and the dot-dash curve shows the effect of a 40% decrease.

8.2.4 High-speed forced oscillations

At the beginning of Section 8.2, it was argued that at high speeds the weave and front wheel hop modes are vulnerable to regular road waves of critical dimensions. The consequent forced oscillations are a significant potential threat to the motorcyclist, because it is a high-speed phenomenon and for typical motorcycle parameters, long-wavelength low-amplitude road undulations will excite these modes. Also, regular long-wavelength low-amplitude undulations are virtually impossible for the rider to see. At a speed of 40 m/s with the motorcycle parameters used here, the weave mode will be excited by road undulations with a wavelength of approximately 14 m, while a 4 m wavelength will excite the front wheel hop mode.

Figure 8.11 shows a Bode magnitude plot of the transfer function that relates the steering angle to regular road height variations. For nominal suspension and steering damper settings, the weave mode gain at 18 rad/s (2.86 Hz) is 58 dB, while the front wheel hop mode gain is 52 dB. As in the case of wobble mode excitation, this diagram shows that relatively low-amplitude road undulations will cause the rider concern. This plot also shows that an increase in the steering damper setting will make matters significantly worse. More particularly, a steering damping increase of 1.5 Nms/rad increases the road forcing gain by 10 dB, or a factor of 3.

Figure 8.11 also shows that the steering damper setting has little impact on the front wheel hop resonance.

Figure 8.12 shows the effect of changes to the rear damper setting. As with the steering damper, an increase in the rear damping increases the weave mode gain by 5 dB, while reducing this damper setting causes the peak value of weave gain to fall by 4 dB. Also, it is clear that

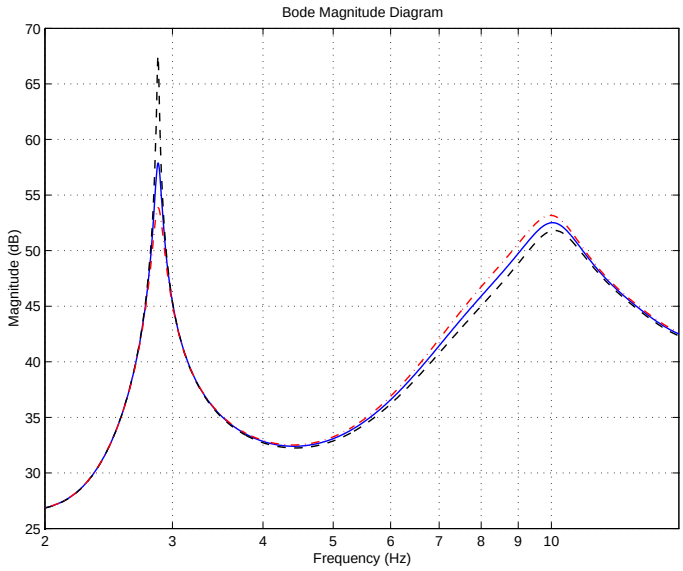

Figure 8.11: Bode magnitude plot of $g(s)$ (0 dB=1 deg/m). Nominal state: 40 m/s, 30 deg roll angle. The solid curve represents the nominal case, the dashed one shows the effect of an increase of 20% in the steering damper setting and the dot-dash curve shows the effect of a 20% decrease.

this change has virtually no influence on the front wheel hop peak gain that remains fixed at approximately 52 dB.

Figure 8.13 shows the effect of changes to the front damping. In contrast to the previous two plots, this diagram shows that increasing the front damper setting has a beneficial impact on the weave and front wheel hop gain peaks. An increase of 220 Ns/m in the front damper coefficient reduces the weave gain peak and the front wheel hop gain peak by approximately 2 dB. If the front damping is reduced by a like amount, the weave mode gain peak increases by approximately 3 dB and the front wheel hop gain peak increases by approximately 6 dB.

8.2.5 Influence of rider parameters

There is anecdotal evidence to suggest that the weight and posture of the rider can influence the vulnerability of the motorcycle-rider system to weave related oscillations. The suggestion that light riders are more likely to experience difficulties with oscillatory instabilities than are heavier ones (Farr, 1997*a*; Dunlop, c1977) will be investigated. The suggestion that the rider can attenuate weave related oscillations by lying down on the tank (Dunlop, c1977) will also be investigated. This study will be carried out at a speed of 40 m/s and a roll angle of 30 deg, via changes in the rider's upper body mass and mass centre location.

The effect of changes in the rider's upper body mass on the transfer function that maps road vertical displacement to the steering angle are studied in Figure 8.14. As suggested in (Farr, 1997*a*), an increase in the rider's upper body mass by 20 kg reduces this gain peak by approximately 8 dB. In the same way, a reduction of the rider's upper body mass by 20 kg increases the peak gain by approximately 7 dB.

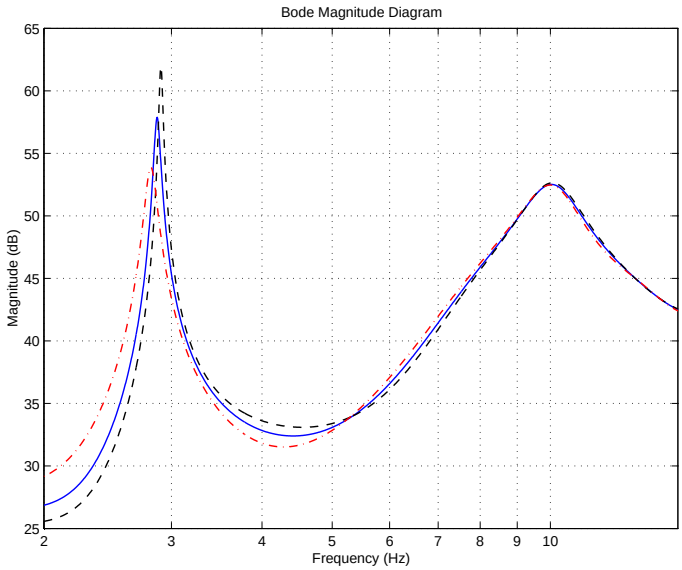

Figure 8.12: Bode magnitude plot of $g(s)$ (0 dB=1 deg/m). Nominal state: 40 m/s, 30 deg roll angle. The solid curve represents the nominal case, the dashed one shows the effect of an increase of 40% in the rear damper setting and the dot-dash curve shows the effect of a 40% decrease.

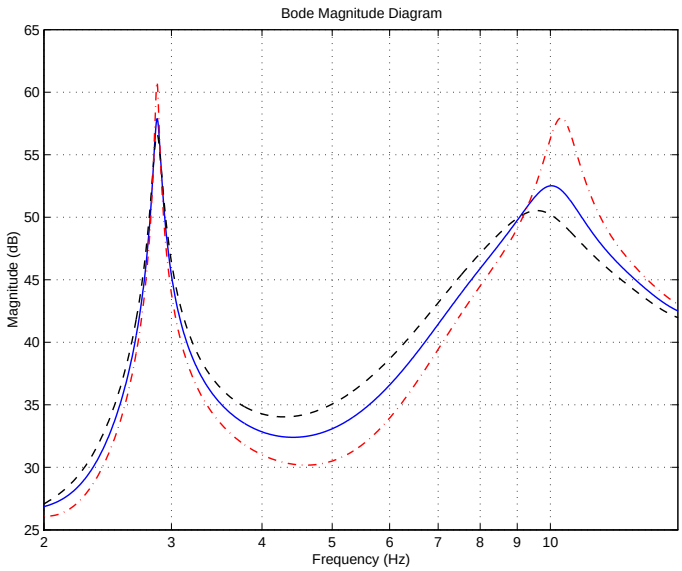

Figure 8.13: Bode magnitude plot of $g(s)$ (0 dB=1 deg/m). Nominal state: 40 m/s, 30 deg roll angle. The solid curve represents the nominal case, the dashed one shows the effect of an increase of 40% in the front damper setting and the dot-dash curve shows the effect of a 40% decrease.

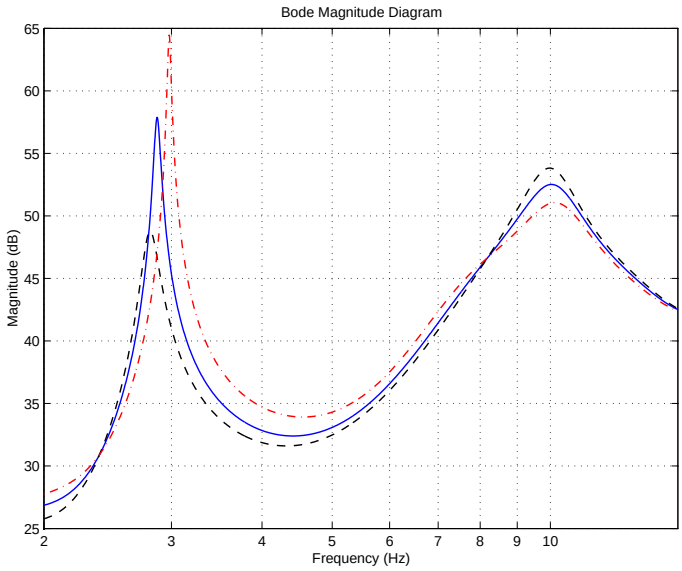

Figure 8.14: Bode magnitude plot of $g(s)$ (0 dB=1 deg/m). Nominal state: 40 m/s, 30 deg roll angle. The solid curve represents the nominal case, the dashed one shows the effect of an increase of 20 kg in the mass of the upper body of the rider and the dot-dash curve shows the effect of a 20 kg decrease.

The effect of variations in the longitudinal location of the rider's centre of mass are studied. As suggested by the video tape (Dunlop, c1977), a forward shift in the rider's upper body mass appears in Figure 8.15 to reduce the vulnerability of the motorcycle to weave related instabilities. In the present study, we see a reduction in the signal transmission gain peak of 5 dB for a forward shift of 15 cm. If the centre of mass is shifted backwards by 15 cm, the transmission gain peak increases by approximately 13 dB.

The effect of variations in the (vertical) z-direction location of the rider's centre of mass on the transfer function that maps road undulations to the steering angle are studied in Figure 8.16. An upward shift of 15 cm reduces the signal transmission gain peak by 13 dB, while a corresponding downward shift increases it by approximately 7 dB.

8.2.6 Nonlinear phenomena

Although it is not the primary purpose of this chapter to study the nonlinear aspects of the road forcing problem, it is desired not to conclude this account without making some introductory observations that will motivate future research. Figure 8.17 shows the build up of oscillations in the roll and steer angles as well as the yaw rate in response to road profiling that is tuned into the front suspension pitch mode at 7.54 rad/s (1.2Hz). The forward speed is 13 m/s and the forcing amplitude is 5 mm. Only the very low-amplitude case can be studied here, because higher amplitude signals take the tyre model out of its domain of validity. It is evident that 7.54 rad/s (1.2Hz) oscillations build up in 2 or 3 seconds. It can also be seen that another consequence of road forcing is a tendency for the roll angle to reduce in response to the onset

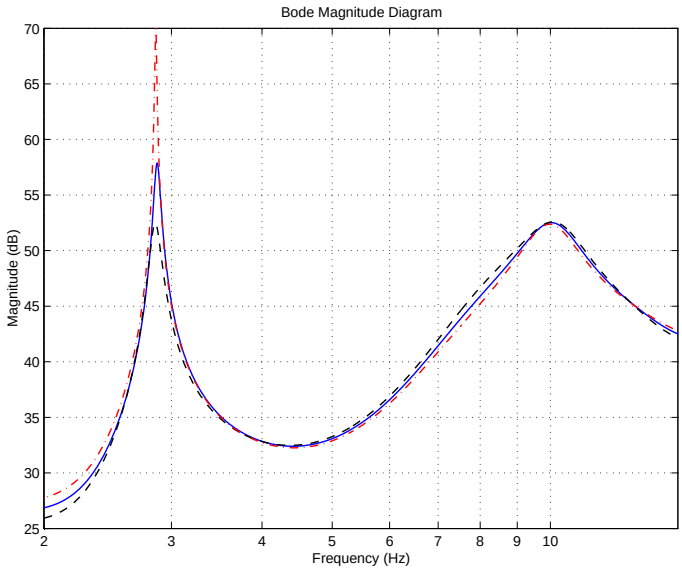

Figure 8.15: Bode magnitude plot of $g(s)$ (0 dB=1 deg/m). Nominal state: 40 m/s, 30 deg roll angle. The solid curve represents the nominal case, the dashed one shows the effect of a forward shift of 15 cm in the centre of mass of the upper body of the rider and the dot-dash curve shows the effect of a rearward shift of 15 cm.

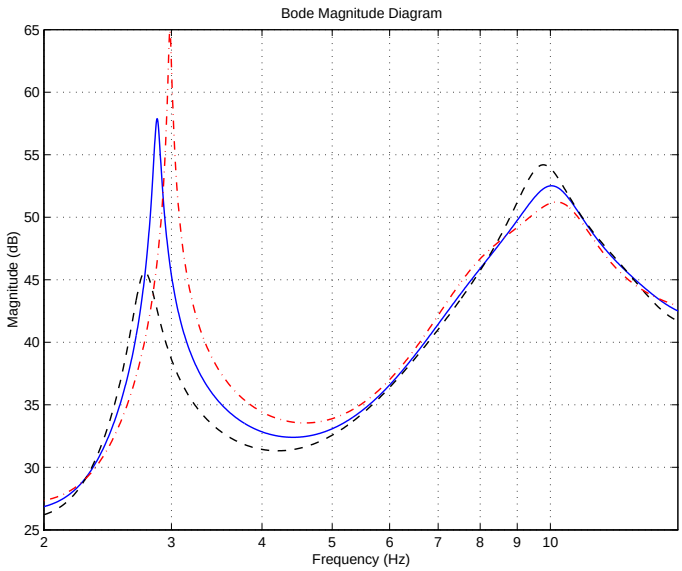

Figure 8.16: Bode magnitude plot of $g(s)$ (0 dB=1 deg/m). Nominal state: 40 m/s, 30 deg roll angle. The solid curve represents the nominal case, the dashed one shows the effect of an upward shift of 15 cm in the centre of mass of the upper body of the rider and the dot-dash curve shows the effect of a downward shift of 15 cm.

of oscillations. This is possibly the result of a slow growth rate instability of the capsize type described in (Sharp, 1971). In practical terms, this effect will cause the vehicle to run wide, a common feature of real accidents involving oscillations. As the roll angle reduces, the road-forcing signal transmission gain will also reduce and we can see evidence of this effect in the yaw rate and steering angle oscillation amplitudes. At approximately 35 s, one can see evidence of the onset of wobble frequency oscillations. This excitation of the wobble mode is the product of nonlinear effects that remain to be analysed.

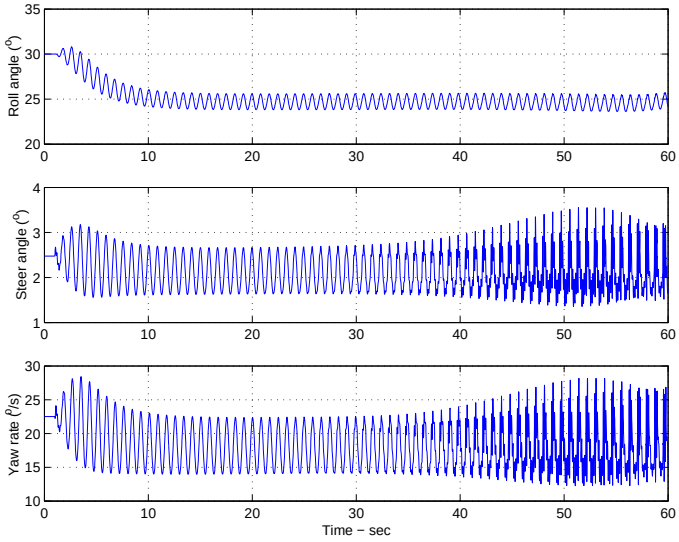

Figure 8.17: Transient behaviour of the roll and steering angles, and the yaw rate in response to sinusoidal road forcing that begins at $t = 1$ s and has a peak amplitude of 0.5 cm. The forcing frequency is tuned to the front suspension pitch mode. The lean angle is 30 deg and the forward speed 13 m/s.

Figure 8.18 shows the response of the machine to low-amplitude road undulations that are tuned into the weave mode. Again, larger amplitude profiling will take the tyre model out of its domain of validity and consequently cannot be used. In common with the previous simulation result, oscillations build up in about 3 s. It is also evident that the roll angle tends to decrease. As can be seen in the video tape (Duke Marketing Ltd, 1999), weave-related instabilities cause the vehicle to run wide. It is also clear that as the roll angle reduces, the steer angle and yaw rate oscillations reduce in consequence. It is believed that this is the result of transmission gain reductions that come about in response to reductions in the roll angle. At approximately 25 s, one sees evidence of waveform distortion, a product of nonlinear mechanisms.

8.3 Conclusions

The results presented show that under cornering conditions, regular low-amplitude road undulations can be a source of considerable difficulty to motorcycle riders. At low machine speeds the wobble and front suspension pitch modes are likely to respond vigorously to resonant forc-

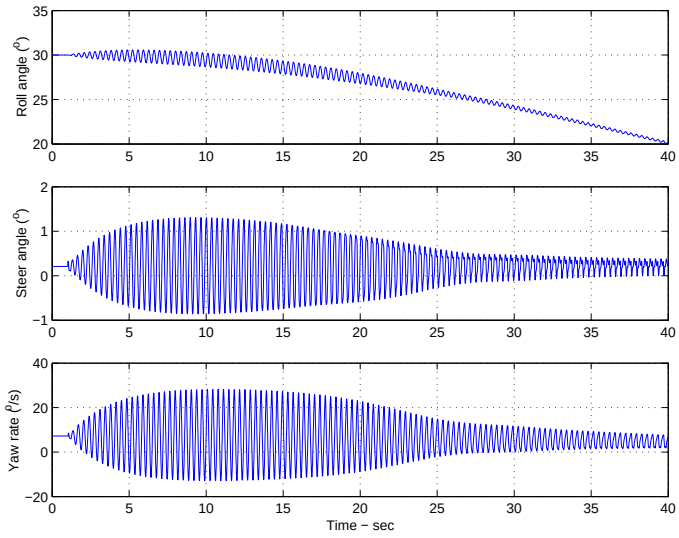

Figure 8.18: Transient behaviour of the roll and steer angles and the yaw rate, in response to sinusoidal road forcing that begins at $t = 1$ s and has a peak amplitude of 0.25 cm. The forcing frequency is tuned to the weave mode. The lean angle is 30 deg and the forward speed 40 m/s.

ing, while at higher speeds, the weave and front wheel hop modes are similarly affected. The vigour of the oscillations is related to the amount of damping present in each mode as predicted by the previously much studied linear stability properties, with low damping factors leading to correspondingly high peak magnification factors. Connections between resonant responses and a class of single vehicle loss-of-rider-control accidents have been postulated.

The individual contributions to these resonances made by each of the two road wheels have been studied. The results show that the wobble and front wheel hop resonance peaks are "front wheel dominated". In other words, difficulties with these modes are likely to be caused by the design and set up of the front of the machine. The same is true, but to a lesser extent, in the case of the front suspension pitch mode. In contrast, the weave mode resonance peak involves the road forcing to both wheels in almost equal measure. As a consequence, weave related problems appear to be more difficult to isolate and remove.

As might be anticipated, the vulnerability of the wobble mode response to road forcing is decreased markedly by an effective steering damper, but changes to the suspension dampers are ineffectual. The front suspension pitch mode resonance is sensitive to the front suspension damping, but is insensitive to the rear suspension and steering damping. The weave mode resonant response is reduced by increasing the front damping, but it is made larger by increasing the rear suspension and steering damper settings. These damping results depend, of course, on the nominal setup and will not be universally true. Increasing the front suspension damping reduces the front wheel hop resonance peak, but this peak does not respond to changes in steering damping, or rear suspension damper settings.

It has also been shown that light riders are more likely to suffer from road forced resonant

weave oscillations than are heavy ones, as has been observed in practice (Farr, 1997*a*) and on the video tape (Dunlop, c1977). The results indicate also that the peak gains associated with the weave mode are brought down by moving the rider upper body mass forwards and upwards. There is not sufficient practical evidence at the moment to indicate whether or not these findings coincide with experience. From the rider's perspective, a worrying feature of the road profile induced oscillations is the tendency of the uncontrolled machine to "sit up" and run wide. This aspect of the machine behaviour can be seen on the video tape (Duke Marketing Ltd, 1999) in the case of a high-speed weave accident.

A preliminary study of motion simulations under resonance conditions has shown the existence of interesting and essentially nonlinear phenomena, that seem to conform with practical experience. These nonlinear phenomena are worthy of further study.

Part IV

Modelling Upgrades

Chapter 9

An improved motorcycle model

This chapter deals with recent work in bringing the already advanced model of Chapter 5 in line with modern motorcycle designs, both at the conceptual level and the parametric description. Some of the work presented here was also covered in (Sharp *et al.*, 2003).

In the base configuration the upgraded model has the same number of bodies and freedoms as the one in Chapter 5. The addition of new bodies will be required for some of the new configurations considered below, such as the chain drive system and telelever front suspension. The new monoshock rear suspension does not require any further bodies. It is possible to switch among the various configurations by activating the appropriate Lisp logical variables at the beginning of the AUTOSIM code to allow the Lisp macros `unless` and `when` to choose the relevant pieces of code from the master file. A similar method was described earlier in Chapters 3 and 4 in the context of choosing between the nonlinear and linearised models, except that this time there are many more flags.

9.1 Parametric description

A measurement campaign to obtain the relevant parameter values of a Suzuki GSX-R1000 motorcycle is currently in progress. One such machine has been disassembled and many parameters of the parts have been measured. At this point the campaign is incomplete and the measurements that are pending will be pointed out below together with those already done. This machine comes with a monoshock rear suspension, and the associated parameters with this type of suspension can be measured. For the front suspension the only parameters possible to obtain are those for the telescopic forks that come with this machine, and parameters for a telelever type suspension should be pursued elsewhere.

9.1.1 Geometry, mass centres, masses and inertias

The workshop manual for the motorcycle includes pictures to scale and key dimensions, like the wheelbase and the steering head angle. Joints between components at the steering head and the swing arm pivot can be identified there and many key points, including those related to

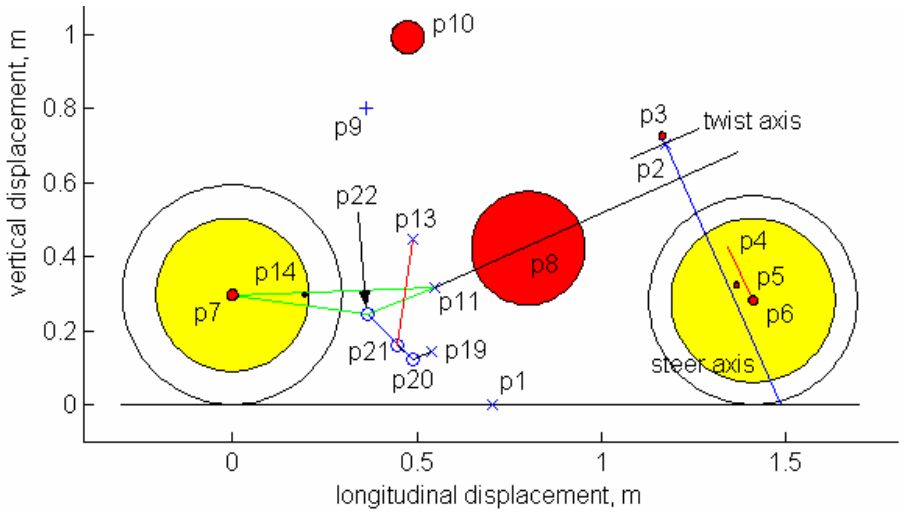

Figure 9.1: Scaled diagrammatic motorcycle in side view.

the monoshock rear suspension, can be located with reasonable precision from these pictures. A scaled diagrammatic representation of the motorcycle with monoshock rear suspension is shown in Figure 9.1. The front frame has been measured separately to give the points p3 and p5 which represent the centre of mass of the front frame steer body and front suspension body respectively. The point p4 is located along the line of the lower front fork translation relative to the upper forks. The exact location of point p2, which is the elastic centre of the rear frame with respect to a moment perpendicular to the steer axis, is not known at this stage.

The rider's total mass is taken as 72 kg, 62% of which is associated with the upper body. The masses of the hands and half of the lower arms are considered to be part of the steering system. The rider upper body pivot axis, p9, the rider upper body mass centre, p10, and the rider lower body mass centre[1], can be estimated. The rider parameters derive from bio-mechanical data (Anon., 1964), accounting for the posture of the rider on the machine.

The wheels, being axi-symmetric, have their mass centres at their geometric centres. Other mass centre locations were found by using plumb lines and taking photographs (Abdelkebir, 2002), while for the remaining main frame mass centre, experiments were conducted and photographs were taken, with the processing of the results remaining.

Wheel and tyre inertias have been obtained by timing oscillations of bi-filar and tri-filar suspension arrangements. Similar bi-filar suspension systems have been used for the front frame. Appropriate contributions from the rider's hands and lower arms are added to the measured values. Bi-filar tests on the rear frame are finished but processing of the results remains to be done. The swing arm inertias are small enough to be obtained by estimation based on the mass centre location and the dimensions.

Parameters for the chain drive (engine sprocket position and inertia) are still to be measured or estimated.

[1]The lower body adds to the mass of the main frame, and their combined mass centre is point p8.

9.1.2 Stiffness and damping properties

Springs and damper units were tested in a standard dynamic materials testing machine (Abdelkebir, 2002). The damper characteristic measurements were limited by the maximum actuator velocity available of about 0.25 m/s. Uni-directional forcing of the steering damper at the maximum rate of the actuator yielded a substantially linear force / velocity relationship with slope 4340 N/(m/s). Using the effective moment arm of the damper (0.04 m) this value was converted to an equivalent rotational coefficient of value 6.944 Nm/(rad/s).

The dimensions of the single steel spring from the monoshock rear suspension were measured, and the standard helical spring formula, $k = Gd^4/(64R^3n)$, was applied to calculating the rate, k, as 55000 N/m. The gas filled damper contributes some suspension preload and a small rate which was determined from the test machine via static measurements as 3570 N/m. The damper unit was stroked at full actuator performance first in compression and then in extension, achieving velocities up to about 0.13 m/s. Allowing for the gas pressure forces in the processing, the damping coefficient in compression was 9600 N/(m/s) and in rebound 13700 N/(m/s). Front spring and damper coefficients need to be measured. Suspension limit stops are included at each end, modelled as fifth powers of displacement from stop contact. The relevant displacements are known from examination of the parts and from information given in the workshop manual.

The torsional stiffness of the main frame, between the steering head and the power unit, is yet to be measured. It is clear from the structural design and materials used that the frame is considerably stiffer than conventional tubular framed motorcycles of some years ago. In those cases, it was established that the frame flexibility was an essential contributor to the stability of the wobble mode, in particular (Sharp and Alstead, 1980; Spierings, 1981). It remains to be seen how significant this area is for modern machines. Tyre radial stiffnesses come directly from (Cossalter and Lot, 2002).

The rider's upper body has roll freedom relative to the main frame, while the lower body is part of the main frame. The upper body is restrained by a parallel spring damper system, stiff enough to give a decoupled natural frequency of 11.7 Hz for the rider upper body lean motion. This allows only a modest participation of the rider body in the motorcycle motions.

9.1.3 Aerodynamics

In-plane aerodynamic effects are included, and associated aerodynamic force and moment data comes from a Triumph motorcycle of similar style and dimensions to the GSX-R1000 (Sharp, 2001). This is steady-state drag force, lift force and pitching moment data from full scale wind tunnel testing, with a prone rider.

9.2 Tyre-road contact modelling

A correct representation of the tyre-road contact is important in the accuracy of predicted behaviour for the motorcycle. The geometries involved are naturally complex, especially at the

front, and special care is needed when modelling this feature. It has been common to represent the tyre as an infinitely thin disc with radial compliance, and with the contact point migrating circumferentially for increased camber and steer angles, as described in Chapter 5. An example of a physically more accurate representation which regards the tyre as having width, was introduced by (Cossalter *et al.*, 1999*a*, 2002; Cossalter and Lot, 2002; Cossalter, 2002). When a disc model is used, it needs to be augmented with an overturning moment description (Chapter 5). This is not necessary with a wide tyre model because in that case the contact point migrates laterally automatically and the overturning moment is a consequence of that movement. A further feature of this model is that longitudinal forces applied to the cambered tyre will lead automatically to realistic aligning moments. A wide tyre model with circular cross-section crown is now modelled, as shown in Figures 9.2 and 9.3, with the rear wheel as the example. The AUTOSIM commands used are described in Appendix B.

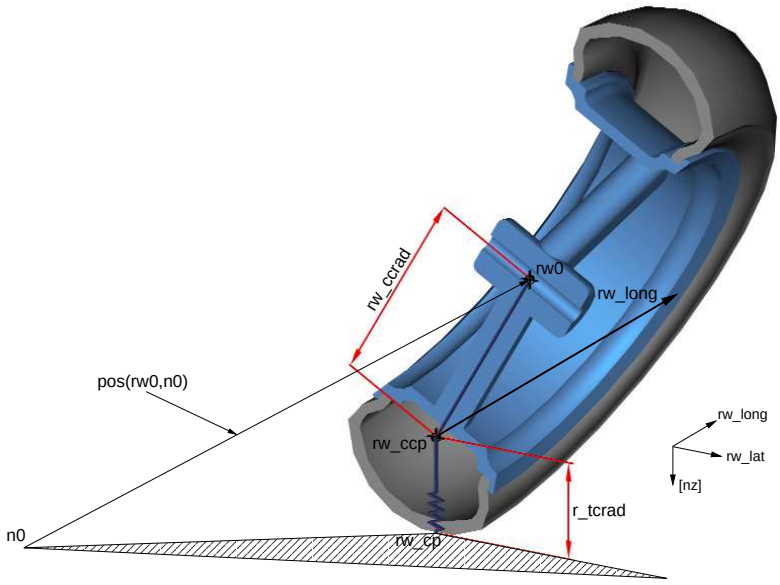

Figure 9.2: Diagrammatic three-dimensional rear wheel contact geometry.

The longitudinal direction with respect to the wheel `rw_long` can be calculated by a cross product between the vertical `[nz]` and wheel spindle `[rwy]` unit vectors. Similarly, the cross product of the longitudinal vector with the wheel spindle vector can be used to obtain a vector in the wheel radial direction. These operations are combined together in a vector triple product with normalisation to obtain the radial unit vector `rw_radl`:

```
dir(cross(cross([rwy],[nz]),[rwy]))
```

The corresponding radial vector from `rw0`, the wheel centre, to `rw_ccp`, the tyre crown centre, is found by multiplying the radial unit vector with the fixed magnitude `rw_ccrad`:

```
@rw_ccrad*@rw_radl
```

As shown in Figures 9.2 and 9.3 the ground contact point `rw_cp` is vertically below the crown centre point `rw_ccp` and the nominal distance between them is `r_tcrad`. In general this distance

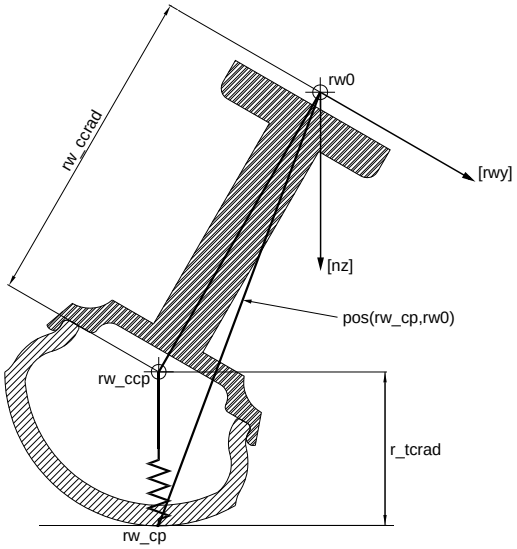

Figure 9.3: Diagrammatic two-dimensional rear wheel contact geometry.

will vary and can be calculated as the magnitude of a vector from the inertial frame origin `n0` to `rw_ccp` projected on to the vertical direction:

```
-dot(pos(rw0,n0)+@rw_ccrad*@rw_radl,[nz])
```

This height is adjusted via a wheel road height variable `r_rht` in the case of a profiled road:

```
-dot(pos(rw0,n0)+@rw_ccrad*@rw_radl,[nz])-r_rht
```

The difference between this distance and the nominal value `r_tcrad`, can be used to calculate the tyre vertical force via the tyre carcass stiffness. Also, combining this distance with the vertical unit vector and adding the radial vector defined above, one obtains a vector with the correct magnitude and direction that points from the wheel spindle axis to the ground contact point:

```
@rw_ccrad*@rw_radl+(-dot(pos(rw0,n0)+@rw_ccrad*@rw_radl,[nz])-r_rht)*[nz])
```

The contact point can now be defined via the coordinates of this vector as a moving point on the tyre outer surface. This point is used to calculate the side-slip and longitudinal slip and it is the point of application of the load and tyre forces. In any case this point remains at road level and when the tyre load becomes negative, which means that the wheel has left the ground, the normal load is reset to zero via a min function, and consequently the shear forces become zero.

In order to find the longitudinal slip the following velocities need to be specified:

(a) **Rolling velocity**. This is the forward velocity of the theoretical ground contact centre (despun as compared with the tread base material). In the absence of camber this is the wheel centre velocity. It is found by taking the dot product of the total velocity of the contact point `rw_cp` with the wheel longitudinal direction `rw_long`:

```
dot(vel(rw_cp),@rw_long)
```

(b) **Tread base velocity**. This is the component of the material contact point velocity in the wheel longitudinal direction, and is found by adding the spin component of the longitudinal velocity to the rolling velocity above:

```
ru(rw)*dot(pos(rw_cp,rw0),@rw_radl)+dot(vel(rw_cp),@rw_long)
```

The spin component of the longitudinal velocity is found by projecting the distance from `rw0` to `rw_cp`, shown in Figure 9.3, onto the wheel radial direction and multiplying by the wheel spin velocity `ru(rw)`.

The tread material longitudinal distortion depends on the ratio of the two velocities specified above. The longitudinal slip is then given by an expression of the form:

$$\kappa = -(\textit{tread base velocity})/\textit{abs}(\textit{rolling velocity})$$

In order to calculate the side-slip, the lateral velocity of the tyre crown centre is defined first as:

```
dot(vel(rw_ccp),@rw_lat)
```

The lateral distortion of the tread material depends on the ratio of the lateral velocity to the rolling velocity. Side-slip is consequently given by:

$$\beta = -(\textit{crown centre lateral velocity})/\textit{abs}(\textit{rolling velocity})$$

Note that the lateral velocity and rolling velocity of the crown centre are equal to the corresponding quantities of the ground contact point because these points always lie in the same vertical line, as shown in Figures 9.2 and 9.3, and consequently they can be interchanged without problem.

In developing the wide tyre model from the previous one (Chapter 5), which treated the wheels as thin discs, subtle differences between the root locus predictions of the old and new versions were observed in circumstances which were at that stage thought physically equivalent. Such differences were found to be associated with the former description of the slip angles as deriving from the lateral velocity components of the disc tyre contact points. When the wheel camber angle is changing these points have a small lateral velocity component not connected with side-slipping, since, with a real tyre, the contact point moves around the circular section sidewall of the tyre. The former model would have provided a more accurate description if it had used the crown centre point velocities to derive the slip angles.

9.3 Tyre forces and moments

9.3.1 Introductory comments

The new tyre model is based on the "Magic Formula" (de Vries and Pacejka, 1997, 1998; Tezuka *et al.*, 2001; Pacejka, 2002). As has been explained earlier, this method was originally developed for car tyres, in which context it became dominant, but recently it has been extended to

motorcycle tyres as well. In the motorcycle case substantial changes are required in order to accommodate the completely different roles of side-slip and camber. In any case, the "Magic Formula" is a set of mathematical equations relating longitudinal slip, side-slip, camber angle and load to longitudinal force, side force and aligning moment with constraints on the equation parameters to preserve at least qualitatively the correctness of the predicted quantities in any operating conditions. Parameter values in the literature are limited, but there is a certain amount of relevant experimental data that can be used for parameter identification.

The requirement here is to find a complete set of parameters to describe modern high performance front and rear tyres. Available test data can be found in (Sakai *et al.*, 1979; Koenen, 1983; Fujioka and Goda, 1995*a*; Ishii and Tezuka, 1997; de Vries and Pacejka, 1997; Tezuka *et al.*, 2001; Pacejka, 2002; Cossalter and Lot, 2002; Cossalter *et al.*, 2003), some of which relate to older tyres. In general, owing to tyre imperfections, these data show bias and left/right asymmetry which is not desired for modelling a generic tyre (rather than a particular tyre), and therefore such imperfections are ignored by omitting certain offset or other terms in the "Magic Formula" relations. The main data sources relied upon here are (de Vries and Pacejka, 1997; Pacejka, 2002), and the others are used for checking purposes. The full set of "Magic Formula" equations is from (Pacejka, 2002) and is reproduced here with minor changes in Appendix C, while the appropriately reduced equations are shown in the following sections.

The data provided were obtained in digital form, either by scanning or from the original source pdf file, and were imported as bitmaps into MATLAB. Manual tracking via the `ginput` (The Mathworks Inc., 2000) command was then necessary to obtain x-y coordinates. The Sequential Quadratic Programming constrained optimisation routine `fmincon` (The Mathworks Inc., 2000) was employed to iteratively improve the elements of a starting vector of parameters appearing in the "Magic Formula" equations, to obtain a best fit (in a least sum of squares of differences sense) of the formula predictions to the measurements. Alternatively, for unconstrained optimisation, the Nelder Mead Simplex routine `fminsearch` (The Mathworks Inc., 2000) was used. Also occasionally, owing to the small amount of data available compared with the number of required parameters, it was necessary to "invent" data outside the range of experimental results available, to force the identified parameters to give sensible predictions over a wide range of operating circumstances, a problem also referred to in (van Oosten *et al.*, 2003). The "brush" model (Pacejka, 2002) behaviour was used on one occasion to guide the choice of constructed data–see 9.3.5. In order to ensure convergence to the optimal solution, it was often needed to provide reasonably accurate starting values for the parameters. The methods should be judged by the results obtained.

9.3.2 List of symbols

F_z	normal load (N)
F_{zo}	nominal normal load (N)
α	side-slip angle (rad)
β	side-slip
γ	camber angle (rad)
κ	longitudinal slip

9.3.3 Longitudinal forces in pure longitudinal slip

From Appendix C, S_{Hx} and S_{Vx} are set to zero to obtain an unbiased[2] tyre. ε_x is a safety term to avoid division by zero and can be set to zero for the present purposes. The "Magic Formula" expressions for the pure longitudinal slip case become:

$$F_{xo} = D_x \sin[C_x \arctan\{B_x\kappa - E_x(B_x\kappa - \arctan(B_x\kappa))\}]$$

$$C_x = p_{Cx1}$$

$$D_x = \mu_x F_z$$

$$\mu_x = p_{Dx1} + p_{Dx2} df_z \qquad (>0)$$

$$E_x = (p_{Ex1} + p_{Ex2} df_z + p_{Ex3} df_z^2) \cdot (1 - p_{Ex4}\,\mathrm{sgn}(\kappa)) \qquad (\leq 1)$$

$$K_{x\kappa} = F_z(p_{Kx1} + p_{Kx2} df_z) \cdot \exp(p_{Kx3} df_z)$$

$$B_x = K_{x\kappa}/(C_x D_x)$$

$$df_z = (F_z - F_{zo})/F_{zo}$$

with the constraints needed to be satisfied as indicated.

Corresponding test data for a 160/70 ZR17 tyre are shown in (Pacejka, 2002) and are reproduced here in Figure 9.4 with the thick lines. F_{zo} was chosen to be 1600 N based on typical usage of such a tyre. That choice is not critical because a change in that value still leads to an optimal set through compensatory changes in other parameters. Optimal parameters were obtained via the `fminsearch` Matlab optimisation function and are given in Table 9.1, with the corresponding fits illustrated in Figure 9.4. The constraint $\mu_x > 0$ is satisfied for loads less than 22452N, while the $E_x \leq 1$ constraint is satisfied for loads less than approximately 20890N. This covers all practical circumstances.

Usable longitudinal force results are not available for any other tyres, so lateral forces are considered next.

9.3.4 Lateral forces in pure side-slip and camber

In exactly the same way, unbiasedness[3] in the tyre and symmetry in side-slip at zero camber angle are preserved by setting S_{Hy} and p_{Ey3} to zero respectively. ε_y was present to avoid the

[2] No longitudinal force for no longitudinal slip.

[3] Zero side force for zero side-slip and camber angle.

	Front tyre **120/70**	Rear tyre **180/55**	Rear tyre **160/70**
p_{Cx1}	1.6064	1.6064	1.6064
p_{Dx1}	1.3806	1.3548	1.2017
p_{Dx2}	-0.041429	-0.060295	-0.092206
p_{Ex1}	0.0263	0.0263	0.0263
p_{Ex2}	0.27056	0.27056	0.27056
p_{Ex3}	-0.076882	-0.076882	-0.076882
p_{Ex4}	1.1268	1.1268	1.1268
p_{Kx1}	25.939	25.939	25.939
p_{Kx2}	-4.2327	-4.2327	-4.2327
p_{Kx3}	0.33686	0.33686	0.33686

Table 9.1: Best-fi t parameter values for longitudinal force from **160/70**, **120/70** and **180/55** tyre.

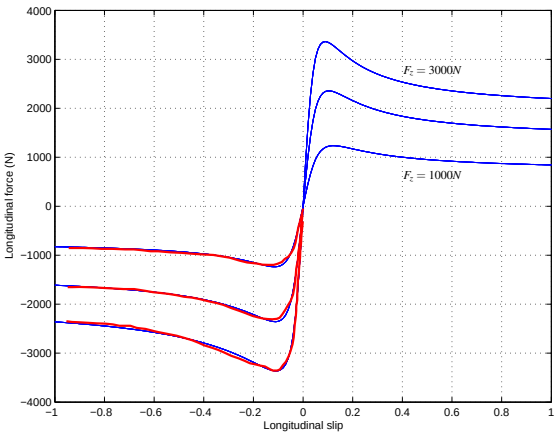

Figure 9.4: **160/70** tyre longitudinal results from (Pacejka, 2002) (thick lines) with best-fi t reconstructions (thin lines) for 0 camber angle and 1000N, 2000N, 3000N normal load.

occurrence of singularities and it can now be ignored. The relevant equations become:

$$F_{yo} = D_y \sin[C_y \arctan\{B_y\beta - E_y(B_y\beta - \arctan(B_y\beta))\} + \\ + C_\gamma \arctan\{B_\gamma\gamma - E_\gamma(B_\gamma\gamma - \arctan(B_\gamma\gamma))\}] \qquad (C_y + C_\gamma < 2)$$

$$C_y = p_{Cy1} \qquad (> 0)$$

$$D_y = \mu_y F_z$$

$$\mu_y = p_{Dy1} \exp(p_{Dy2} df_z)/(1 + p_{Dy3}\gamma^2) \qquad (> 0)$$

$$E_y = p_{Ey1} + p_{Ey2}\gamma^2 + p_{Ey4}\gamma \mathrm{sgn}(\beta) \qquad (\leq 1)$$

$$K_{y\alpha o} = p_{Ky1} F_{zo} \sin[p_{Ky2} \arctan\{F_z/((p_{Ky3} + p_{Ky4}\gamma^2)F_{zo})\}]$$

$$K_{y\alpha} = K_{y\alpha o}/(1 + p_{Ky5}\gamma^2)$$

$$B_y = K_{y\alpha}/(C_y D_y)$$

$$C_\gamma = p_{Cy2} \qquad (> 0)$$

$$K_{y\gamma} = (p_{Ky6} + p_{Ky7} df_z) F_z$$

$$E_\gamma = p_{Ey5} \qquad (\leq 1)$$

$$B_\gamma = K_{y\gamma}/(C_\gamma D_y)$$

with the relevant constraints indicated. For the same tyre as before, the parameter optimisation process gives the results illustrated in Figure 9.5 with parameter values given in Table 9.2. The

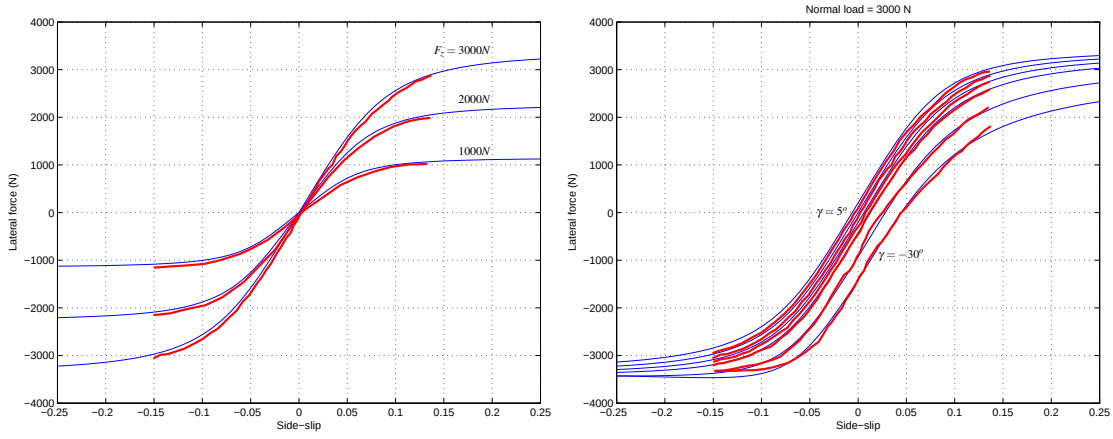

Figure 9.5: **160/70** tyre lateral force results from (Pacejka, 2002) (thick lines) with best-fi t reconstructions (thin lines) for 0 camber angle and 1000N, 2000N, 3000N normal load on the left and for 5^o, 0^o, -5^o, -10^o, -20^o, -30^o camber angles and 3000N normal load on the right.

coefficient of friction μ_y, apart from the constraint shown above, was also limited to values no greater than 1.3 and this was adhered to by the solver for camber angles up to 70 deg. For this particular tyre, the only non-zero camber experimental results available are for only one case of normal load, and therefore p_{Ky7} is set to zero. This is consistent with the relatively small value obtained for the same parameter for tyres 120/70 and 180/55 (see below). The constraint $E_y \leq 1$

is satisfied for camber angles up to 73.6 deg in absolute value as shown in Figure 9.6. All other constraints are globally satisfied.

	Front tyre **120/70**	Rear tyre **180/55**	Rear tyre **160/70**
p_{Cy1}	0.83266	0.9	0.93921
p_{Dy1}	1.3	1.3	1.1524
p_{Dy2}	0	0	-0.01794
p_{Dy3}	0	0	-0.065314
p_{Ey1}	-1.2556	-2.2227	-0.94635
p_{Ey2}	-3.2068	-1.669	-0.098448
p_{Ey4}	-3.9975	-4.288	-1.6416
p_{Ky1}	22.841	15.791	26.601
p_{Ky2}	2.1578	1.6935	1.0167
p_{Ky3}	2.5058	1.4604	1.4989
p_{Ky4}	-0.08088	0.669	0.52567
p_{Ky5}	-0.22882	0.18708	-0.24064
p_{Cy2}	0.86765	0.61397	0.50732
p_{Ky6}	0.69677	0.45512	0.7667
p_{Ky7}	-0.03077	0.013293	0
p_{Ey5}	-15.815	-19.99	-4.7481

Table 9.2: Best-fi t parameter values for lateral force from **160/70**, **120/70** and **180/55** tyre.

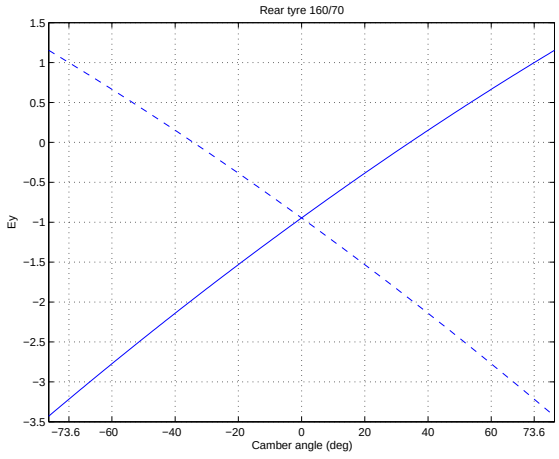

Figure 9.6: Identifi ed **160/70** tyre parameter E_y against camber angle for positive (dashed line) and negative (continuous line) side-slip. The required constraint is $E_y \leq 1$.

The lateral force fitting is repeated for the experimental results included in (de Vries and Pacejka, 1997) for a 120/70 ZR17 front tyre and a 180/55 ZR17 rear tyre. It is recognised

here that the relevant results suffer from an unreasonable positive force offset, especially at larger camber angles and lower loads, which would imply a friction coefficient greater than 2 if they were true. To avoid responding too strongly to these apparently spurious features, μ_y is constrained as before not to exceed 1.3, being a realistic value for a typical road tyre coefficient of friction. The p_{Cy1} parameter is also constrained to values no greater than 0.9 to avoid having an increasing fall of the side force asymptotic saturation level with increasing camber angle at large positive side-slip values. In addition, the measurements for side-slip angles greater than +5 deg (or 0.0875) from the 120/70 tyre are ignored to make the data set used approximately symmetric. F_{zo} was chosen to be 1100 N for the 120/70 tyre and 1600 N for the 180/55 tyre. Best-fit parameters are shown in Table 9.2, and the quality of the fits for the front and rear tyres is shown in Figures 9.7 and 9.8 respectively. All the constraints are satisfied by these parameters. The situation with the $E_y \leq 1$ constraint can be seen in closer detail in Figure 9.9.

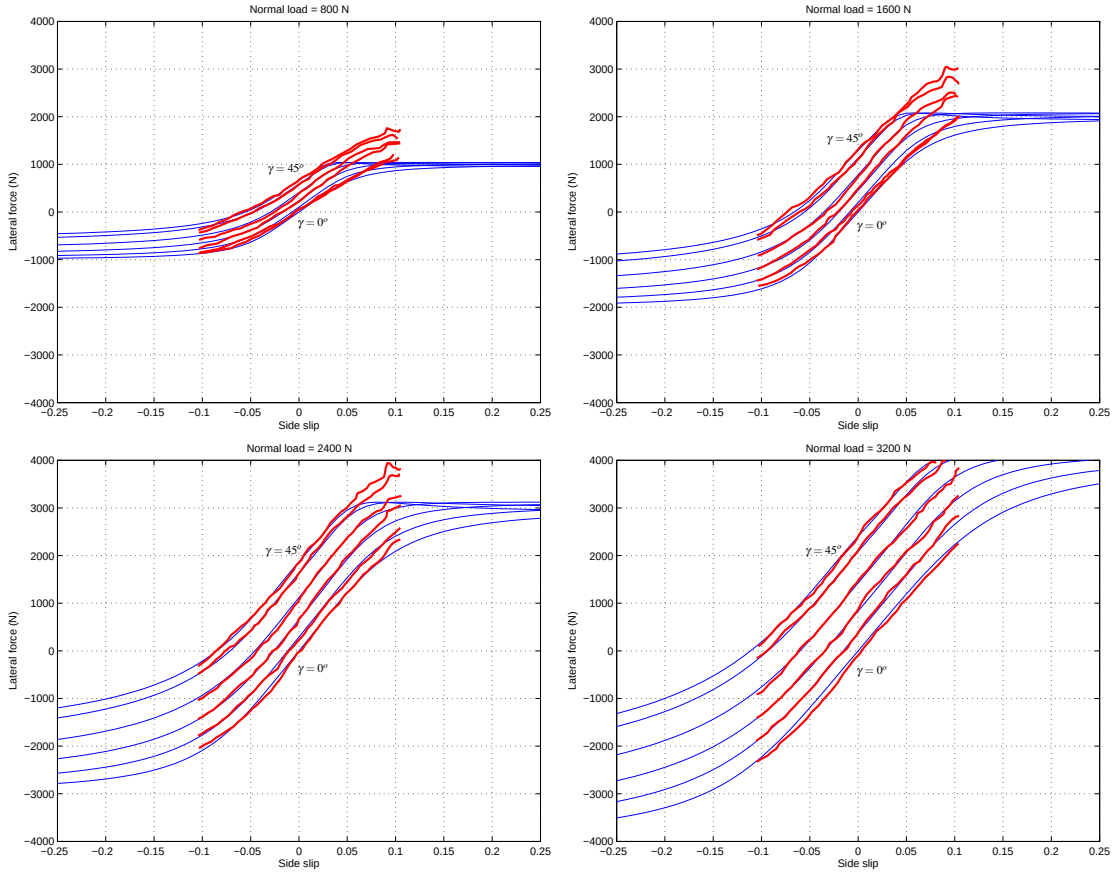

Figure 9.7: **120/70** tyre lateral force results from (de Vries and Pacejka, 1997) (thick lines) with best-fi t reconstructions (thin lines) for 0º, 10^o, 20^o, 30^o, 40^o, 45^o camber angles and 800N, 1600N, 2400N, 3200N normal loads.

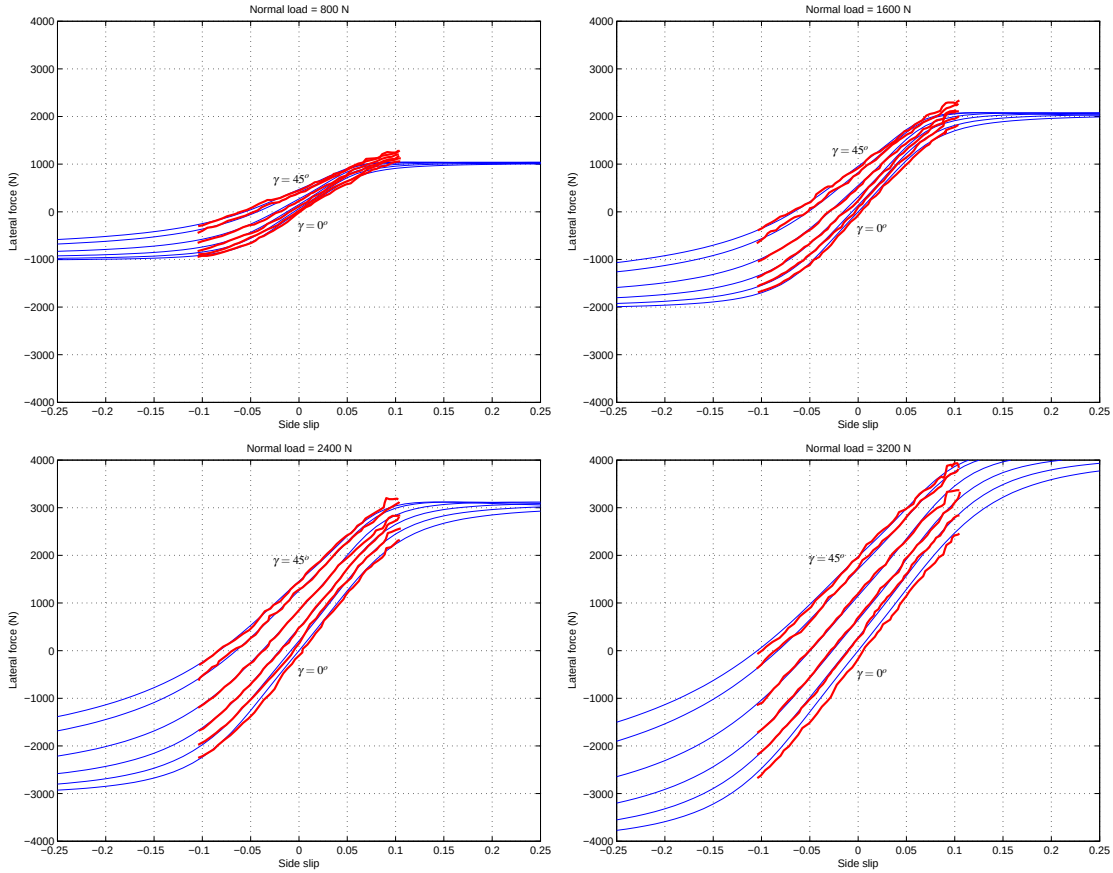

Figure 9.8: **180/55** tyre lateral force results from (de Vries and Pacejka, 1997) (thick lines) with best-fi t reconstructions (thin lines) for 0º, 10^o, 20^o, 30^o, 40^o, 45^o camber angles and 800N, 1600N, 2400N, 3200N normal loads.

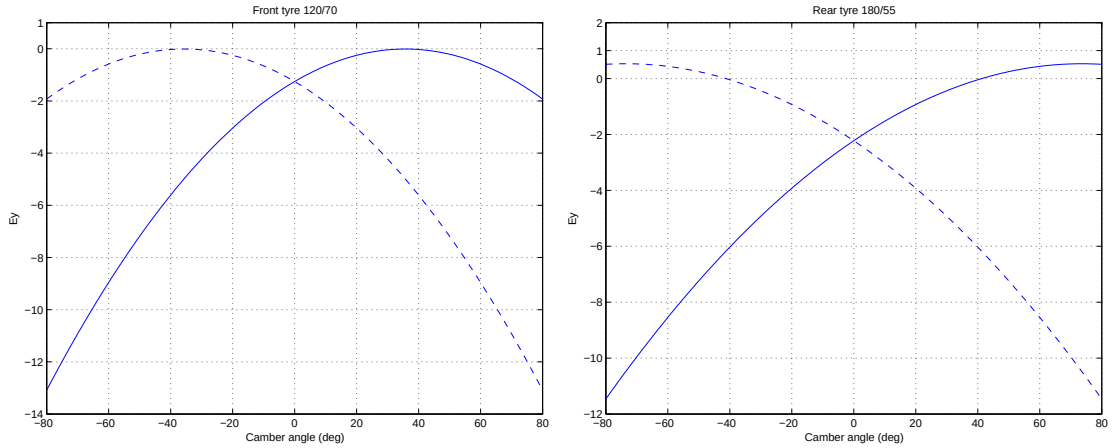

Figure 9.9: Identifi ed parameter E_y against camber angle for front **120/70** and rear **180/55** tyre for positive (dashed line) and negative (continuous line) side-slip. The required constraint is $E_y \leq 1$.

9.3.5 Aligning moment in side-slip and camber

Aligning moment results are included in (Pacejka, 2002) for the 160/70 tyre and in (de Vries and Pacejka, 1997) for the 120/70 and 180/55 tyre. Three loads are covered in (Pacejka, 2002) but only two in (de Vries and Pacejka, 1997), which makes the model very heavy in parameters for the amount of experimental data available. See for example parameters B_t and E_t from the corresponding equations in Appendix C. In setting the parameters for the 160/70 tyre of (Pacejka, 2002) assuming the full quadratic dependency of B_t on load, the fitting is good within the load range used for the measurements but the extrapolation is poor, with constraint violations at low and high loads. With linear dependency, the fitting is almost as good and the extrapolation problem can be eliminated. Consequently, B_t is considered linear with load by setting q_{Bz3} to zero. This linear relationship also proves adequate for the aligning moment stiffness of the tyre (product $B_tC_tD_t$), which should be approximately proportional to load to the power of 1.5. Properly constructed data need to be added to the existing data set outside the measured range for this to happen. The required dependence of the aligning moment stiffness with load comes from physical reasoning via the "brush" model (Pacejka, 2002). It predicts the aligning moment stiffness to be proportional to the contact length to the power of 3. The assumption that the contact length changes quadratically with radial tyre deflection and that the load depends linearly on the radial deflection, implies that the load depends on the contact length to the power of 2. Consequently, the dependence of aligning moment stiffness on load follows. This is used to alleviate the burden associated with the disproportionately large number of model parameters with respect to the existing measured data. Also, in order to aid the $E_t \leq 1$ constraint, q_{Ez3} is not allowed to become positive. As before right/left symmetry (with respect to camber) and zero bias[4] are assumed, making q_{Hz1}, q_{Hz2} and q_{Ez4}, and q_{Dz6} and q_{Dz7} zero respectively.

The relevant "Magic Formula" equations become[5]:

$$M_{zo} = M_{zto} + M_{zro}$$

$$M_{zto} = -t_o \cdot F_{yoo}$$

$$t_o = t_o(\beta) = D_t \cos[C_t \arctan\{B_t\beta - E_t(B_t\beta - \arctan(B_t\beta))\}] / \sqrt{1+\beta^2}$$

$$M_{zro} = M_{zro}(\alpha_r) = D_r \cos[\arctan(B_r\alpha_r)]$$

$$\alpha_r = \beta + S_{Hr}$$

$$S_{Hr} = (q_{Hz3} + q_{Hz4} df_z)\gamma$$

$$B_t = (q_{Bz1} + q_{Bz2} df_z) \cdot (1 + q_{Bz5}|\gamma| + q_{Bz6}\gamma^2) \qquad (>0)$$

$$C_t = q_{Cz1} \qquad (>0)$$

$$D_{to} = F_z(R_o/F_{zo}) \cdot (q_{Dz1} + q_{Dz2} df_z)$$

$$D_t = D_{to}(1 + q_{Dz3}|\gamma| + q_{Dz4}\gamma^2)$$

$$E_t = (q_{Ez1} + q_{Ez2} df_z + q_{Ez3} df_z^2) \cdot \{1 + q_{Ez5}\gamma(2/\pi)\arctan(B_tC_t\beta)\} \qquad (\leq 1)$$

[4] Zero moment for zero side-slip and camber angles.

[5] F_{yoo} is equal to F_{yo} with $\gamma = 0$.

$$B_r = q_{Bz9} + q_{Bz10} B_y C_y$$
$$D_r = F_z R_o \{(q_{Dz8} + q_{Dz9} df_z)\gamma + (q_{Dz10} + q_{Dz11} df_z)\gamma|\gamma|\}/\sqrt{1+\beta^2}$$

also indicating the associated constraints. For the 160/70 tyre, q_{Hz4} in S_{Hr} equation and q_{Dz9} and q_{Dz11} in D_r equation above are set to zero, because experimental results at non-zero camber angle are only provided for one load. For the 120/70 and 180/55 tyres test data at side-slip angles greater than +5 deg are ignored to make those used approximately symmetric, and also some constructed data are added to prevent the absolute value of E_t from becoming large.

The tyre crown radius R_o is found from the cross-sectional geometry as 0.08 m for 160/70, 0.06 m for 120/70 and 0.09 m for 180/55 (Cossalter and Lot, 2002). Identification of the parameters using the MATLAB routines as before gives the values in Table 9.3. The fit qualities are shown in Figures 9.10, 9.11 and 9.12. Figures 9.13 and 9.14 illustrate the match achieved between the aligning moment stiffness ($B_tC_tD_t$ product) and the load to the power of 1.5. The $E_t \leq 1$ constraint violation is summarised in Table 9.4. This includes all practical running conditions. The other constraints are always satisfied.

	Front tyre **120/70**	Rear tyre **180/55**	Rear tyre **160/70**
q_{Hz3}	-0.0037886	-0.028448	-0.049075
q_{Hz4}	-0.01557	-0.0098618	0
q_{Bz1}	10.486	10.041	10.354
q_{Bz2}	-0.0011536	-1.6065e-08	4.3004
q_{Bz5}	-0.68973	-0.76784	-0.34033
q_{Bz6}	1.0411	0.73422	-0.13202
q_{Cz1}	1.0917	1.3153	1.3115
q_{Dz1}	0.19796	0.26331	0.20059
q_{Dz2}	0.065629	0.030987	0.052816
q_{Dz3}	0.2199	-0.62013	-0.21116
q_{Dz4}	0.21866	0.98524	-0.15941
q_{Ez1}	-0.91586	-0.19924	-3.9247
q_{Ez2}	0.11625	-0.017638	10.809
q_{Ez3}	-0.0024085	0	-7.5785
q_{Ez5}	1.4387	3.6511	0.9836
q_{Bz9}	27.445	16.39	10.118
q_{Bz10}	-1.0792	-0.35549	-1.0508
q_{Dz8}	0.3682	0.50453	0.30941
q_{Dz9}	0.1218	0.36312	0
q_{Dz10}	0.25439	-0.19168	0.10037
q_{Dz11}	-0.17873	-0.40709	0

Table 9.3: Best-fi t parameter values for aligning moment from 160/70, 120/70 and 180/55 tyre.

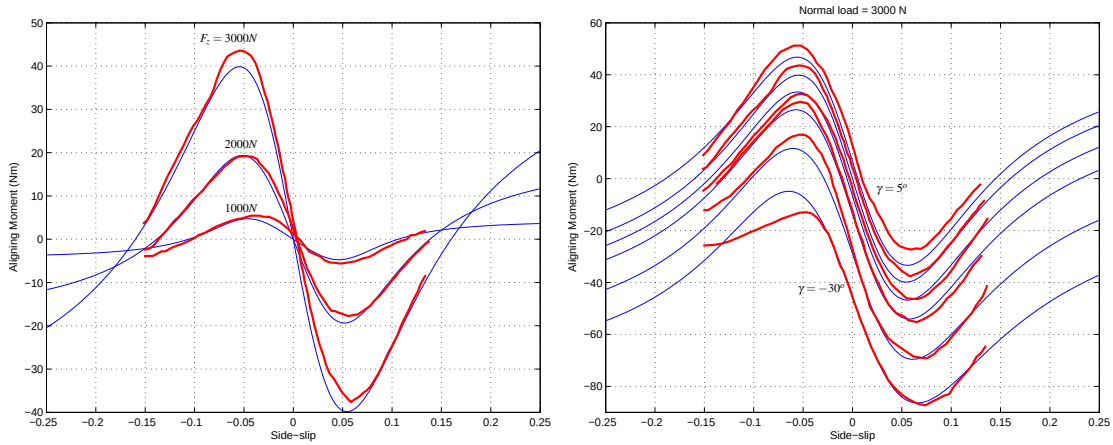

Figure 9.10: **160/70** tyre aligning moment results from (Pacejka, 2002) (thick lines) with best-fi t reconstructions (thin lines) for 0 camber angle and 1000 N, 2000 N, 3000 N normal loads on the left fi gure and -30^o, -20^o, -10^o, -5^o, 0^o, 5^o camber angles and 3000 N normal load on the right fi gure.

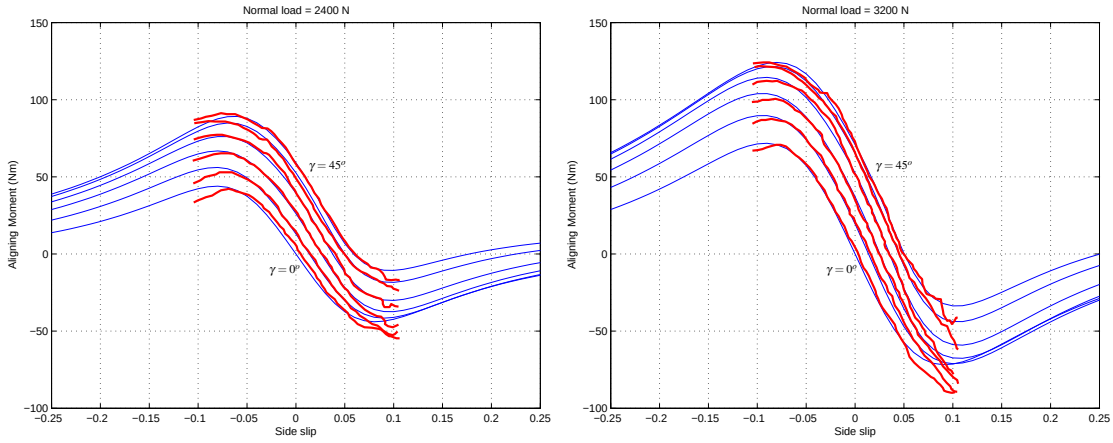

Figure 9.11: **120/70** aligning moment results from (de Vries and Pacejka, 1997) (thick lines) with best-fi t reconstructions (thin lines) for 0^o, 10^o, 20^o, 30^o, 40^o, 45^o camber angles and 2400 N, 3200 N normal loads.

	Front tyre **120/70**	Rear tyre **180/55**	Rear tyre **160/70**
side-slip	∞	∞	1
camber angle (deg)	70	70	60
load (N)	20000	11000	12000

Table 9.4: Maximum values of side-slip, camber angle and load for which $E_t \leq 1$ constraint is satisfi ed for 160/70, 120/70 and 180/55 tyre.

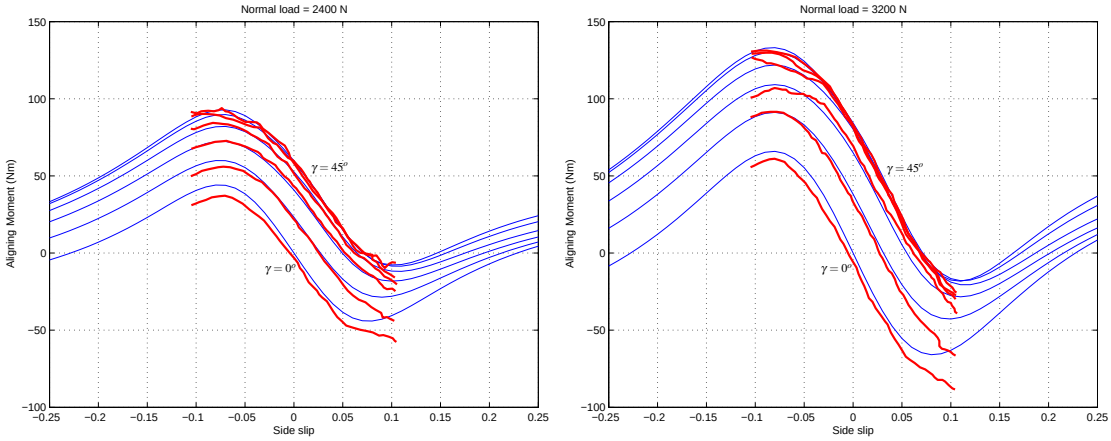

Figure 9.12: **180/55** aligning moment results from (de Vries and Pacejka, 1997) (thick lines) with best-fi t reconstructions (thin lines) for 0º, 10^o, 20^o, 30^o, 40^o, 45^o camber angles and 2400 N, 3200 N normal loads.

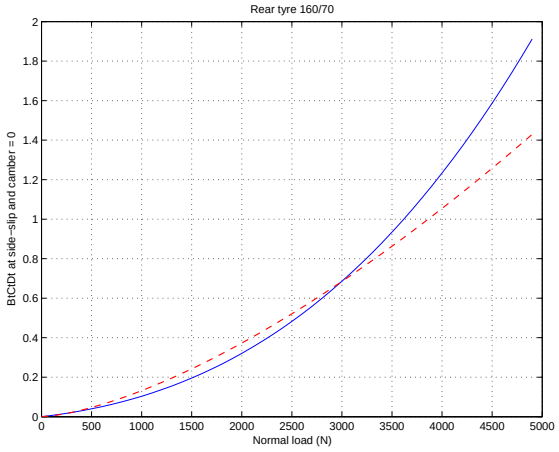

Figure 9.13: **160/70** tyre aligning moment slope at the origin ($B_tC_tD_t$ product at zero side-slip and camber angle) (continuous line) with scaled load to the power of 1.5 (dashed line).

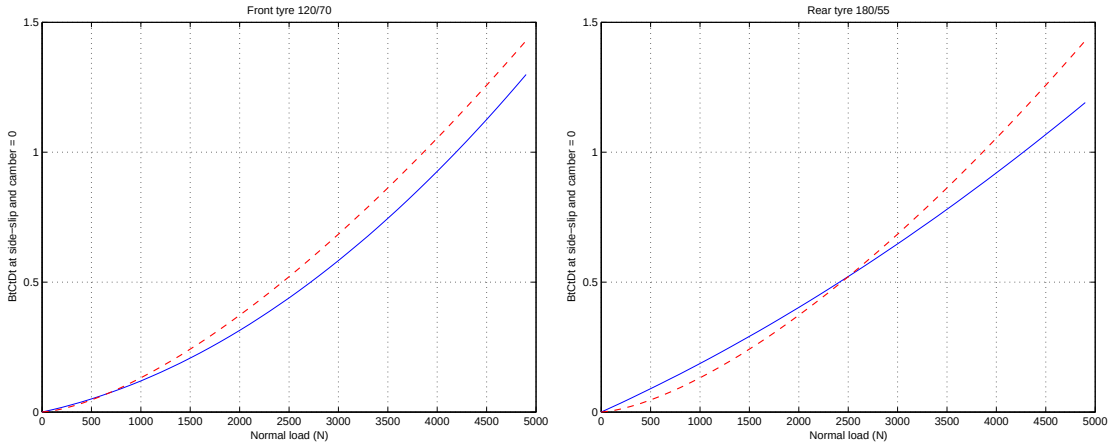

Figure 9.14: **120/70** and **180/55** tyre aligning moment slope at the origin ($B_tC_tD_t$ product at zero side-slip and camber angle) (continuous lines) with scaled load to the power of 1.5 (dashed lines).

9.3.6 Combined slip results

9.3.6.1 Longitudinal forces

In the "Magic Formula" scheme, the loss of longitudinal force due to side-slipping is described by a "loss function" to be applied to the pure slip force expression described earlier in Section 9.3.3. In the absence of any data or other indication to the contrary, it is assumed that wheel camber will not affect the loss of longitudinal force due to side-slipping ($r_{Bx3} = 0$), and as before the generic tyres of interest are presumed to be symmetric ($S_{Hx\alpha} = 0$). Thus the equations describing the loss are:

$$F_x = G_{x\alpha} F_{xo}$$

$$G_{x\alpha} = \cos[C_{x\alpha} \arctan(B_{x\alpha}\beta)] \qquad (> 0)$$

$$B_{x\alpha} = r_{Bx1} \cos[\arctan(r_{Bx2}\kappa)] \qquad (> 0)$$

$$C_{x\alpha} = r_{Cx1}$$

with two constraints shown.

The only relevant combined slip data available are from (Pacejka, 2002) for the 160/70 tyre for 3000 N load and zero camber angle. These together with the pure slip force data shown in Figure 9.4 were used in a parameter identification process as before and yielded the optimum parameter values as $r_{Bx1} = 13.476$; $r_{Bx2} = 11.354$; $r_{Cx1} = 1.1231$, with the fit quality shown in Figure 9.15. The loss function is illustrated in Figure 9.16. The constraint on $B_{x\alpha}$ is always satisfied while that on $G_{x\alpha}$ is satisfied for side-slip angles less than approximately 23 degrees, which is considered to provide an adequate operating range.

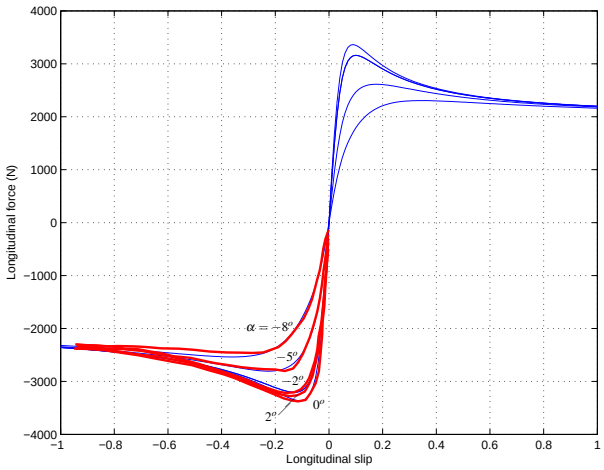

Figure 9.15: Influence of side-slip on longitudinal force for **160/70** tyre at 3000 N load and 0 camber angle. Data from (Pacejka, 2002) (thick lines) with best-fi t reconstructions (thin lines).

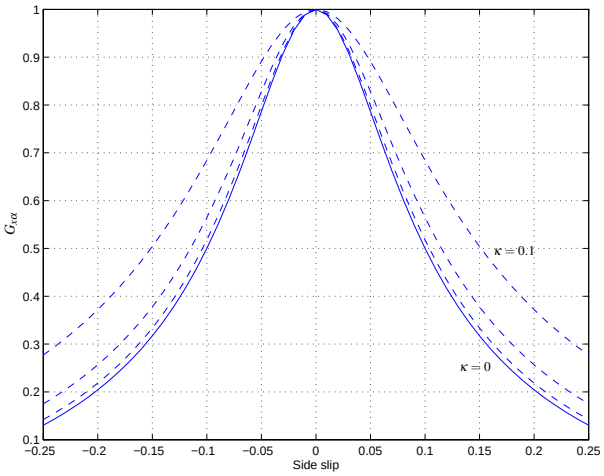

Figure 9.16: Longitudinal force loss function for longitudinal slip of 0, 0.025, 0.5 and 0.1. The continuous line is for zero longitudinal slip.

9.3.6.2 Lateral forces

In the same way (with $S_{Vy\kappa} = S_{Hy\kappa} = r_{By4} = 0$ for zero bias[6], symmetry with longitudinal slip and no camber influence on loss function respectively), the equations describing the loss of lateral force due to longitudinal slip are:

$$F_y = G_{y\kappa} F_{yo}$$

$$G_{y\kappa} = \cos[C_{y\kappa} \arctan(B_{y\kappa}\kappa)] \qquad (> 0)$$

$$B_{y\kappa} = r_{By1} \cos[\arctan\{r_{By2}(\beta - r_{By3})\}] \qquad (> 0)$$

$$C_{y\kappa} = r_{Cy1}$$

[6]Longitudinal slip alone cannot produce a side force.

needing to satisfy the indicated constraints.

Data again comes from (Pacejka, 2002) and are for the 160/70 tyre at 3000 N and zero camber angle. These together with the pure side-slip force data shown in Figure 9.5 were used and yielded the best-fit parameters as $r_{By1} = 7.7856$, $r_{By2} = 8.1697$, $r_{By3} = -0.05914$ and $r_{Cy1} = 1.0533$. The fit quality is shown in Figures 9.17 and 9.18. The loss function is illustrated in Figure 9.19. Both constraints are satisfied.

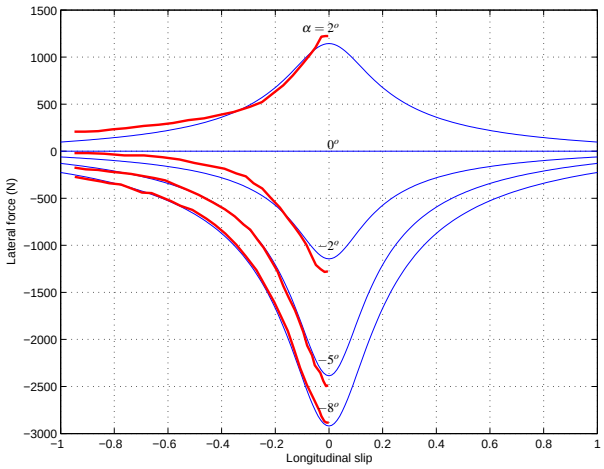

Figure 9.17: Influence of longitudinal slip on lateral force for 160/70 tyre at 3000 N load and 0 camber angle. Data from (Pacejka, 2002) (thick lines) with best-fi t reconstructions (thin lines).

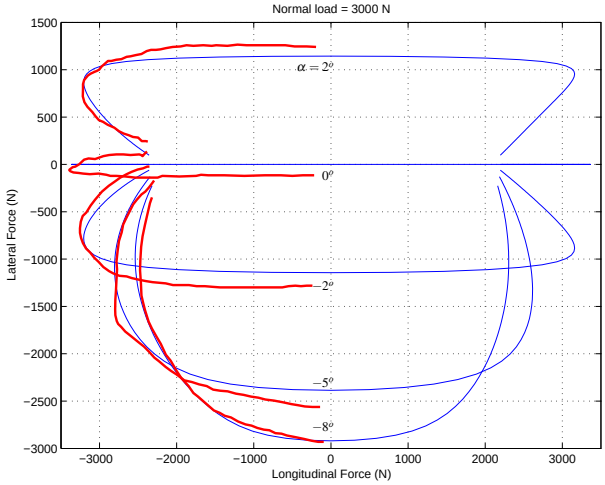

Figure 9.18: Influence of side-slip on longitudinal and lateral forces for 160/70 tyre at 3000 N load and 0 camber angle. Data from (Pacejka, 2002) (thick lines) with best-fi t reconstructions (thin lines). The longitudinal slip varies from -1 to 1.

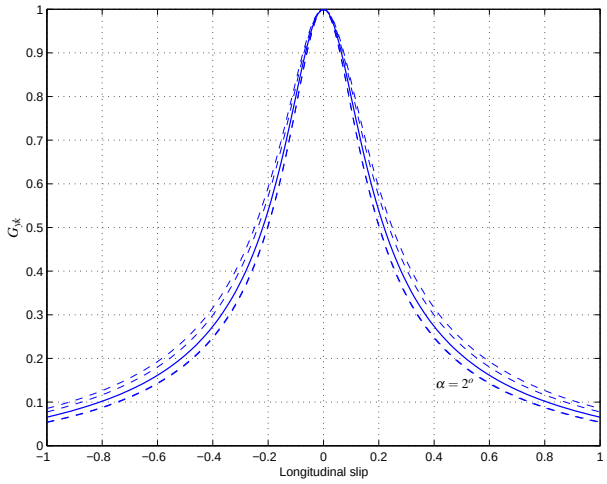

Figure 9.19: Lateral force loss function for side-slip angles of 2^o, 0^o, -2^o, -5^o, -8^o. The continuous line is for 0 side-slip angle. The curves for 2^o and -2^o coincide.

9.3.6.3 Aligning moments

In much the same way, with $s = S_{Vy\kappa} = 0$, the relevant equations from Appendix C become[7]:

$$M_z = M_{zt} + M_{zr}$$

$$M_{zt} = -t \cdot F_{y,\gamma=0}$$

$$t = t(\lambda_t) = D_t \cos[C_t \arctan\{B_t\lambda_t - E_t(B_t\lambda_t - \arctan(B_t\lambda_t))\}]/\sqrt{1+\beta^2}$$

$$F_{y,\gamma=0} = G_{y\kappa}F_{yoo}$$

$$M_{zr} = M_{zr}(\lambda_r) = D_r \cos[\arctan(B_r\lambda_r)]$$

$$\lambda_t = \sqrt{\beta^2 + \left(\frac{K_{x\kappa}}{K_{y\alpha oo}}\right)^2 \kappa^2} \cdot \mathrm{sgn}(\beta)$$

$$\lambda_r = \sqrt{\alpha_r^2 + \left(\frac{K_{x\kappa}}{K_{y\alpha oo}}\right)^2 \kappa^2} \cdot \mathrm{sgn}(\alpha_r)$$

The contribution associated with the $s \cdot F_x$ term in the original equations is included automatically here since the moment reference point is the actual contact point (wide tyre model).

All parameters here can be traced in previous sections, therefore further identification is unnecessary and the combined slip moments can be predicted from what is already known. The aligning moment for the 160/70 tyre at 3000 N load and 0 camber angle, as a function of longitudinal slip, for several side-slip angles, is shown in Figure 9.20.

[7] $K_{y\alpha oo}$ is equal to $K_{y\alpha}$ with $\gamma = 0$.

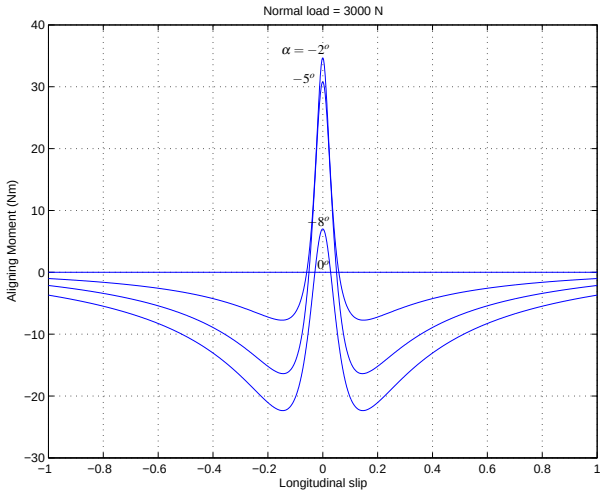

Figure 9.20: Aligning moment for 160/70 tyre at 3000 N load and 0 camber as a function of longitudinal slip for each of four side-slip cases.

9.3.7 Longitudinal force models for 120/70 and 180/55 tyres

Longitudinal forces for 120/70 and 180/55 tyres were not measured in (de Vries and Pacejka, 1997). In order to complete a general description of those tyres, it is necessary to make up, using the best evidence available, appropriate parameter values to describe their longitudinal properties. The strategy for doing so is to use the 160/70 tyre as a model and to scale its data according to some criterion to obtain the other tyres' properties. Longitudinal pure slip parameters for the 160/70 tyre are given in Table 9.1, while those for pure lateral slip appear in Table 9.2. The criterion used is that the ratio of the peak longitudinal and lateral forces, D_x/D_y, remains constant for all tyres. This ratio can be completely defined for the 160/70 tyre for the three different loads for which measured data exist, as shown in Figure 9.21. For the other two tyres, D_y is already known and it remains to find D_x via the following expressions:

$$D_{x_{120/70}} = \frac{D_{x_{160/70}}}{D_{y_{160/70}}} \times D_{y_{120/70}}$$

and

$$D_{x_{180/55}} = \frac{D_{x_{160/70}}}{D_{y_{160/70}}} \times D_{y_{180/55}}.$$

Once D_x is calculated for each of the three loads, local parameter identification via `fminsearch` gives the corresponding p_{Dx1} and p_{Dx2} parameters in the longitudinal force equations for each of the 120/70 and 180/55 tyres. Their shapes are assumed to be the same as those for the 160/70, thus only these parameters need to be changed, as shown in Table 9.1. Predicted longitudinal forces for these tyres are shown in Figure 9.22. The longitudinal force peaks are about 1.33 ($= \mu_y \times (D_x/D_y)$) times the tyre load in the usual operating range of loads, which is compatible with contemporary motorcycle performance in acceleration or deceleration.

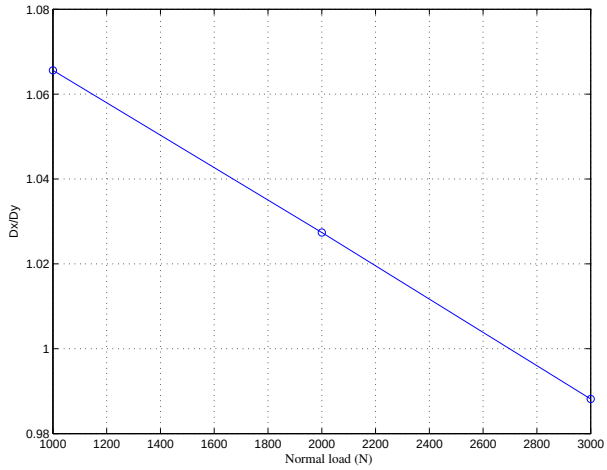

Figure 9.21: **160/70** tyre D_x/D_y ratio against normal load at 0 camber angle.

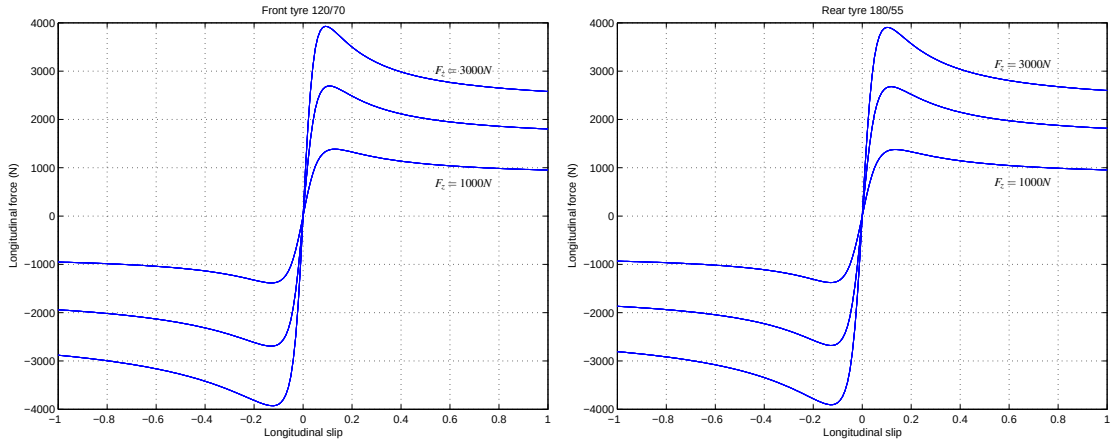

Figure 9.22: **120/70** and **180/55** tyre longitudinal force predictions for 0 camber angle and 1000 N, 2000 N, 3000 N normal loads.

9.3.8 Combined slip force models for 120/70 and 180/55 tyres

The combined slip parameters given for the 160/70 tyre in section 9.3.6.1 are regarded as describing the behaviour of the 120/70 and 180/55 tyres also. Combination of longitudinal force under pure longitudinal slip from section 9.3.3 with the longitudinal loss function data from 9.3.6.1, and combination of lateral force under pure side-slip and camber from section 9.3.4 with the lateral loss function data of 9.3.6.1 allows the prediction of combined slip forces generally. Combination of pure side-slip and camber aligning moments from section 9.3.5 with loss function data from 9.3.6.1 also allows combined slip aligning moments to be predicted.

9.3.9 Checking against other data

The full tyre model has been used to obtain force and moment predictions corresponding to running conditions for which data have been published, for comparison purposes. Each case is

treated individually.

In Figure 9.23 an older rear tyre from (Sakai *et al.*, 1979) is compared with the present model. Even though there is a clear difference in absolute values between the measurements and the model, it seems that there is agreement throughout the range with respect to the slopes involved, with slightly better agreement for the 160/70 tyre.

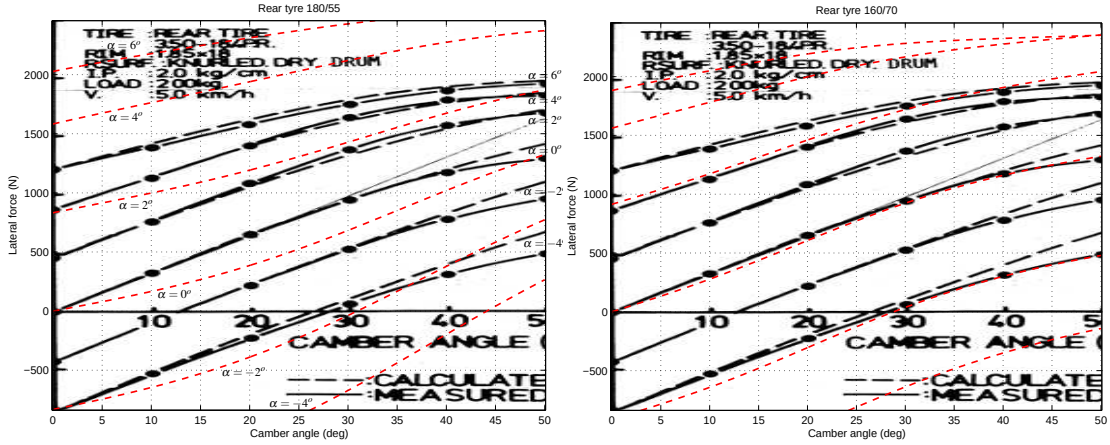

Figure 9.23: **3.50-18.4P.R.** rear tyre lateral force results (Sakai *et al.*, 1979) (continuous lines) with **180/55** tyre (dashed lines on left fi gure) and **160/70** tyre (dashed lines on right fi gure) predictions for six side-slip angles and 1962 N normal load.

The agreement between the model prediction and the tyre results from (Koenen, 1983), shown in Figure 9.24, is within acceptable bounds. The falling slope with camber angle apparent in the results, does not seem to be predicted by the magic formula model.

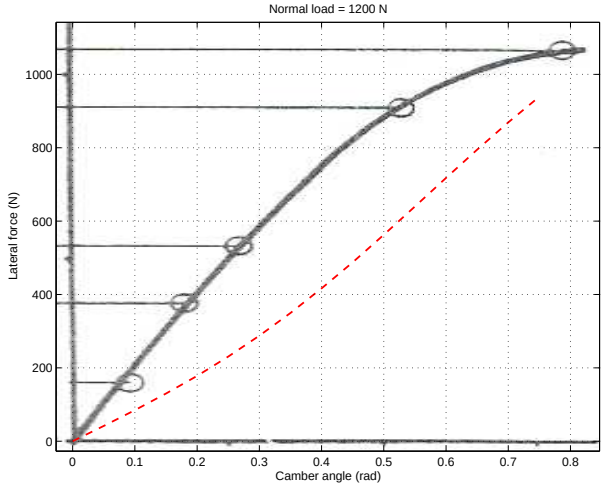

Figure 9.24: Tyre camber thrust results at zero side-slip (Koenen, 1983) (continuous line) with **120/70** tyre (dashed line) predictions for 1200 N normal load.

The model is compared with a 120/70 tyre from (Fujioka and Goda, 1995*a*) in Figure 9.25. In this case it was necessary to reverse the sign of the side-slip, camber angles, side force and

aligning moment to correspond to the different coordinate system used in (Fujioka and Goda, 1995*a*)[8]. There is very good agreement in the lateral force results, and good agreement in the aligning moment for relatively small side-slip angles.

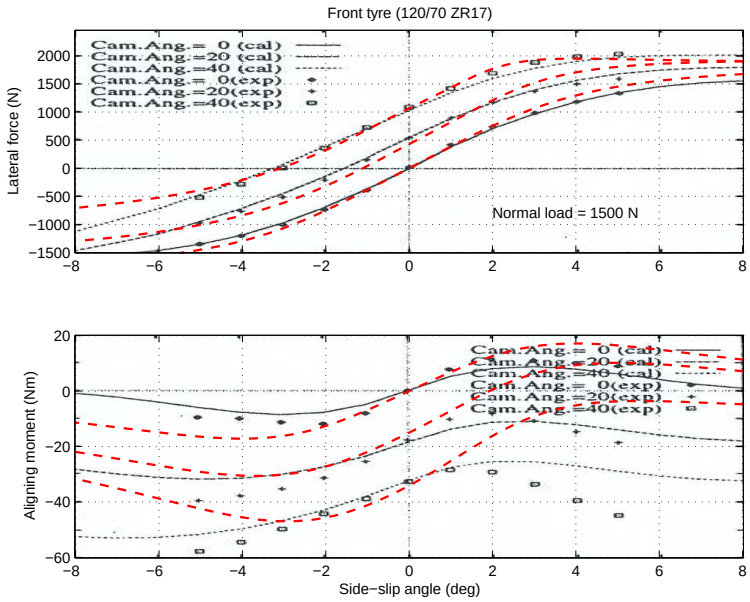

Figure 9.25: **120/70** tyre lateral force and aligning moment results (Fujioka and Goda, 1995*a*) (discrete points) with same tyre model predictions (dashed lines) for 0^o, 20^o, 40^o camber angles and 1500 N normal load.

Next, front and rear tyres from (Ishii and Tezuka, 1997) are given in Figure 9.26 together with the corresponding predictions from the present model. The correlations are acceptable in most cases except for aligning moments at large values of side-slip. Note that the aligning moment experimental results for the rear tyre seem to have a scaling problem which has been corrected in the predicted values.

In the case of Figure 9.27, results from (Cossalter and Lot, 2002) are compared. These relate to a modern set of tyres and agree very well with the model predictions almost everywhere.

The plots on the left column of Figure 9.28 show normalised tyre side force changes with camber angle when side-slip is zero. The top plot is for three different front 120/70 tyres. The "Magic Formula" model predicts a camber force that is less in magnitude by an approximately constant percentage at each camber angle. The bottom plot is for three different rear 180/55 tyres and when compared with the model predictions the same pattern of constant difference is observed, with bigger differences in this case. Similar behaviour is found in the middle plot where one 120/70 tyre is shown at three different normal loads. The systematic difference tends to reinforce the argument that there was a larger error than what was thought with the calculation of the curvature force due to the rotating disc test machine in (Cossalter *et al.*, 2003), and that the model predictions behave normally. A further observation from the results presented in the

[8]The sign of the aligning moment in (Fujioka and Goda, 1995*a*) seems to be inconsistent with its associated coordinate system.

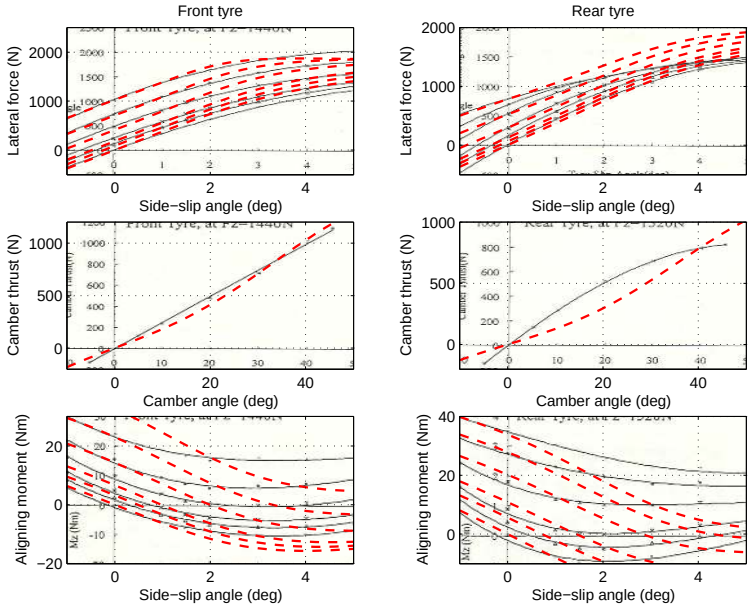

Figure 9.26: Front **130/70** and rear **190/50** tyre lateral force, camber thrust (at 0 side-slip) and aligning moment results (Ishii and Tezuka, 1997) (continuous lines), with front **120/70** and rear **180/55** tyre (dashed lines) predictions, for 1440 N front tyre load and 1520 N rear tyre load. The lateral force and aligning moment are for 0^o, 5^o, 10^o, 20^o, 30^o and 40^o camber angles.

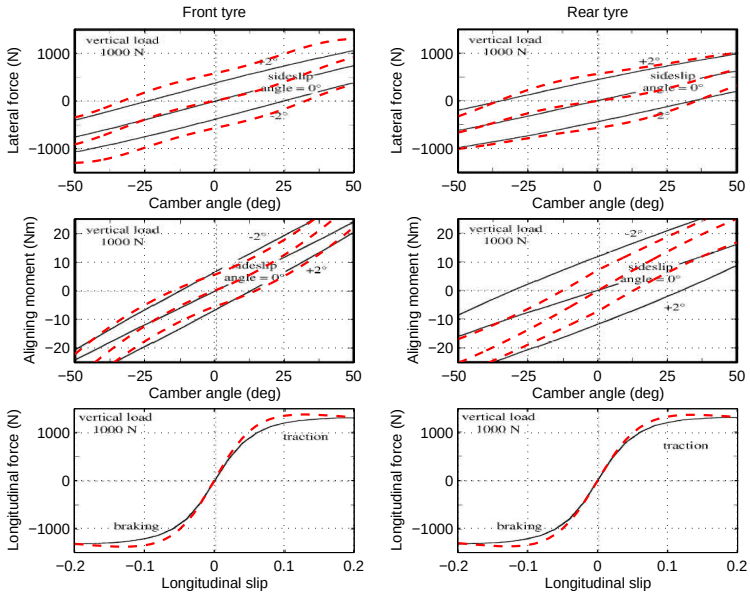

Figure 9.27: Aprilia RSV 1000 tyres lateral, longitudinal force and aligning moment results (Cossalter and Lot, 2002) (continuous lines) with front **120/70** and rear **180/55** tyre (dashed lines) predictions for 1000 N normal load, and in the case of the lateral forces and aligning moments, for -2^o, 0^o, 2^o side-slip angles.

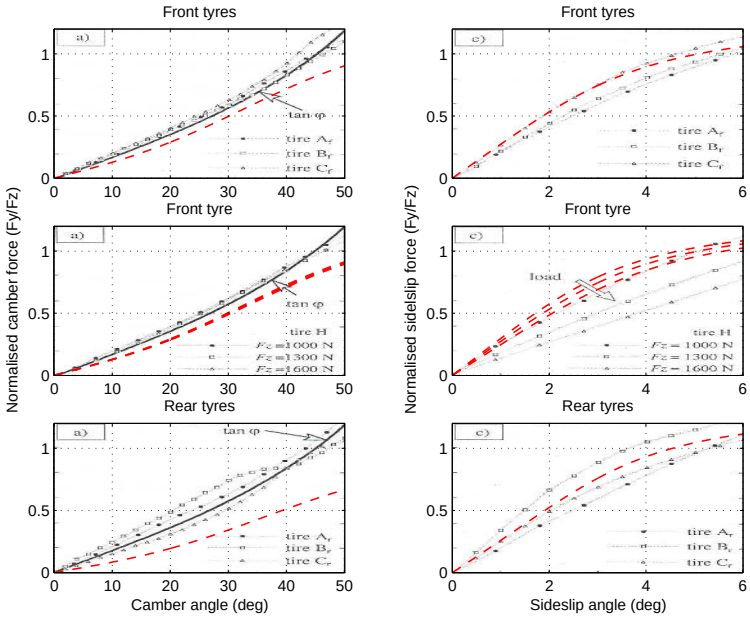

Figure 9.28: Front **120/70** and rear **180/55** tyres normalised camber force (side-slip = 0) and side-slip force (camber = 0) results (Cossalter *et al.*, 2003) (continuous lines with symbols) with front **120/70** and rear **180/55** tyre (dashed lines) predictions for 1300 N load in the top and bottom plots and 1000 N, 1300 N, 1600 N load in the middle.

middle plot is that the variation with load in the normalised camber force (F_y/F_z) is very small which is also verified by the model predictions. The constant ratio between camber force and normal load is physically based, since the camber force is generated by changes in the tyre geometry (tangent law) (Pacejka and Sharp, 1991), and this is correctly represented here.

The plots on the right column of Figure 9.28 show normalised side-slip force against side-slip angle when camber is zero. The same tyres and loads are considered as before. The middle plot shows that there is a decrease in the normalised side force due to side-slip when the load is increased. This is consistent with tyre practice. As the load is increased the contact patch becomes larger but eventually the carcass starts to buckle, which leads to a reduction in side force. The amount by which the side force is reduced with increased load is predicted to be smaller by the model equations than with the results in (Cossalter *et al.*, 2003).

The plots in Figure 9.29 show the twisting torque, self aligning torque and the combined yaw torque results for three different front 120/70 tyres. The model predicts slightly bigger twisting torque and smaller self aligning torque.

In general the results presented here are in agreement with the "Magic Formula" model predictions, with naturally better correlation with newer tyres that the model is intended to represent. In this way reassurance is provided that the generic model with its parameters can be employed with confidence.

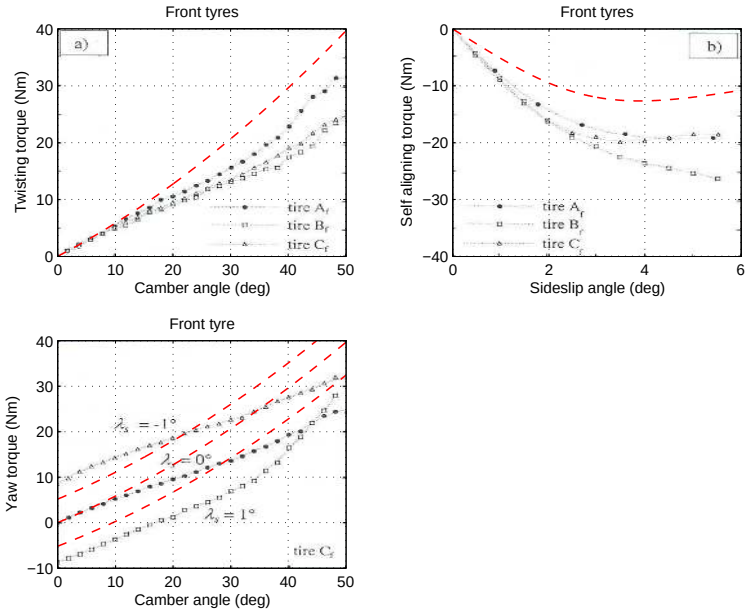

Figure 9.29: **120/70** tyres twisting torque (side-slip = 0), self aligning torque (camber = 0) and yaw torque results (Cossalter *et al.*, 2003) (continuous lines with symbols) with **120/70** tyre (dashed lines) predictions, for 1300 N normal load, and in the case of the yaw torque, for -1^o, 0^o, 1^o side-slip angles.

9.3.10 Relaxation length description and data

It is essential when modelling motorcycle tyres to include relaxation effects so that the higher frequency mode properties are correctly replicated. Conventionally, a constant relaxation length for each tyre is employed but it was found in (de Vries and Pacejka, 1997) that the tyre relaxation length varies with load roughly as the cornering stiffness does and that it grows with speed. Using the data for front 120/70 and rear 180/55 tyres in Table 9.5 that come directly from (de Vries and Pacejka, 1997) and fitting a quadratic function of speed to the results in each case, we obtain the descriptions:

$$\sigma_f = K_{y\alpha f,\gamma=o}(8.633\times10^{-6} + 3.725\times10^{-8}\cdot V + 8.389\times10^{-10}\cdot V^2)$$

$$\sigma_r = K_{y\alpha r,\gamma=o}(9.694\times10^{-6} - 1.333\times10^{-8}\cdot V + 1.898\times10^{-9}\cdot V^2)$$

where V is the forward speed, and σ_f/σ_r the relaxation length and $K_{y\alpha f,\gamma=o}/K_{y\alpha r,\gamma=o}$ the cornering stiffness for zero camber and side-slip angles for front/rear tyres respectively. The cornering stiffnesses come from the "Magic Formula" computations through the equations in section 9.3.4. The fit quality is shown in Figure 9.30.

Relaxation is applied to the side-slip rather than the side forces, through equations of the form: $\sigma\dot{\beta}_1/V + \beta_1 = \beta$. This implies that only forces and moments arising from side-slip are lagged, while those arising from camber are treated as occurring instantaneously. Such a representation is considered to be more physically accurate in view of the nature of the force generating mechanism in each case: camber leads to forces geometrically, while side-slip leads

	front 120/70	rear 180/55
20 km/h	0.91×10^{-5}	0.97×10^{-5}
59 km/h	0.90×10^{-5}	0.99×10^{-5}
100 km/h	1.04×10^{-5}	1.09×10^{-5}
140 km/h	1.16×10^{-5}	1.20×10^{-5}
200 km/h	1.32×10^{-5}	1.48×10^{-5}
251 km/h	1.53×10^{-5}	1.80×10^{-5}

Table 9.5: Front **120/70** and rear **180/55** tyre 'Relaxation length'/'cornering stiffness' results from (de Vries and Pacejka, 1997).

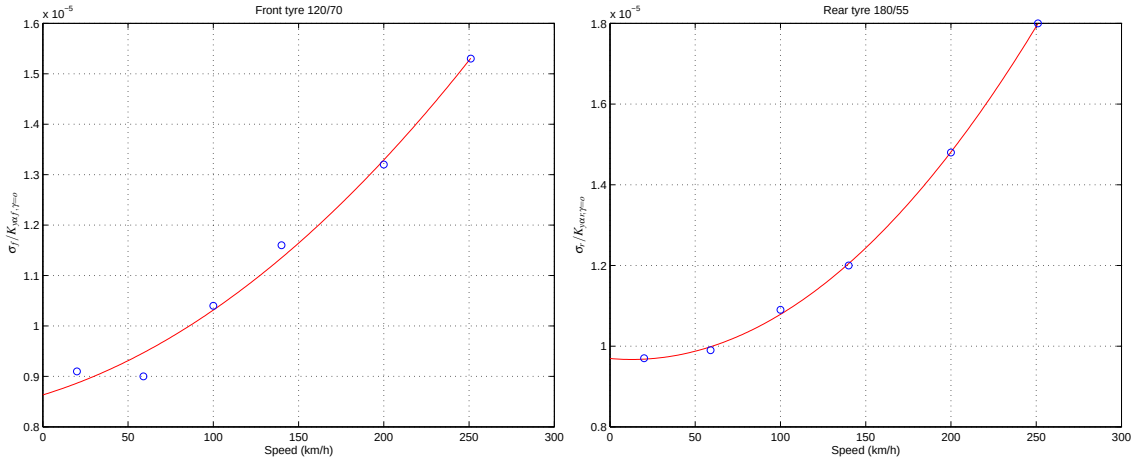

Figure 9.30: **120/70** and **180/55** tyre 'Relaxation length'/'cornering stiffness' results (circles) with polynomial fi t (continuous line).

to forces via distortion of the tyre carcass, which distortion requires time (or distance rolled) to establish.

9.4 "Monoshock" rear suspension

A "monoshock" rear suspension is modelled here as an alternative to the twin-shock system already present in the established motorcycle model. The mechanical arrangement of such a system is shown diagrammatically in Figure 9.31. In its present form, it is fitted to the Suzuki GSX-R1000, and it uses a single spring/damper unit with a mechanical linkage connection between the main frame and the swinging arm of the motorcycle. Many modern rear suspensions found on other machines are of this type, although several variants of it exist. It involves a closed kinematic loop which, when added directly into the model, will provide equations of motion which integrate relatively slowly, since the simulation has to solve the kinematic loop equations at each integration step. When modelling such a suspension it is preferred to do this off-line via a separate geometric pre-analysis. Such a pre-analysis may yield an analytic relationship between

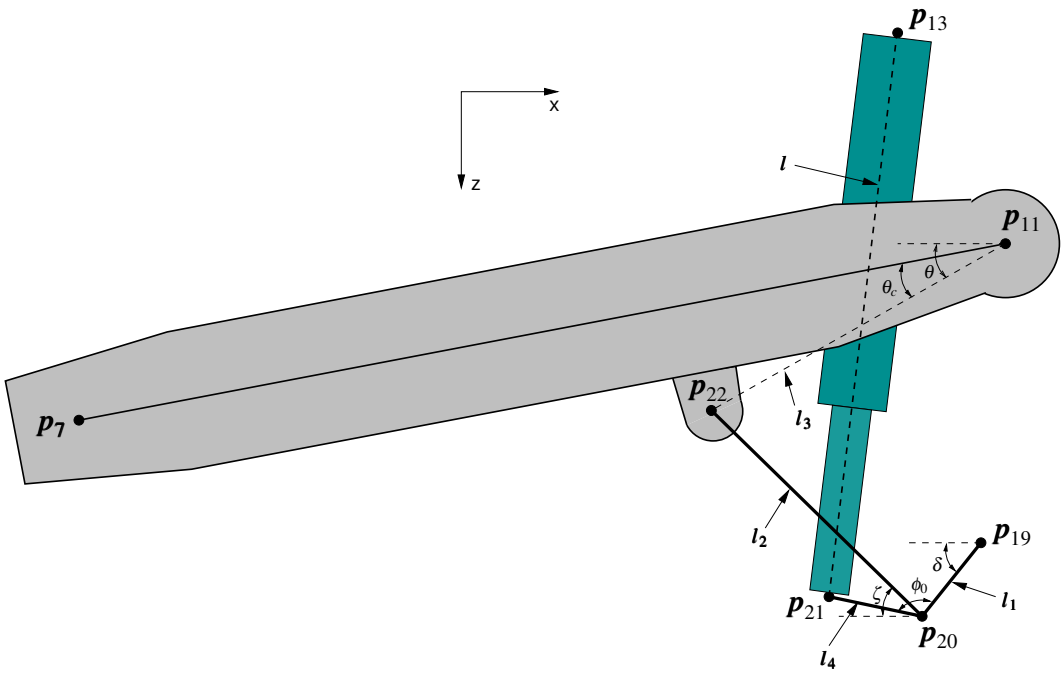

Figure 9.31: Geometry of monoshock suspension arrangement on GSX-R1000 motorcycle.

the swinging arm angle change and angular speed, and the moment of the spring/damper force about the swinging arm pivot, which is then added directly in the motorcycle model building. The analysis follows.

Points p_{11}, p_{13} and p_{19} are fixed to the main frame. l_1, l_4 and ϕ_o are dimensions of the swinging link and l_2 the length of the pull rod. l_3 is a fixed length in the swinging arm. The spring/damper unit is of variable length l. θ is the sum of the angle of the swinging arm to the horizontal x-axis and the fixed angle θ_c, which is the angle of the line connecting points p_{11} and p_{22} to the horizontal in the nominal configuration (the swinging arm is not necessarily horizontal in the nominal configuration). δ and ζ are angles to the horizontal for the swinging link and pull rod respectively. Traversing the loop p_{19}-p_{20}-p_{22}-p_{11}-p_{19}, both x and z displacements are nil, since we end where we begin. Therefore:

$$x_{11} - x_{19} - l_3 \cos\theta + l_2 \cos\zeta + l_1 \cos\delta = 0$$

and

$$z_{11} - z_{19} + l_3 \sin\theta + l_2 \sin\zeta - l_1 \sin\delta = 0$$

Forming l_2^2 as $(l_2^2 \sin^2\zeta + l_2^2 \cos^2\zeta)$ and substituting:

$$c_1 = -x_{11} + x_{19} + l_3 \cos\theta$$

and

$$c_2 = -z_{11} + z_{19} - l_3 \sin\theta$$

we obtain:

$$l_2^2 = (c_1 - l_1\cos\delta)^2 + (c_2 - l_1\sin\delta)^2$$

from which it can be shown that:

$$\delta = \arcsin\left(\frac{l_2^2 - l_1^2 - c_1^2 - c_2^2}{2l_1\sqrt{c_1^2 + c_2^2}}\right) + \arctan\left(\frac{c_1}{c_2}\right),$$

which is a function of θ only. Also:

$$x_{21} = x_{19} - l_1\cos\delta + l_4\cos(\phi_o + \delta)$$

and

$$z_{21} = z_{19} + l_1\sin\delta - l_4\sin(\phi_o + \delta)$$

with

$$l = \sqrt{(x_{13} - x_{21})^2 + (z_{13} - z_{21})^2}$$

so that l can be found as a function of θ, $l = f_1(\theta)$ say, by substitution for x_{21} and z_{21} in this expression. Figure 9.32 illustrates the outcome[9]. If a small change $\delta\theta$ in θ occurs, in which the corresponding change in l is δl, the moment M corresponding to a spring/damper force $f_2(l,\dot{l})$ is $f_2(l,\dot{l}) \cdot dl/d\theta$ by virtual work. The properties of the spring/damper unit can thus be expressed in terms of an equivalent moment $M(\theta,\dot{\theta})$ about the swing-arm pivot, as:

$$M = f_2\{f_1(\theta), \frac{df_1(\theta)}{d\theta}\dot{\theta}\} \cdot \frac{df_1(\theta)}{d\theta},$$

which can be fully automated.

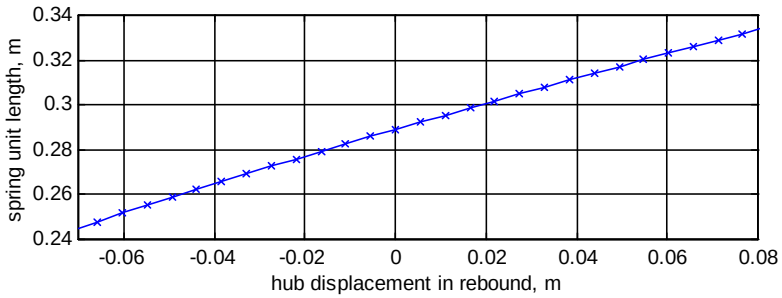

Figure 9.32: Spring / damper unit length to wheel displacement relationship for GSX-R1000 motorcycle.

9.5 Chain drive

A chain drive system is modelled in this section. The mechanical arrangement of such a system is shown diagrammatically in Figure 9.33. Under driving conditions the upper part of the chain

[9]The hub displacement is 'swing arm length' $\times\sin(\theta - \theta_c)$

between the engine sprocket and the rear wheel sprocket can carry tension to transfer the engine torque to the rear wheel. Alternatively the rear wheel's motion is opposed by engine braking carried by the lower part of the chain, with some dead zone (slack) in the middle. The modelling of this system involves finding analytic relationships between the coordinates of points chp_1, chp_3 on the rear wheel and chp_2, chp_4 on the engine sprocket (added as a separate body), shown in Figure 9.33, and the swinging arm angle so that the points' locations can be completely specified. Then the appropriate forces can be applied between them. In the present analysis the angles η_1 and η_2 are found analytically as functions of the swinging arm angle, and then are connected to the coordinates of the points. The tension forces can subsequently be found via a chain deflection calculation converted into a force via the chain stiffness. The calculation of the deflections is complicated because it involves the relative position of the swinging arm and the difference in rotational displacement between the wheel and engine sprocket, further complicated by the presence of slack in the chain. This requires AUTOSIM commands such as `min` and `ifthen` to be used. The method is currently being developed and will not be described here any further. The geometric analysis follows.

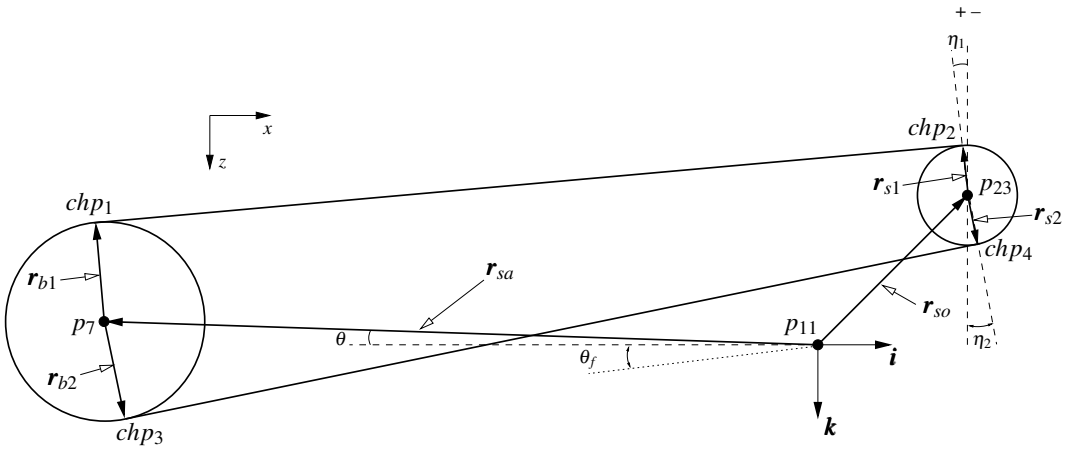

Figure 9.33: Geometry of chain drive arrangement.

Points p_{11} and p_{23} are fixed to the main frame and p_7 to the rear wheel. θ is the angle of the swinging arm centreline (p_{11} to p_7) to the horizontal. In Figure 9.33 θ is shown with a negative value. θ_f is fixed and is the nominal value of θ, thus θ is found by summing the swing arm rotation and θ_f. By defining the following vectors with point p_{11} as the origin and $\boldsymbol{i}$, $\boldsymbol{k}$ as horizontal and vertical unit vectors:

$$\boldsymbol{r}_{sa} = -r_{sa}\cos\theta\boldsymbol{i} + r_{sa}\sin\theta\boldsymbol{k}$$

$$\boldsymbol{r}_{so} = r_{sox}\boldsymbol{i} + r_{soz}\boldsymbol{k}$$

$$\boldsymbol{r}_{b1} = -r_b\sin\eta_1\boldsymbol{i} - r_b\cos\eta_1\boldsymbol{k}$$

$$\boldsymbol{r}_{s1} = -r_s\sin\eta_1\boldsymbol{i} - r_s\cos\eta_1\boldsymbol{k}$$

$$\boldsymbol{r}_{b2} = r_b\sin\eta_2\boldsymbol{i} + r_b\cos\eta_2\boldsymbol{k}$$

$$\boldsymbol{r}_{s2} = r_s\sin\eta_2\boldsymbol{i} + r_s\cos\eta_2\boldsymbol{k}$$

and taking the scalar product of the radius vector $\boldsymbol{r}_{s1}$ and the vector joining points chp_1 and chp_2, which is tangent to both the wheel and engine sprockets and perpendicular to their radii $\boldsymbol{r}_{s1}$ and $\boldsymbol{r}_{b1}$, we get:

$$(\boldsymbol{r}_{sa} + \boldsymbol{r}_{b1} - \boldsymbol{r}_{so} - \boldsymbol{r}_{s1}) \cdot \boldsymbol{r}_{s1} = 0$$

from which, with some manipulation, it can be shown that:

$$\eta_1 = \arcsin\left(\frac{r_s - r_b}{\sqrt{(r_{sa}\cos\theta + r_{sox})^2 + (r_{sa}\sin\theta - r_{soz})^2}}\right) + \arctan\left(\frac{r_{sa}\sin\theta - r_{soz}}{r_{sa}\cos\theta + r_{sox}}\right)$$

which is a function of θ only. In the same way, by taking the dot product of the vector joining points chp_3 and chp_4, and the radial vector $\boldsymbol{r}_{s2}$ we obtain:

$$(\boldsymbol{r}_{sa} + \boldsymbol{r}_{b2} - \boldsymbol{r}_{so} - \boldsymbol{r}_{s2}) \cdot \boldsymbol{r}_{s2} = 0$$

and similarly after some algebra:

$$\eta_2 = \arcsin\left(\frac{-r_s + r_b}{\sqrt{(r_{sa}\cos\theta + r_{sox})^2 + (r_{sa}\sin\theta - r_{soz})^2}}\right) + \arctan\left(\frac{r_{sa}\sin\theta - r_{soz}}{r_{sa}\cos\theta + r_{sox}}\right)$$

which is also a function of θ only. Vectors pointing from the engine sprocket centre to points chp_2 and chp_4, and from the wheel centre to points chp_1 and chp_3 can now be determined. These four points can then be defined via the coordinates of the associated vectors as moving points on the wheel or engine sprocket.

9.6 Telelever front suspension

Work is currently in progress to obtain a full description for a telelever front suspension, which is common in new BMW machines, and has a number of different properties from the widespread telescopic fork suspension. The mechanical arrangement used is shown in Figure 9.34. In this case the suspension is modelled on-line, link by link and joint by joint. It would be preferred to avoid having a closed kinematic loop in the equations of motion, which is a feature of this type of suspension, using ideas similar to those described in Section 9.4 for the "monoshock" rear suspension. Such a solution will be sought in the future.

The model building sequence is described next:

- define all points in global coordinates
- define point p_{15} in main frame
- add *front frame pitch body* (massless) on main frame at p_2 with y rotational freedom
- define x' and z' directions
- add *upper forks body* to *front frame pitch body* with z' rotational freedom

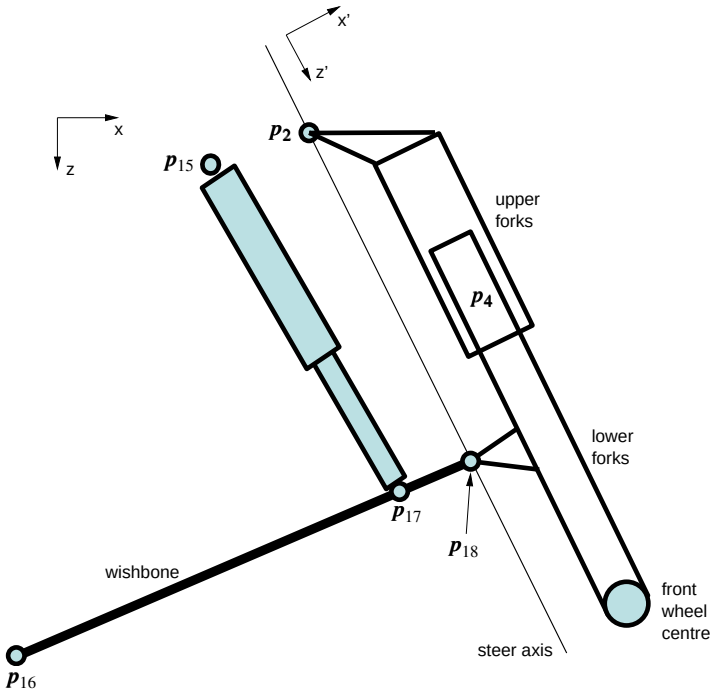

Figure 9.34: Geometry of telelever suspension arrangement.

- define point p_4 in *upper forks body*
- add *lower forks body* to *upper forks body* at p_4 with z' translational freedom
- define point p_{18} in *lower forks body*
- add *wishbone* (massless) on main frame at p_{16} with y rotational freedom
- define points p_{17} and p_{18} in *wishbone*
- constrain movement in z' direction between points p_{18} on *lower forks body* and p_{18} on *wishbone* to eliminate rotational freedom of the *wishbone*
- constrain movement in x' direction between points p_{18} on *lower forks body* and p_{18} on *wishbone* to eliminate rotational freedom of the *front frame pitch body*
- add spring/damper force between points p_{15} on main frame and p_{17} on *wishbone*

For the linear model the movement constraints are replaced by speed constraints.

9.7 Improved equilibrium checking

Equilibrium checking processes were described earlier in Section 5.2, and some further fine detail improvements have been developed here. The underlying principles behind the checks in any case remain the same, and require that under equilibrium conditions:

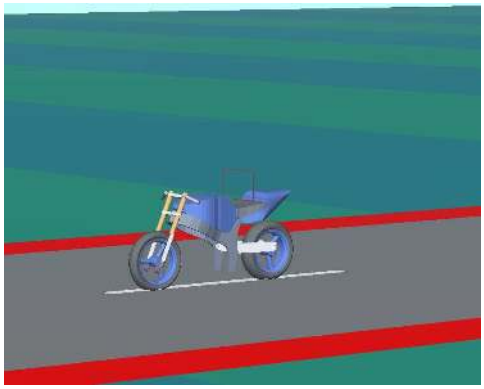

Figure 9.35: 3D motorcycle shape in stereolithography surface form.

- the external forces acting on the motorcycle-rider system must match the sum of the inertial and gravitational forces,
- the external moments acting on the motorcycle-rider system must sum to zero and
- the power supply and dissipation must be equal.

The main new addition is contributions from acceleration induced inertial forces and moments, such that under acceleration/deceleration conditions the 'equilibrium' checks still hold. The $\boldsymbol{v} \times \boldsymbol{\omega}$ product was used earlier to calculate the acceleration of the main body, where $\boldsymbol{v}$ is the velocity and $\boldsymbol{\omega}$ the yaw rate of the main body respectively. This term includes only the acceleration towards the centre of the path i.e the centripetal acceleration. It is now replaced by $d\boldsymbol{v}/dt$ that gives a complete description of the acceleration. Such terms are computed for each body individually with $\boldsymbol{v}$ for each body being the velocity vector of its centre of mass. Wheel spin inertial moments are also added for each wheel as $Id\omega/dt$ terms, where in this case I is the moment of inertia and ω the spin of the relevant wheel. Also included are the power used to accelerate the motorcycle using a term $Mvdv/dt$ with M the total mass of the vehicle and v its forward speed, the power used to accelerate the wheels via terms of the form $I\omega d\omega/dt$, and the power dissipated by the braking moments.

9.8 Animations

The animations generated from the animator program described in Chapter 6 were in the form of a sequence of wireframe objects. A newer version of the same program allows the use of stereolithography (STL) surface files to define 3D shapes as a group of triangles, making the animation more realistic as shown in Figure 9.35. 3D graphics programs and CAD programs need to be used to create STL files. Other input files to the animator remain the same as before. The animation of the various motorcycles modes using eigenvalue and eigenvector information is also in progress and description of these tasks is a future job.

Part V

Conclusions and Future Work

Chapter 10

Conclusions

The use of automated methods for generating equations of motion and analysing motorcycle dynamics has been demonstrated. In particular it has been shown that the hand derived results in (Sharp, 1971, 1994*b*) can be reproduced by the multi-body modelling code AUTOSIM. As is the case with many nonlinear systems, local stability is investigated via the eigenvalues of linearised models that are associated with equilibrium points of the nonlinear system. The full nonlinear equations of motion in each case are obtained in FORTRAN or C code that is used to generate time histories, and the linearised state-space model is obtained in symbolic form as a MATLAB m-file. The employment of feedback controllers is necessary to establish specified straight running or cornering equilibrium states prior to testing the stability. A typical local stability study requires the importation of quasi-steady time histories from the nonlinear model to the symbolic linearised equations of motion.

A more comprehensive model has also been presented, capable of more general equilibrium conditions, acceleration/deceleration conditions and road forcing on the wheels. The relevant account given here is based on previous work from (Sharp and Limebeer, 2001). There is novelty in the development of animation runs with the same model.

The modern theoretical techniques developed have been employed to investigate the behaviour of motorcycles under acceleration and deceleration. Extensive use has been made of both nonlinear and linearised models. Control systems have been used to control the motorcycle drive and braking systems in order that the machine maintains preset rates of acceleration or deceleration. The results show that the wobble mode damping of a motorcycle is significantly reduced when the machine is descending an incline or braking on a level surface. Conversely, the wobble mode is substantially stabilised when the machine is ascending an incline at constant speed or accelerating on a level surface. Ascending, descending inclines, acceleration and deceleration appear to have very little influence on the damping or frequency of the weave mode. (Sharp, 1976*b*) reported that acceleration can reduce weave mode damping by a large amount and that the weave and wobble modes can lose their identities because of the narrowing of the frequency gap between these modes. Neither of these observations were predicted in this study which reinforces the idea that the model and ideas employed in (Sharp, 1976*b*) were too simpli-

fied for the intended purpose.

The known problems to do with rear tyre adhesion in heavy rear-wheel-dominated braking situations have also been exposed by nonlinear simulations. The analysis has quantified the transfer of normal tyre loading to the front tyre under heavy braking, which implies that the rear tyre cannot perform its task under such conditions. If an attempt is made to slow the machine using rear-wheel-dominated braking, it very likely that the rear tyre will go into a slide, causing an irrecoverable loss of control. The aerodynamic drag does some of the braking and reduces these difficulties at high speeds.

Theoretical analysis with the use of the techniques developed has also been carried out to examine the behaviour of motorcycles under road forcing conditions. The results presented show that under cornering, regular low-amplitude road undulations can be a source of considerable difficulty to motorcycle riders. At low machine speeds the wobble and front suspension pitch modes are likely to respond vigorously to resonant forcing, while at higher speeds, the weave and front wheel hop modes are similarly affected. The vigour of the oscillations is related to the amount of damping present in each mode, with low damping factors leading to correspondingly high peak magnification factors.

The individual contributions to these resonances made by each of the two road wheels have been studied. The results show that the wobble and front wheel hop resonance peaks are "front wheel dominated". In other words, difficulties with these modes are likely to be caused by the design and set up of the front of the machine. The same is true, but to a lesser extent, in the case of the front suspension pitch mode. In contrast, the weave mode resonance peak involves the road forcing to both wheels in almost equal measure. As a consequence, weave related problems appear to be more difficult to isolate and remove.

As might be anticipated, the vulnerability of the wobble mode response to road forcing is decreased markedly by an effective steering damper, but changes to the suspension dampers are ineffectual. The front suspension pitch mode resonance is sensitive to the front suspension damping, but is insensitive to the rear suspension and steering damping. The weave mode resonant response appears to be reduced by increasing the front damping, but it is made larger by increasing the rear suspension and steering damper settings. Increasing the front suspension damping reduces the front wheel hop resonance peak, but this peak does not respond to changes in steering damping, or rear suspension damper settings.

It has also been shown that light riders are more likely to suffer from road forced resonant weave oscillations than are heavy ones, as has been observed in practice (Farr, 1997*a*) and on the video tape (Dunlop, c1977). The results indicate also that the peak gains associated with the weave mode are brought down by moving the rider upper body mass forwards and upwards. There is not sufficient practical evidence at the moment to indicate whether or not these findings coincide with experience. From a safety point of view, a worrying feature of the road profile induced oscillations is the tendency of the uncontrolled machine to "sit up" and run wide. This aspect of the machine behaviour can be seen on the video tape (Duke Marketing Ltd, 1999) in the case of a high-speed weave accident.

The work reported here has a number of practical consequences. It appears to provide an explanation for a class of single vehicle loss-of-rider-control accidents reported in the popular literature, and it helps to explain why motorcycles that behave perfectly well for long periods can suddenly suffer serious and dangerous oscillation problems. Such oscillations are likely to be difficult to reproduce and study in practice, because they occur under a rare combination of running conditions, characterised by the machine speed, the lean angle, the rider's mass and posture, and the road profile wavelength. The safety of the rider is also an issue. The kind of theoretical analysis presented here provides a safe and economical way for reproducing and studying these dangerous oscillatory phenomena associated with motorcycles, and can easily be used by motorcycle manufacturers to determine "worst case" operating conditions for their new products.

New work has also been started and described here, relating to modelling improvements to the already advanced motorcycle model described earlier in this thesis. The tyre model, in particular, has been fully developed to provide a generic description of a set of modern high performance motorcycle tyres with a wide range of validity. The basis for the shear force and moment description is the powerful Magic Formula method, for which parameters have been derived from recent published tyre results. The tyre relaxation properties have also been updated, and the tyre-road contact geometry has been adapted to correspond to the geometry of a wide tyre, as opposed to the previously infinitely thin tyre assumed. Improved equilibrium checking procedures have also been developed. A monoshock rear suspension has been described through a separate off-line geometric analysis. Significant progress has been made in modelling other parts of the motorcycle design–chain drive, front telelever suspension–, and in obtaining a complete parametric description of a contemporary, high performance motorcycle, although further work is required to complete these tasks.

Chapter 11

Future Work

The immediate work that needs to be completed in the future involves the pending modelling improvements described earlier and the parametric description of a modern sports bike. The chain drive and telelever front suspension, in particular, need to be finalised and the remaining unknown parameters to be measured. More advanced animations, that involve the use of eigenvalue and eigenvector information from linearised models, can show the various normal modes of the motorcycle in a 3-dimensional form. Further work is required to complete such animation tasks or animations of any other general motion of the motorcycle with the newly developed solid object form.

In the improved motorcycle model, a first order relaxation model has been used to capture the transient behaviour of the tyre. Although this is adequate for the present purposes it might be advantageous, in other circumstances, to model the tyre carcass as a rigid ring, that correctly represents the tyre behaviour for a larger range of frequencies. This feature when included complicates the tyre model substantially and the benefits to be gained have to outweigh the increase in complexity, if it is to be used.

A preliminary time domain study of motion simulations under resonance conditions has been presented earlier. It has shown the existence of interesting and essentially nonlinear phenomena, that seem to conform with practical experience. The task of understanding these nonlinear phenomena has been undertaken in a separate project and time-frequency signal processing techniques have been employed in an attempt to detect super-harmonic or sub-harmonic excitations of the resonant motorcycle modes. The results appear to indicate that road forcing induced oscillations are mainly explained by the linear theory presented in this thesis and the use of nonlinear techniques is not necessary, but further investigation is clearly required before anything can be said with certainty. Bifurcation theory can also help to further examine nonlinear stability, particularly with respect to the not so well understood high speed wobble, commonly known as a "tank slapper".

The completed representation of a modern high performance machine will be used to determine steady turning, stability, response and parameter sensitivity data to be compared with older information and determine to what extent it remains valid in order to acquire a better un-

derstanding of modern machines. In addition, the linearised version of the motorcycle model can be used to develop the rider's feedback stabilisation and path following response via linear optimal preview steering and rider lean control.

Part VI

Appendices

Appendix A

The weave, wobble and capsize modes

A.1 Body capsize

When the motorcycle has zero forward velocity and the steering freedom is removed, it behaves like an inverted pendulum that is about to fall over. For small camber angles, one can balance inertial and gravitational moments to obtain:

$$(\sum I_i)\ddot{\phi} = g\phi(\sum m_i l_i) \tag{A.1}$$

in which ϕ is the camber angle and $\sum I_i$ is the total moment of inertia of the vehicle about the line joining the two wheel ground contact points in the nominal configuration as shown in Figure A.1. The sum $g\phi \sum m_i l_i$ is the total torque generated by the gravitational forces. It is easy to see that the second order differential equation (A.1) has two real poles associated with it:

$$\alpha = \pm\sqrt{\frac{g(\sum m_i l_i)}{\sum I_i}}. \tag{A.2}$$

Figure A.2 shows the right-half plane part of the root-locus corresponding to the "Sharp 1971"

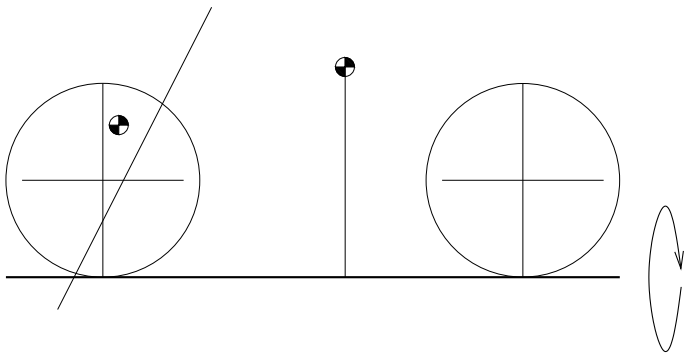

Figure A.1: Motorcycle as an inverted pendulum.

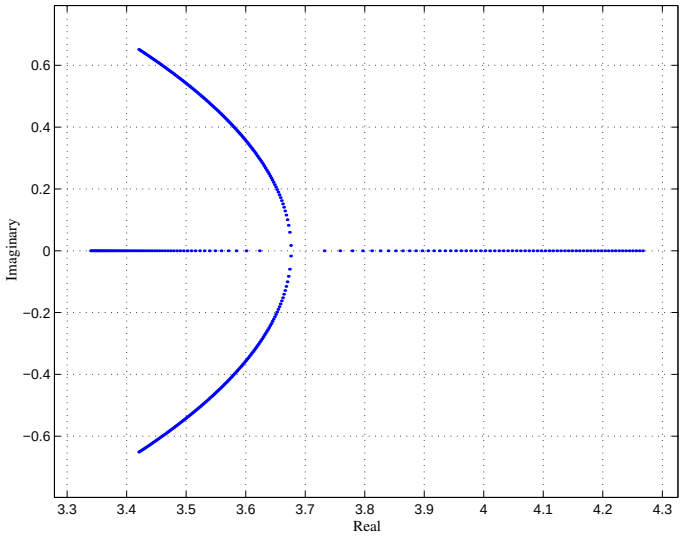

Figure A.2: Capsize portion of the root-locus plot.

model for low values of forward speed. As the machine speed increases, these poles meet, coalesce and become the complex pole pair associated with the weave motion of the machine. The pole with the larger initial value of about 4.27 corresponds to the positive solution of equation (A.2) which can be solved to yield 3.46 for the "Sharp 1971" model parameters. The reason for the discrepancy between these two values (4.27 and 3.46) can be traced to the vehicle's steering action. Indeed, when steering is inhibited, the "Sharp 1971" model has a positive real pole located at 3.494 rather than at 4.27 as shown in Figure (A.2). The reason for this increased capsize growth rate under steering is interesting. Suppose the machine begins to fall to the rider's right. In this case the motorcycle's steering geometry causes the machine to steer right thereby moving the front wheel ground contact point towards the rider's left. Consequently, the ground contact line that joins the front and rear wheel ground contact points rotates to the rider's left. This means that the gravitational torque produced by the $g\phi \sum m_i l_i$ terms increase and so the machine capsizes more quickly.

A.2 Steering capsize

Consider the simplified situation in which the rear frame is fixed (in body n) and the *Front Frame* is free to steer (ground contact effects being ignored). This situation is shown in Figure A.3. As before, balancing the gravitational and inertial torques gives:

$$I_{fz}\ddot{\delta} = (M_f g e \sin\varepsilon)\delta \tag{A.3}$$

in which all the symbols have their usual meaning. This second order system has the real poles:

$$\zeta = \pm\sqrt{\frac{M_f g e \sin\varepsilon}{I_{fz}}} \tag{A.4}$$

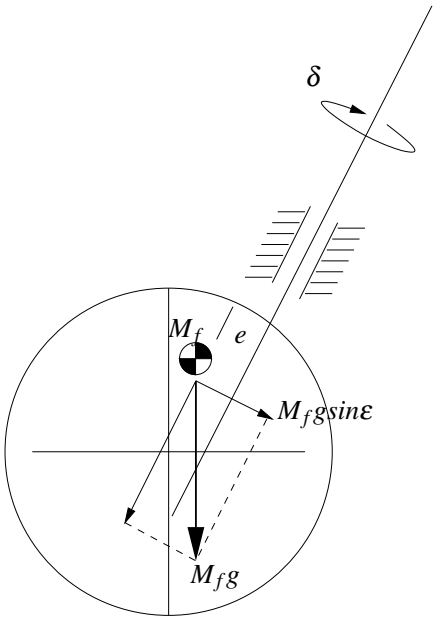

Figure A.3: Steering mechanism as it relates to the steering capsize mode.

associated with it. Substituting the "Sharp 1971" model parameters into (A.4) gives the positive real pole a value of 2.742. As will be explained, this root is related to the smaller of the real roots in Figure A.2. The initial agreement is not very good, because equation (A.4) predicts a growth rate of $\sim e^{2.742t}$, while the "Sharp 1971" model predicts a rate of about $\sim e^{3.33t}$. It turns out that this discrepancy is due to a combination of the steering damping, which is neglected in equation (A.4), and the front wheel tyre forces. In order to show this, one can multiply the steering damping factor and the front wheel tyre forces terms in the "Sharp 1971" AUTOSIM code by a parameter λ, and then consider reducing the value of λ from $1 \rightarrow 0$. It turns out that the real pole corresponding to the steering capsize mode varies from $3.33 \rightarrow 2.69$. This latter value is much closer to the figure of 2.74 predicted by equation (A.4). If in addition the rolling motion of the rear frame is inhibited by setting `Irx` to some large value, the pole predicted by the AUTOSIM (full model) code becomes even closer to that predicted by equation (A.4); agreement to three significant figures was obtained.

A.3 Wobble frequency

As will be shown, the wobble frequency for small forward speeds can be calculated by considering the front frame and the front wheel tyre side force. The situation of interest is shown in Figure A.4. Balancing the inertial torque with that generated by the side-slip tyre force gives:

$$I_{fz}\ddot{\delta} = -tC_{f1}\alpha \tag{A.5}$$

and since $\alpha = \delta cos\varepsilon$

$$I_{fz}\ddot{\delta} = -tC_{f1}\delta cos\varepsilon. \tag{A.6}$$

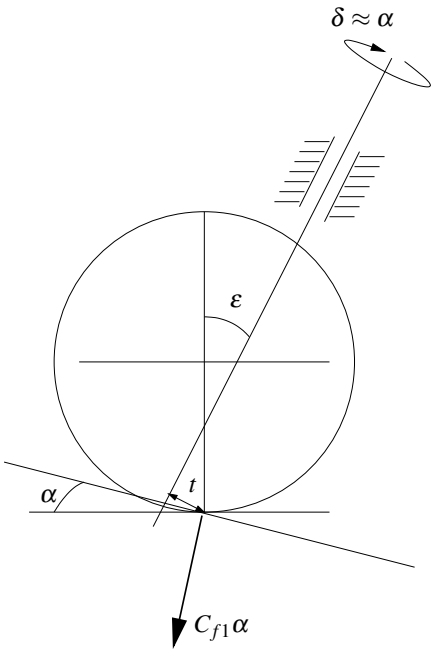

Figure A.4: The steering system and the tyre forces associated with the wobble mode.

This gives a predicted wobble frequency of:

$$\omega_{wobble} = \sqrt{\frac{tC_{f1}cos\varepsilon}{I_{fz}}}. \tag{A.7}$$

The "Sharp 1971" model predicts a low-speed wobble frequency of 57.7, which is good agreement with the value of 51.1 computed from equation (A.7).

Appendix B

AUTOSIM commands

This appendix contains a brief description of the AUTOSIM functions used in this thesis. A much fuller account can be found in the AUTOSIM reference manual (Anon., 1998).

Vector Algebra	
Autosim code	Mathematical interpretation
`angle(v1,v2,v3)`	the angle between vectors v_1 and v_2 (v_3 determines the sign)
`cross(v1,v2)`	the cross product between vectors v_1 and v_2
`dir(v1)`	unit vector in the direction of vector v_1
`dot(v1,v2)`	inner product between vectors v_1 and v_2
`dplane(v1,v2)`	projection of vector v_1 onto the plane perpendicular to vector v_2
`euler(b,i,ref)`	ith euler angle of body b relative to body ref
`pos(p1,p2)`	vector going from point p_2 to point p_1
`rq(b,i)`	ith rotational coordinate of body b
`ru(b,i)`	ith rotational speed of body b
`tu(b,i)`	ith translational speed of body b
`vel(p1)`	absolute velocity vector of point p_1
`[fwy]`	symbol is a unit-vector when enclosed in braces

Appendix C

Complete Magic Formulae

C.1 List of symbol changes

Symbol as it appears in (Pacejka, 2002)	Symbol used here
$\lambda_i,\ \lambda_i',\ \lambda_i^*$	1
α^*	β
$\alpha_{t,eq}$	λ_t
$\alpha_{r,eq}$	λ_r
F_y'	F_{yt}
$F_{yo,\gamma=0}$	F_{yoo}
$K_{y\alpha}'$	$K_{y\alpha oo}$
M_z'	M_{zt}
M_{zo}'	M_{zto}
$\cos'\alpha\ (=\frac{V_{cx}}{V_c+\varepsilon_V})$	$\frac{1}{\sqrt{1+\beta^2}}$

V_{cx} is the rolling velocity of the tyre crown centre, V_c is the velocity of the tyre crown centre and ε_V is a safety factor.

C.2 Magic Formulae

$df_z = (F_z - F_{zo})/F_{zo}$

C.2.1 Longitudinal force in pure longitudinal slip

$F_{xo} = D_x sin[C_x \arctan\{B_x\kappa_x - E_x(B_x\kappa_x - \arctan(B_x\kappa_x))\}] + S_{Vx}$

$\kappa_x = \kappa + S_{Hx}$

$C_x = p_{Cx1}$

$D_x = \mu_x F_z$

$$\mu_x = p_{Dx1} + p_{Dx2} df_z \qquad (>0)$$
$$E_x = (p_{Ex1} + p_{Ex2} df_z + p_{Ex3} df_z^2) \cdot (1 - p_{Ex4} \mathrm{sgn}(\kappa_x)) \qquad (\leq 1)$$
$$K_{x\kappa} = F_z (p_{Kx1} + p_{Kx2} df_z) \cdot \exp(p_{Kx3} df_z)$$
$$B_x = K_{x\kappa} / (C_x D_x + \varepsilon_x)$$
$$S_{Hx} = -(q_{sy1} F_z + S_{Vx}) / K_{x\kappa}$$
$$S_{Vx} = F_z (p_{Vx1} + p_{Vx2} df_z) \cdot \{|V_{cx}| / (\varepsilon_{Vx} + |V_{cx}|)\}$$

C.2.2 Lateral force in pure side-slip and camber

$$F_{yo} = D_y \sin[C_y \arctan\{B_y \alpha_y - E_y (B_y \alpha_y - \arctan(B_y \alpha_y))\} + \\ + C_\gamma \arctan\{B_\gamma \gamma - E_\gamma (B_\gamma \gamma - \arctan(B_\gamma \gamma))\}] \qquad (C_y + C_\gamma < 2)$$
$$\alpha_y = \beta + S_{Hy}$$
$$C_y = p_{Cy1} \qquad (>0)$$
$$D_y = \mu_y F_z$$
$$\mu_y = p_{Dy1} \exp(p_{Dy2} df_z) / (1 + p_{Dy3} \gamma^2) \qquad (>0)$$
$$E_y = p_{Ey1} + p_{Ey2} \gamma^2 + (p_{Ey3} + p_{Ey4} \gamma) \mathrm{sgn}(\alpha_y) \qquad (\leq 1)$$
$$K_{y\alpha o} = p_{Ky1} F_{zo} \sin[p_{Ky2} \arctan\{F_z / ((p_{Ky3} + p_{Ky4} \gamma^2) F_{zo})\}]$$
$$K_{y\alpha} = K_{y\alpha o} / (1 + p_{Ky5} \gamma^2)$$
$$B_y = K_{y\alpha} / (C_y D_y + \varepsilon_y)$$
$$S_{Hy} = p_{Hy1}$$
$$C_\gamma = p_{Cy2} \qquad (>0)$$
$$K_{y\gamma} = (p_{Ky6} + p_{Ky7} df_z) F_z$$
$$E_\gamma = p_{Ey5} \qquad (\leq 1)$$
$$B_\gamma = K_{y\gamma} / (C_\gamma D_y + \varepsilon_y)$$

C.2.3 Aligning moment in pure side-slip and camber

$$M_{zo} = M_{zto} + M_{zro}$$
$$M_{zto} = -t_o \cdot F_{yoo}$$
$$t_o = t_o(\alpha_t) = D_t \cos[C_t \arctan\{B_t \alpha_t - E_t (B_t \alpha_t - \arctan(B_t \alpha_t))\}] / \sqrt{1 + \beta^2}$$
$$\alpha_t = \beta$$
$$M_{zro} = M_{zro}(\alpha_r) = D_r \cos[\arctan(B_r \alpha_r)]$$
$$\alpha_r = \beta + S_{Hr}$$
$$\gamma_z = \gamma$$
$$S_{Hr} = q_{Hz1} + q_{Hz2} df_z + (q_{Hz3} + q_{Hz4} df_z) \gamma_z$$
$$B_t = (q_{Bz1} + q_{Bz2} df_z + q_{Bz3} df_z^2) \cdot (1 + q_{Bz5} |\gamma_z| + q_{Bz6} \gamma_z^2) \qquad (>0)$$

$$C_t = q_{Cz1} \qquad (>0)$$
$$D_{to} = F_z(R_o/F_{zo}) \cdot (q_{Dz1} + q_{Dz2} df_z)$$
$$D_t = D_{to}(1 + q_{Dz3}|\gamma_z| + q_{Dz4}\gamma_z^2)$$
$$E_t = (q_{Ez1} + q_{Ez2} df_z + q_{Ez3} df_z^2) \cdot \{1 + (q_{Ez4} + q_{Ez5}\gamma_z)\tfrac{2}{\pi}\arctan(B_t C_t \alpha_t)\} \qquad (\leq 1)$$
$$B_r = q_{Bz9} + q_{Bz10} B_y C_y$$
$$D_r = F_z R_o\{(q_{Dz6} + q_{Dz7} df_z) + (q_{Dz8} + q_{Dz9} df_z)\gamma_z + (q_{Dz10} + q_{Dz11} df_z)\gamma_z|\gamma_z|\}/\sqrt{1+\beta^2}$$

C.2.4 Combined slip

C.2.4.1 Longitudinal force

$$F_x = G_{x\alpha} F_{xo}$$
$$G_{x\alpha} = \cos[C_{x\alpha}\arctan(B_{x\alpha}\alpha_S)]/G_{xao} \qquad (>0)$$
$$G_{x\alpha o} = \cos[C_{x\alpha}\arctan(B_{x\alpha} S_{Hx\alpha})]$$
$$\alpha_S = \beta + S_{Hx\alpha}$$
$$B_{x\alpha} = (r_{Bx1} + r_{Bx3}\gamma^2)\cos[\arctan(r_{Bx2}\kappa)] \qquad (>0)$$
$$C_{x\alpha} = r_{Cx1}$$
$$S_{Hx\alpha} = r_{Hx1}$$

C.2.4.2 Lateral force

$$F_y = G_{y\kappa} F_{yo} + S_{Vy\kappa}$$
$$G_{y\kappa} = \cos[C_{y\kappa}\arctan(B_{y\kappa}\kappa_S)]/G_{y\kappa o} \qquad (>0)$$
$$G_{y\kappa o} = \cos[C_{y\kappa}\arctan(B_{y\kappa} S_{Hy\kappa})]$$
$$\kappa_S = \kappa + S_{Hy\kappa}$$
$$B_{y\kappa} = (r_{By1} + r_{By4}\gamma^2)\cos[\arctan\{r_{By2}(\beta - r_{By3})\}] \qquad (>0)$$
$$C_{y\kappa} = r_{Cy1}$$
$$S_{Hy\kappa} = r_{Hy1}$$
$$S_{Vy\kappa} = D_{Vy\kappa}\sin[r_{Vy5}\arctan(r_{Vy6}\kappa)]$$
$$D_{Vy\kappa} = \mu_y F_z(r_{Vy1} + r_{Vy2} df_z + r_{Vy3}\gamma) \cdot \cos[\arctan(r_{Vy4}\beta)]$$

C.2.4.3 Aligning moment

$$M_z = M_{zt} + M_{zr} + s \cdot F_x$$
$$M_{zt} = -t \cdot F_{yt}$$
$$t = t(\lambda_t) = D_t\cos[C_t\arctan\{B_t\lambda_t - E_t(B_t\lambda_t - \arctan(B_t\lambda_t))\}]/\sqrt{1+\beta^2}$$
$$F_{yt} = F_{y,\gamma=0} - S_{Vy\kappa}$$

$$F_{y,\gamma=0} = G_{y\kappa} \cdot F_{yoo}$$

$$M_{zr} = M_{zr}(\lambda_r) = D_r \cos[\arctan(B_r \lambda_r)]$$

$$s = R_o \cdot \{s_{sz1} + s_{sz2}(F_y/F_{zo}) + (s_{sz3} + s_{sz4} df_z)\gamma\}$$

$$\lambda_t = \sqrt{\alpha_t^2 + \left(\frac{K_{x\kappa}}{K_{y\alpha oo}}\right)^2 \kappa^2} \cdot \mathrm{sgn}(\alpha_t)$$

$$\lambda_r = \sqrt{\alpha_r^2 + \left(\frac{K_{x\kappa}}{K_{y\alpha oo}}\right)^2 \kappa^2} \cdot \mathrm{sgn}(\alpha_r)$$

Bibliography

Abdelkebir, A. (2002). Measurements of inertia, stiffness and damping components of a Suzuki GSX-R1000. Technical report. Imperial College London, Mechanical Engineering Department.

Anon. (1964). *Bio-astronautus data book*. NASA SP 3006.

Anon. (1993*a*). BMW statement to all (UK) chief constables.

Anon. (1993*b*). Boxer comeback. *Which Motorcycle* pp. 26–32.

Anon. (1993*c*). An interview with Dr. Goeschel. *Motorcycle Sport* pp. 234–235.

Anon. (1997*a*). *Chapter 5 of CarsimEd Manual*. Mechanical Simulation Corporation. 709 West Huron, Ann Arbor MI. http://www.carsim.com.

Anon. (1997*b*). Operating stable. *Performance Bikes* pp. 44–51.

Anon. (1997*c*). Safety recall notice, American Suzuki Motor Corporation. *Motorcycle*.

Anon. (1998). *Autosim 2.5+ Reference Manual*. Mechanical Simulation Corporation. 709 West Huron, Ann Arbor MI. http://www.carsim.com.

Bakker, E., H.B. Pacejka and L. Lidner (1989). A new tyre model with an application in vehicle dynamics studies. *SAE 890097*.

Bayer, B. (1988). Flattern und pendeln bei kraftradern. *Automobil_Industrie* **2**, 193–197.

Bridges, P. and J.B. Russell (1987). The effect of topboxes on motorcycle stability. *Vehicle System Dynamics* **16**(5–6), 345–354.

Cooper, K.R. (1974). The effects of aerodynamics on the performance and stability of high speed motorcycles. In: *2nd AIAA Symp. on Aerodynamics of Sport and Competition Automobiles*. Los Angeles.

Cossalter, V. (2002). *Motorcycle Dynamics*. Race Dynamics. Greendale (WI).

Cossalter, V., A. Doria and R. Lot (1999*a*). Steady turning of two-wheeled vehicles. *Vehicle System Dynamics* **31**(3), 157–181.

Cossalter, V., A. Doria, R. Lot, N. Ruffo and M. Salvador (2003). Dynamic properties of motorcycle and scooter tires: Measurement and comparison. *Vehicle System Dynamics* **39**(5), 329–352.

Cossalter, V. and R. Lot (2002). A motorcycle multi-body model for real time simulations based on the natural coordinates approach. *Vehicle System Dynamics* **37**(6), 423–447.

Cossalter, V., M. Da Lio, R. Lot and L. Fabbri (1999*b*). A general method for the evaluation of vehicle manoeuvrability with special emphasis on motorcycles. *Vehicle System Dynamics* **31**(2), 113–135.

Cossalter, V., R. Lot and M. Fabiano (2002). The influence of tire properties on the stability of a motorcycle in straight running and curves. *SAE 2002-01-1572*.

Cutts, J. (1993). The boxer rebellion. *Superbike* pp. 4–10.

de Vries, E.J.H. and H.B. Pacejka (1997). Motorcycle tyre measurements and models. In: *Proc. 15th IAVSD Symposium on the Dynamics of Vehicles on Roads and on Tracks* (L. Palkovics, Ed.). Budapest Hungary. Suppl. Vehicle System Dynamics, **28**, 1998, 280–298.

de Vries, E.J.H and H.B. Pacejka (1998). The effect of tyre modeling on the stability analysis of a motorcycle. In: *Proc. AVEC'98*. SAE of Japan. Nagoya. pp. 355–360.

Desoer, C.A. (1969). Slowly varying system $\dot{x} = a(t)x$. *IEEE Trans Auto Control (Correspondence)* **AC-14**(12), 780–781.

Duke Marketing Ltd (1999). Motorcycle magic.

Duke, O. (1997). Planet bike—Radical thriller or flawed killer. *Bike* pp. 14–17.

Dunlop (c1977). Wobble and weave videotape.

Eaton, D.J. (1973). Man-Machine dynamics in the stabilization of single-track vehicles. PhD thesis. University of Michigan.

Evangelou, S. and D.J.N. Limebeer (2000*a*). Lisp programming of the "sharp 1971" motorcycle model. http://www.ee.ic.ac.uk/control/motorcycles.

Evangelou, S. and D.J.N. Limebeer (2000*b*). Lisp programming of the "sharp 1994" motorcycle model. http://www.ee.ic.ac.uk/control/motorcycles.

Evangelou, S. and D.J.N. Limebeer (2001). Animation of the "sl2001" motorcycle model. http://www.ee.ic.ac.uk/control/motorcycles.

Evans, J. (1993). BMW R1100RS. *Motor Cycle International* pp. 58–64.

Farr, K. (1997*a*). Fats the way to. *Motorcycle News*.

Farr, K. (1997*b*). Suzuki TL1000 recalled in UK. *Motorcycle News*.

Farrar, S. (2002). Orritt's story to explain the phenomena. *Times Higher Educational Supplement*.

Fujioka, T. and K. Goda (1995*a*). Discrete brush tire model for calculating tire forces with large camber angle. In: *Proc. 14th IAVSD Symposium on the Dynamics of Vehicles on Roads and on Tracks* (L. Segel, Ed.). Suppl. Vehicle System Dynamics, **25**, 1996, 200–216.

Fujioka, T. and K. Goda (1995*b*). Tire cornering properties at large camber angles: mechanism of the moment around the vertical axis. *JSAE Review* **16**(3), 257–261.

Giles, C.G. and R.S. Sharp (1983). Static and dynamic stiffness and deflection mode measurements on a motorcycle, with particular reference to steering behaviour. In: *Proc. Inst. Mech. Eng./MIRA Conference on Road Vehicle Handling*. Mechanical Engineering Publications. London. pp. 185–192.

Hales, F.D. (1965). Lateral stability problems of simply articulated vehicles. In: *Proceedings of IUTAM Symposium on Recent Progress in Linear Mechanical Vibrations*. pp. 17–34.

Hasegawa, A. (1985). Analysis of controllability and stability of motorcycles – Analysis of stability at high speed driving. In: *10th International Technical Conference on Experimental Safety Vehicles*. Oxford. pp. 479–500.

Imaizumi, H. and T. Fujioka (1998). Motorcycle-rider system dynamics by multibody dynamics analysis—effects of the rear load and the suspension assembly on wobble and weave motions. *JSAE Review* **19**(1), 54–57.

Imaizumi, H., T. Fujioka and M. Omae (1996). Rider model by use of multibody dynamics analysis. *JSAE* **17**, 75–77.

Ishii, H. and Y. Tezuka (1997). Considerations of turning performance for motorcycles. In: *Proc. SETC'97*. Yokohama. pp. 383–389. JSAE 9734601; SAE 972127.

Jennings, G. (1974). A study of motorcycle suspension damping characteristics. *SAE 740628*.

Kailath, T. (1980). *Linear Systems*. Chap. 9, p. 607. Prentice-Hall. ISBN 0-13-536961-4.

Kamioka, T., N. Yoshimura and S. Sato (1997). Influence of the front fork on the movement of a motorcycle. In: *Proc. SETC'97*. Yokohama. pp. 397–403. SAE 972129.

Kane, T.R. and D.A. Levinson (1983). Multibody dynamics. *Transactions of the ASME, Journal of Applied Mechanics* **50**, 1071–1078.

Kane, T.R. and D.A. Levinson (1985). *Dynamics: theory and applications*. McGraw-Hill Series in Mechanical Engineering. McGraw-Hill. New York.

Katayama, T., A. Aoki and T. Nishimi (1988). Control behaviour of motorcycle riders. *Vehicle System Dynamics* **17**, 211–229.

Knight, M. (2000). Triumph Designs private communication.

Koenen, C. (1983). The dynamic behaviour of motorcycles when running straight ahead and when cornering. PhD thesis. Delft University of Technology.

Koenen, C. and H.B. Pacejka (1980). Vibrational modes of motorcycles in curves. In: *Proc. International Motorcycle Safety Conference*. Vol. II. Motorcycle Safety Foundation. Washington DC. pp. 501–543.

Koenen, C. and H.B. Pacejka (1981). The influence of frame elasticity, simple rider body dynamics, and tyre moments on free vibrations of motorcycles in curves. In: *Proc. 7^{th} IAVSD Symp. on Dynamics of Veicles on Roads and on Railway Tracks*. Swets and Zeitlinger, Lisse. Cambridge UK. pp. 53–65.

Limebeer, D.J.N., R.S. Sharp and S. Evangelou (2001). The stability of motorcycles under acceleration and braking. *Proc. Inst. Mech. Eng.* **215**(C9), 1095–1109.

Limebeer, D.J.N., R.S. Sharp and S. Evangelou (2002). Motorcycle steering oscillations due to road profiling. *Transactions of the ASME, Journal of Applied Mechanics* **69**(6), 724–739.

Metropolitan Police (2000). Metropolitan Police, private communication.

Nishimi, T., A. Aoki and T. Katayama (1985). Analysis of straight running stability of motorcycles. In: *10th International Technical Conference on Experimental Safety Vehicles*. Oxford. p. 33.

Otto, W.M. (1980). Effect of motorcycle accessories on stability. In: *Proc. International Motorcycle Safety Conference*. Motorcycle Safety Foundation. Linthicum MD 21090, Washington DC. pp. 1560–1581.

Pacejka, H.B. (2002). *Tyre and Vehicle Dynamics*. Butterworth Heinemann. Oxford.

Pacejka, H.B. and E. Bakker (1991). The magic formula tyre model. In: *Proc. 1st International Colloquium on Tyre Models for Vehicle Dynamics Analysis*. Swets and Zeitlinger, Lisse. Delft. Suppl. Vehicle System Dynamics, **21**, 1993, 1–18.

Pacejka, H.B. and I.J.M. Besselink (1997). Magic formula tyre model with transient properties. In: *Proc. 2nd International Colloquium on Tyre Models for Vehicle Dynamics Analysis*. Berlin. Suppl. Vehicle System Dynamics, **27**, 1997, 234–249.

Pacejka, H.B. and R.S. Sharp (1991). Shear force development by pneumatic tyres in steady state conditions: A review of modelling aspects. *Vehicle System Dynamics* **20**, 121–176.

Raymond, K. (1993). Could do better. *Performance Bikes* pp. 34–36.

Roe, G.E. and T.E. Thorpe (1976). A solution of the low-speed wheel flutter instability in motorcycles. *Jour. Mech. Eng. Sci.* **18**(2), 57–65.

Sakai, H., O. Kanaya and H. Iijima (1979). Effect of main factors on dynamic properties of motorcycle tires. *SAE 790259*.

Sayers, M.W. (1991*a*). Symbolic computer language for multibody systems. *Journal of Guidance, Control, and Dynamics* **14**(6), 1153–1163.

Sayers, M.W. (1991*b*). Symbolic vector/dyadic multibody formalism for tree-topology systems. *Journal of Guidance, Control, and Dynamics* **14**(6), 1240–1250.

Segel, L. and R. Wilson (1975). Requirements for describing the mechanics of tires used on single-track vehicles. In: *IAVSD-IUTAM Symp. on Dynamics of Vehicles on Roads and Railway Tracks*. Swets and Zeitlinger, Lisse. Delft. pp. 173–186.

Sharp, R.S. (1971). The stability and control of motorcycles. *Jour. Mech. Eng. Sci.* **13**(5), 316–329.

Sharp, R.S. (1974). The influence of frame flexibility on the lateral stability of motrcycles. *Jour. Mech. Eng. Sci.* **15**(2), 117–120.

Sharp, R.S. (1976*a*). The influence of the suspension system on motorcycle weave-mode oscillations. *Vehicle System Dynamics* **5**, 147–154.

Sharp, R.S. (1976*b*). The stability of motorcycles in acceleration and deceleration. In: *Inst. Mech. Eng. Conference Proceedings on "Braking of Road Vehicles"*. MEP. London. pp. 45–50.

Sharp, R.S. (1985). The lateral dynamics of motorcycles and bicycles. *Vehicle System Dynamics* **14**, 265–283.

Sharp, R.S. (1991). Tyre structural mechanisms influencing shear force generation: Ideas from a multi-radial-spoke model. In: *Proc. 1st International Colloquium on Tyre Models for Vehicle Dynamics Analysis* (H.B. Pacejka, Ed.). Swets and Zeitlinger, Lisse. Delft. Suppl. Vehicle System Dynamics, **21**, 1993, 145–155.

Sharp, R.S. (1994*a*). The application of multi-body computer codes to road vehicle dynamics modelling problems. *Proc. Inst. Mech. Eng., Part D, Journal of Automobile Engineering* **208**(D1), 55–61.

Sharp, R.S. (1994*b*). Vibrational modes of motorcycles and their design parameter sensitivities. In: *Vehicle NVH and Refinement, Proc Int Conf.*. Mech. Eng. Publications, London. Birmingham. pp. 107–121.

Sharp, R.S. (2000). Variable geometry active rear suspension for motorcycles. In: *Proc. of the 5th International Symposium on Automotive Control (AVEC 2000)*. Ann Arbor MI. pp. 585–592.

Sharp, R.S. (2001). Stability, control and steering responses of motorcycles. *Vehicle System Dynamics* **35**(4–5), 291–318.

Sharp, R.S. and C.J. Alstead (1980). The influence of structural flexibilities on the straight running stability of motorcycles. *Vehicle System Dynamics* **9**(6), 327–357.

Sharp, R.S. and C.J. Jones (1977). The straight-running stability of single-track vehicles. In: *Proc. 5th IAVSD Symp. on The Dynamics of Vehicles on Roads and on Railway Tracks*. Swets and Zeitlinger, Lisse. Vienna. pp. 334–342.

Sharp, R.S. and D.J.N. Limebeer (2001). A motorcycle model for stability and control analysis. *Multibody System Dynamics* **6**(2), 123–142.

Sharp, R.S. and M.A. El-Nashar (1986). A generally applicable digital computer based mathematical model for the generation of shear forces by pneumatic tyres. *Vehicle System Dynamics* **15**, 187–209.

Sharp, R.S., D.J.N. Limebeer and M.R. Gani (1999). A motorcycle model for stability and control analysis. In: *Euromech Colloquium 404, Advances in Computational Multibody Dynamics* (J.A.C. Ambrosio and W.O. Schiehlen, Eds.). pp. 287–312.

Sharp, R.S., S. Evangelou and D.J.N. Limebeer (2003). Improvements in the modelling of motorcycle dynamics. In: *ECCOMAS Thematic Conference on Advances in Computational Multibody Dynamics* (J.A.C. Ambrósio, Ed.). Lisbon. MB2003-029 (CD-ROM).

Singh, D.V. and V.K. Goel (1975). Stability of single track vehicles. In: *IAVSD-IUTAM Symp. on Dynamics of Vehicles on Roads and Railway Tracks*. Swets and Zeitlinger, Lisse. Delft. pp. 187–196.

Singh, D.V., V.K. Goel and M. Bhattacharya (1974). Rolling characteristics of small size pneumatic tyres. *Proc. Inst. Mech. Engrs.* **188**(AD), 701–713.

Skoog, R.A. and C.G.Y. Lau (1972). Instability of slowly varying systems. *IEEE Trans Auto Control* **AC-17**(1), 86–92.

Spierings, P.T.J. (1981). The effects of lateral front fork flexibility on the vibrational modes of straight-running single-track vehicles. *Vehicle System Dynamics* **10**(1), 21–35.

Steele, Jr. and L. Guy (1984). *COMMON LISP: the language*. Digital Press. Burlington, Mass.

Strang, G. (1988). *Linear Algebra and its applications*. 3rd ed.. Saunders HBJ.

Takahashi, T., T. Tatsuo and T. Nakamura (1984). Experimental and theoretical study of the influence of tires on straight-running motorcycle weave response. *SAE 840248*.

Tezuka, Y., H. Ishii and S. Kiyota (2001). Application of the magic formula tire model to motorcycle maneuverability analysis. *JSAE Review* **22**, 305–310.

The Mathworks Inc. (2000). *MATLAB 6 Reference Manual*. http://www.mathworks.com.

van Oosten, J.J.M., E. Kuiper, G. Leister, D. Bode, H. Schindler, J. Tischleder and S. Köhne (2003). A new tyre model for TIME measurement data. in press.

Weir, D.H. (1972). Motorcycle handling dynamics and rider control and the effect of design configuration on response and performance. PhD thesis. University of California at Los Angeles.

Weir, D.H. and J.W. Zellner (1978). Lateral-directional motorcycle dynamics and rider control. *SAE 780304*.

Weir, D.H. and J.W. Zellner (1979). Experimental investigation of the transient behaviour of motorcycles. *SAE 790266*.

Zellner, J.W. and D.H. Weir (1978). Development of handling test procedures for motorcycles. *SAE 780313*.